Analysis of the Kinesin-13 gene family in plants

FISCHER, NICHOLAS,JAMES,KILBURN

Analysis of the Kinesin-13 gene family in plants

Nicholas Fischer

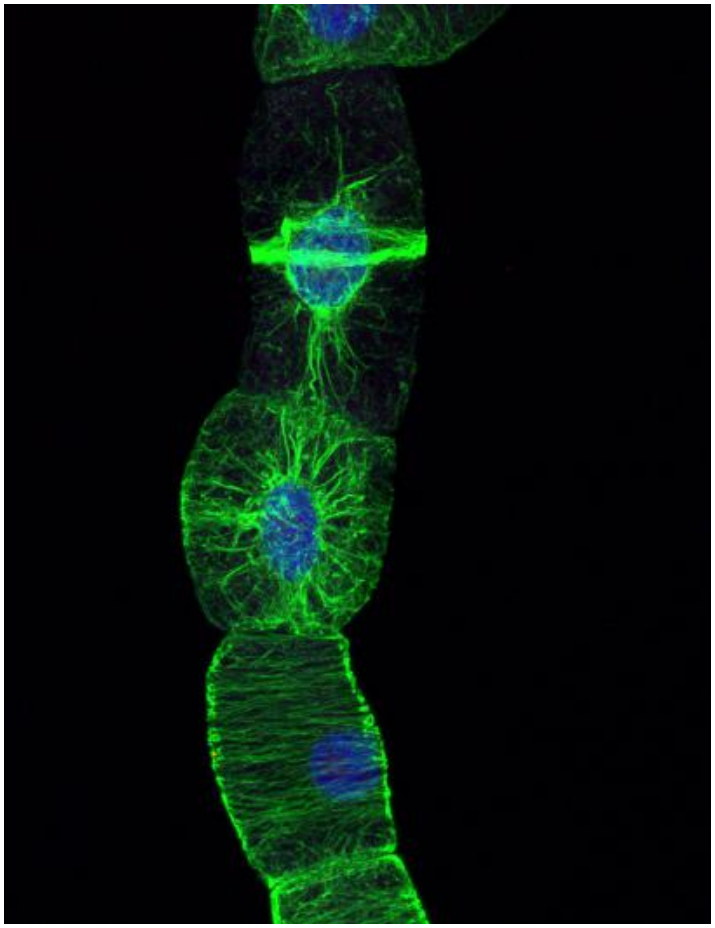

Submitted in Accordance with the Requirements for the Degree of

Masters of Science

School of Biological and Biomedical Sciences

Durham University

December 2011

Abstract

Although the depolymerizing effects of animal kinesin-13 proteins have been well characterized, little is known of the two *Arabidopsis* kinesin-13 proteins. This project aimed to investigate in more detail the functions of AtKinesin-13A/B and their effect on microtubule dynamics. The first aim was to analyse the function of both proteins *in vitro* using biochemical studies. Proteins were expressed in both bacterial and insect cells before undergoing co-sedimentation and turbidimetric assays to assess their activity and microtubule-interacting properties. The second aim of this project was to investigate the *in vivo* effects of these proteins on microtubule dynamics throughout the cell cycle. Tobacco BY2 cell lines were transformed with AtKinesin-13A and 13B, as well as human HsKinesin-13 for comparison under the expression of an estradiol-inducible promoter. This inducible system allowed transient expression of recombinant protein to analyse the effect of expression on cell growth, nuclear morphology and microtubule dynamics by immunofluorescence microscopy.

These experiments show that AtKin13B appears to function during metaphase in aiding activation of the metaphase spindle checkpoint and subsequent progression through the cell cycle. Biochemical studies into its relationship with microtubules, combined with *in vivo* induction data, suggest that AtKin13B may have a subtle destabilizing effect on microtubules. Biochemical studies with AtKin13A showed that it binds specifically to microtubules, and it localized to chromosome arms in a similar pattern to AtKin13B, but may have different effects in plants. Human Kinesin-13 localized exclusively to spindle microtubules throughout the cell cycle showing that the activity of kinesin-13 proteins is species-specific and animal kinesins have little effect in plant systems.

Contents

Cell Biology

Acknowledgements

There are many people to whom I would like to express my thanks for this project. Firstly, I would like to thank my supervisor, Professor Patrick Hussey, for inspiring me to continue my studies in such an interesting area of Biology and for his guidance along the way.

A huge thank you to Dr Andrei Smertenko, for his unceasing support and enthusiasm throughout the year. Throughout the ups and downs, he was always there to offer advice and to instil confidence. I've learnt so much from working with him, and without his help couldn't have got to where I am now!

Finally, my thanks go to everyone in the Hussey lab who were a source of knowledge, advice and laughter throughout the year. Dr Tim Hawkins, who carried out the initial work on this project and made the antibodies I used throughout the year, and Dr Mike Deeks were always on hand for technical advice and support. My fellow postgraduates Martin, Frances, Orla and Lizzy - it's been huge!

1. INTRODUCTION

1.1. Microtubules

Microtubules represent key structural components of the eukaryotic cell cytoskeleton, important in many cellular processes such as division, cell expansion, vesicular transport and specifically for plants, cell wall formation.

Built from subunits of the αβ-tubulin heterodimer, each tubulin monomer consists of around 450 amino acids with a molecular mass of 50kDa. Although a total of seven tubulin proteins are known to exist in nature, the only three present ubiquitously in eukaryotic organisms are α-tubulin, β-tubulin and γ-tubulin (Dutcher 2001). The two proteins which construct the heterodimer from which microtubules are assembled, α- and β-tubulin, share a 50% homology, whereas the more specialized γ-tubulin is involved in microtubule nucleation (Burns 1991). Each tubulin monomer can bind to a single GTP molecule, which is exchangeable in β-tubulin (at the E-site) but non-exchangeable in α-tubulin (N-site). GTP-bound β-tubulin is required for microtubule assembly, and its hydrolysis follows the addition of a tubulin heterodimer to the growing microtubule end, whereupon it is made nonexchangeable within the microtubule (Kirchner & Mandelkow 1985).

During microtubule formation, tubulin heterodimers associate in an end-to-end fashion to form linear protofilaments (Desai & Mitchison 1997). Interactions between neighbouring α- and β-tubulin monomers allows lateral association between protofilaments to form sheets which subsequently fold into long, hollow-tubed cylinders (Chretien et al 1995). Each microtubule cylinder has a diameter of 25nm and typically consists of 13 protofilaments, although genetic studies have indicated that protofilament number can be influenced by specific β-tubulin isoforms (Raff et al 1997) (FIG 1).

As tubulin heterodimers polymerize in the same orientation, an intrinsic polarity exists within the microtubule polymer which produces structural and kinetic differences at each end. The slower growing minus end has α-tubulin exposed, whereas the faster growing

plus end has β-tubulin dimers exposed. The polar nature of microtubule filaments is an essential prerequisite for the establishment of cell polarity and the directional movement of motor proteins (such as members of the kinesin and dynein family) along the microtubule.

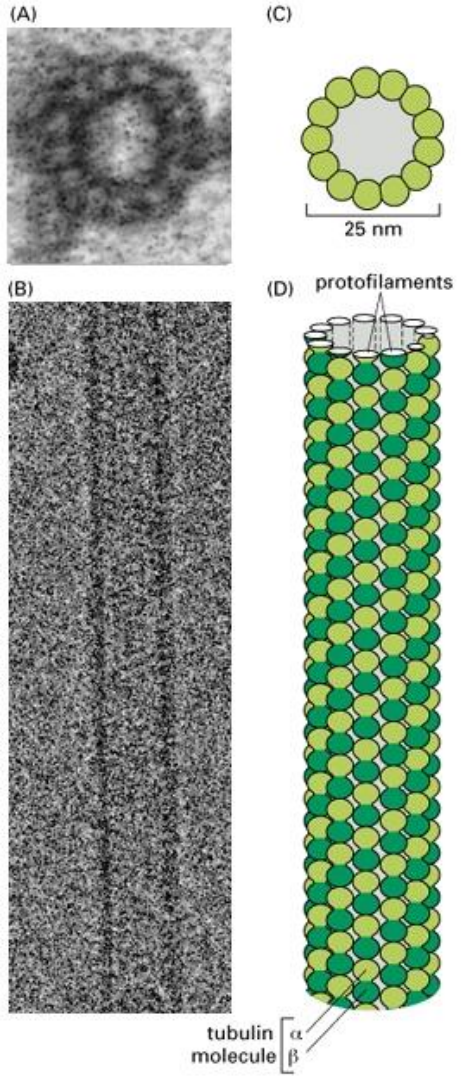

Figure 1: Microtubule structure. Electron micrographs of (A) the cross-section through a microtubule showing the thirteen protofilaments, and (B) a cryoelectron micrograph of an assembled microtubule *in vitro*. (C) and (D) show schematic representations of the microtubule, showing how the tubulin subunits fit together within the tubular lattice (Alberts et al 2002)

.

1.2. Microtubule Dynamics

1.2.1. Assembly

Microtubule assembly takes place in three distinct phases: nucleation, elongation and steady state. Nucleation involves the spontaneous formation and subsequent growth of microtubules from seeds of oligomers proposed to contain between 6 and 13 dimers (Fygenson et al 1995, Voter & Erickson 1984). One factor identified as a key requirement for microtubule nucleation is the presence of GTP-tubulin. Furthermore, polymerization only occurs if a threshold of tubulin concentration known as the critical concentration is reached; above this threshold tubulin dimers add to the elongating microtubule (Valiron et al 2001).

Although the rate of nucleation is strongly dependent on the initial concentration of free GTP-tubulin, the rate remains constant through most of the assembly phase despite subsequent drops in tubulin concentration. The elongation rate is also unaffected by free tubulin concentration, and is instead limited by the probability of tubulin dimers binding to the microtubule (Caudron et al 2000). Elongating microtubules are typically not blunt-ended polymers, as mentioned earlier growing protofilaments form open-ended sheets which eventually close to form a tube.

During the steady state phase a fixed proportion of tubulin is assembled in the microtubule lattice, with a second pool of tubulin remaining soluble. Throughout this stage the microtubule system remains out of equilibrium, that is, a continual supply of energy is required for GTP hydrolysis and thus the maintenance of steady state microtubules. This energy is used to drive the exchange of integral subunits with the tubulin dimers of the soluble pool (Valiron et al 2001). Clearly, despite the net proportion of bound tubulin remaining constant, individual tubulin monomers are in a state of constant flux between bound and soluble pools. This highly dynamic and seemingly misleading characteristic of ‘steady-state’ microtubules can be explained by two mechanisms: treadmilling and dynamic instability.

1.2.2. Treadmilling

Treadmilling is the first mechanism by which steady state microtubules exhibit dynamic properties. It relies on the differing behaviour of steady state microtubule ends: the plus end continuously incorporates new tubulin dimers whilst the minus end continuously loses them (FIG 2) (Margolis & Wilson 1978). These opposing behaviours are due to net differences in critical subunit concentrations at either end. If both ends of the microtubule are untethered, this asymmetry allows apparent translocation of the microtubule around the cytoplasm, whereas if one end of the microtubule is fixed then treadmilling produces a unidirectional flux of tubulin dimers through the polymer length travelling from the plus end to the minus end (Margolis & Wilson 1981).

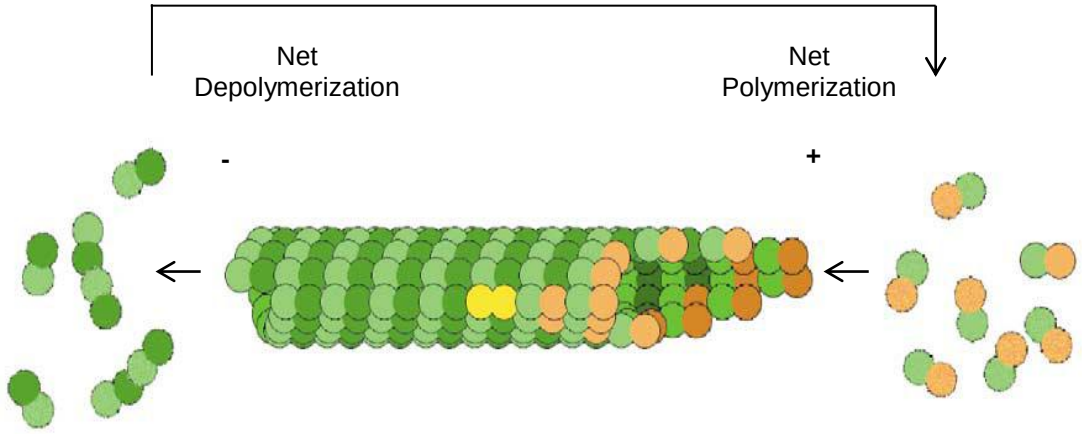

Figure 2: Treadmilling: free microtubules undergo dynamic behaviour at both ends, with the minus end favouring depolymerization. When rates of polymerization and depolymerization rates are balanced at both ends, microtubules stay at constant net length despite a flow of tubulin dimers from the plus to minus end (Adapted from Hashimoto 2003)

Two models have been proposed to explain treadmilling in microtubules: the Wegner model and differential dynamic instability at each end. The Wegner model (posited before the discovery of dynamic instability) basically translates an explanation of actin filament assembly to that of microtubules: GTP hydrolysis upon tubulin binding at one end allows the critical concentrations for growth to be different, so the end with the lower critical concentration will grow whilst the end with the higher critical concentration will persistently shorten (Wegner & Engel 1975). Alternatively, treadmilling could also occur if stages of dynamic instability had a net bias at each end (Grego et al 2001).

1.2.3. Dynamic Instability

First proposed following an analysis of the length distribution of fixed microtubules (Mitchison & Kirschner 1984a, Mitchison & Kirschner 1984b), the finding that microtubules can stochastically switch between phases of growth and shrinkage, without complete disassembly or maintenance of a steady length, represents a unique phenomenon known as dynamic instability. An intrinsic property of tubulin observable even in purified extracts, dynamic instability enables rapid rearrangement of the microtubule network to accommodate different structural and functional requirements throughout cell division and the cell cycle. Additionally, by repeated phases of growth and shrinkage the cell is able to respond to changing environmental cues and stresses (Komarova et al 2002) (FIG 3).

The classical chemical kinetics model posits that microtubule stability is normally maintained by the presence of a GTP-tubulin 'cap' at the growing (plus) end. During the polymerization phase, GTP-bound tubulin dimers add to the plus end of a MT to cause elongation or growth. However, soon after the addition of GTP-dimers the tubulin subunits can hydrolyze their bound GTP to GDP and subsequently release a phosphate molecule (P_i). If the rate of GTP hydrolysis is faster than the addition of new tubulin dimers, the 'GTP-cap' is dissolved and GDP-tubulin subunits are exposed and lost at a rapid rate, resulting in MT depolymerization. Depolymerizing microtubules can be switched back to growth if GTP-tubulin dimers are added to the plus end before bound GTP is hydrolysed (FIG 3) (Desai & Mitchison 1997).

The nature of the GTP-cap has been well-studied *in vitro*, though direct evidence of its size was traditionally hard to obtain. Initial data suggested that a monolayer of GTP-tubulin subunits covers the 13-14 protofilaments of the microtubule (Caplow & Shanks 1996, Drechsel & Kirschner 1994, Panda et al 2002). However, experiments using 'optical tweezers' to track microtubule assembly dynamics showed evidence of a multi-layered and highly variable GTP-cap (Schek et al 2007). This was confirmed in recent computational studies of microtubule dynamics, which suggested that the GTP-cap may in fact be up to several microns in length, comprising an average of forty GTP-tubulin dimers (Piette et al 2009).

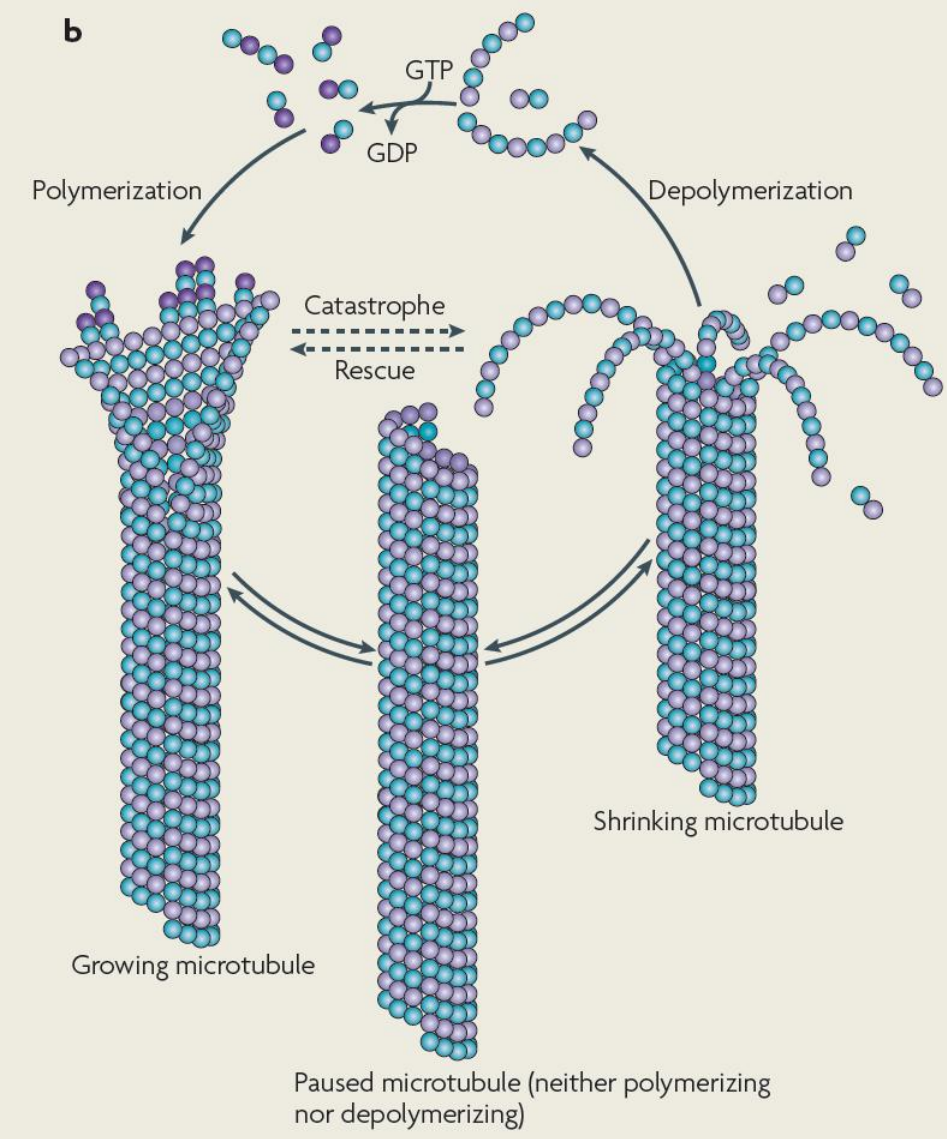

Figure 3: Dynamic instability: GTP-bound tubulin dimers are added at the plus end. Contact with exposed α-tubulin subunits leads to hydrolysis of GTP to GDP and subsequent depolymerization due to a conformational change. Growing microtubules have a GTP-cap structure at plus end which prevents depolymerization. Random loss of this cap leads to rapid depolymerization (catastrophe) and stochastic gain of a cap restores microtubule growth (rescue). Interestingly, the structure of growing and shrinking microtubule ends is markedly different, indicating that different mechanisms operate (Conde & Caceres 2009).

This switch from growth to rapid shrinkage is known as 'catastrophe' and the switch from shrinkage to growth is called 'rescue'. Interestingly, microtubules *in vivo* are frequently seen to 'pause' where they neither grow nor shrink (Shelden & Wadsworth 1993), and *in vitro* microtubules with pure tubulin pause much less frequently (Walker et al 1988).

The energy needed to power dynamic instability is generated during the hydrolysis of a GTP molecule during polymerization. Although both α- and β-subunits associate with one molecule of GTP, in α-tubulin this molecule is non-hydrolysable. The GTP molecule

associated with β-tubulin, however, is exchangeable: GTP is hydrolysed to GDP during polymerization, which is then exchanged for GTP when released upon depolymerization

1.2.4. Structural basis of microtubule dynamics

Although a general model for the principles of dynamic instability is widely accepted, details of the structural and molecular mechanisms underpinning this process are still poorly understood.

The first evidence suggesting a relationship between microtubule dynamics and the geometry of inter-subunit bonds came from early studies using cryoelectron microscopy. Protofilaments in microtubules were seen as relatively straight, whereas the intermediate depolymerization products of microtubules adopted curved structures and protofilaments seemed to peel from the microtubule ends forming 'ram horns' (FIG 3) (Mandelkow & Mandelkow 1985, Mandelkow et al 1991).

These observations, combined with more recent structural studies (Lowe et al 2001, Ravelli et al 2004), led to the formulation of an 'allosteric' model in which the tubulin heterodimer exists in two differing conformations dependent on the nucleotide bound at the β-tubulin E-site (Wang & Nogales 2005). A relatively straight GTP-tubulin would allow the formation of linear protofilaments, whereas a curved GDP-tubulin conformation would account for the curved protofilaments seen in cryoelectron studies, but would not allow microtubule polymerization. Within the microtubule, however, GDP-tubulin subunits are held in a straightened, GTP-like state owing to structural constraints of the microtubule lattice (Melki et al 1989, Wang & Nogales 2005). This hypothesis of tubulin kinetics is in line with thermodynamic studies of dynamic instability: the energy produced by GTP hydrolysis is stored within the MT lattice as mechanical 'strain' needed to maintain the GDP-subunits in their unfavoured, straight conformation (Caplow et al 1994). When the GTP cap is lost, therefore, rapid depolymerization ensues as GDP-subunits convert into the low-energy, curved state (Nogales & Wang 2006).

Recently, though, an opposing 'lattice' model has been proposed which posits that the αβ-heterodimer adopts the curved conformation in solution, regardless of the state of its

attached nucleotide (Buey et al 2006, Rice et al 2008). Structural rearrangements, therefore, do not occur in response to GTP binding. Rather, the tubulin dimers straighten as a result of incorporation into the growing microtubule lattice as a consequence of protofilament straightening during tube closure (Valiron 2011). The role of GTP in this model is to strengthen the lattice contacts and stabilize the MT-bound straight tubulin conformation (Rice et al 2008). After GTP hydrolysis, then, the microtubule protofilaments curve outwards either as a result of weaker lateral interactions with their neighbours, or due to decreased stability of the curved GDP-tubulin conformation.

A paucity of direct experimental evidence means this question is still unresolved. The problem is that analysis usually involves external influences such as destabilizing agents or large structural assemblies which may impose geometric constraints on tubulin curvature. Support for the allosteric model, for example, comes from evidence that the curvature of tubulin bound to a non-hydrolysable GTP analogue, GMPCPP, is less than that of GDP-bound tubulin (Wang & Nogales 2005). Conversely, analysis of the crystal structures of γ-tubulin (Rice et al 2008) and more distantly related bacterial homologues (Gigant et al 2005, Oliva et al 2007) showed curved GTP-bound tubulin in support of the lattice model.

Despite this, computational studies may prove useful alternatives as they eliminate the influence of external factors on tubulin conformation. A plethora of recent computational simulations have helped to better understand tubulin and MT properties, binding sites and the conformation of their termini (Summarized in Grafmueller & Voth 2011). A recent study, using atomistic simulations of short protofilaments, concluded that both the GDP- and GTP-bound tubulin states adopt a similar curved conformation in solution (Grafmueller & Voth 2011), supporting the lattice model for MT assembly.

These recent structural investigations place growing importance on the geometric states of microtubule intermediates in microtubule dynamics, independent of the chemical state of the bound nucleotide. Traditionally dominant models based on chemical kinetics, extolling the stabilizing role of a GTP cap, are becoming increasingly hard to reconcile with these structural studies. Although the chemical kinetics viewpoint is not invalidated, it is clear that future, sophisticated analyses should encompass these features of ‘structural plasticity’ (Kueh & Mitchison 2009).

Interestingly, the recent characterisation of an antibody specific to GTP-tubulin has allowed new insights into the localization of GTP-tubulin *in vivo*, pointing to the role of GTP 'remnants' in aiding microtubule rescue (Dimitrov et al 2008). This antibody adds to a growing list of new tools allowing the study of polymerization/depolymerization at increasingly small experimental resolutions, one step further to unravelling the mechanics of microtubule dynamics at a molecular level.

1.3. Plant Microtubule Arrays

The cellular architecture of higher plants is fundamentally different to that of animal or fungal cells, containing a peripheral cytosolic layer at the cell cortex surrounding a large vacuole. Organelles and other cytoplasmic components are dispersed throughout the cytosol and in a state of constant movement due to the action of actin-/myosin-based cytoplasmic streaming. Importantly, absence of centrosomes or spindle pole bodies found in animal cells poses an interesting challenge for microtubule assembly and maintenance in plants. In animal cells, the centrosome plays a dominant role in creating the architecture of the interphase array, by nucleating microtubules and stabilizing their bound minus ends. Microtubule organization in plant cells, therefore, differs significantly to that of their animal counterparts, forming four distinct arrangements prominent at different stages of the cell cycle (FIG 4).

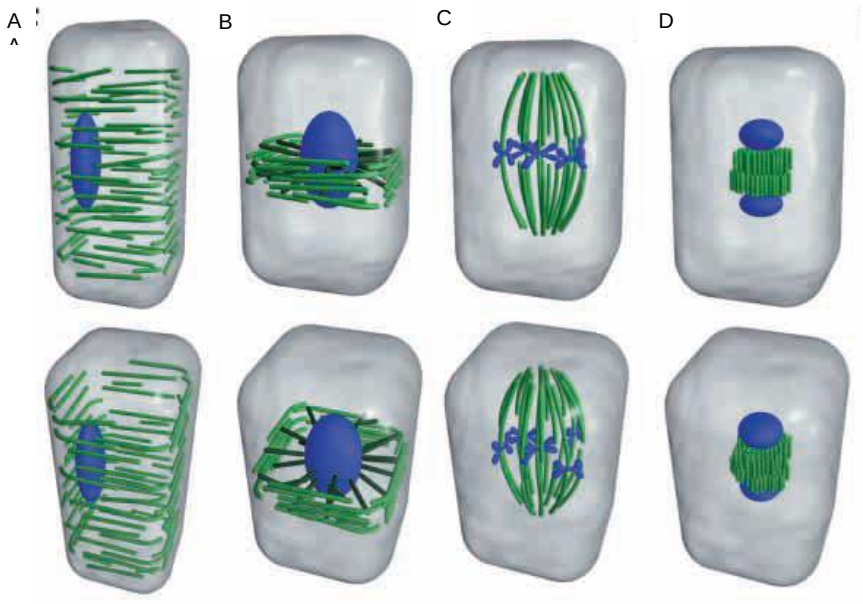

Figure 4: Schematic representation of the four microtubule arrays. (A) The cortical interphase array arranged perpendicular to cell axis (B) the preprophase band, marking the site of future cell division (C) the mitotic spindle and (D) the phragmoplast aiding formation of the cell plate. (Adapted from Wasteneys 2002)

1.3.1. The Interphase Arrays: Cortical microtubules and the Preprophase Band

In the cortical interphase array, microtubules are present at the cell periphery and lie perpendicular to the cell axis, closely coincident with cell wall fibers (Fig 4A). In growing interphase cells, microtubules and cell wall microfibrils are found parallel to each other, transverse to the direction of cell expansion. This apparent co-alignment led to the hypothesis that cortical microtubules have a role in cell wall formation, acting as guides for cellulose deposition by constraining the distribution of cellulose synthase complexes (Giddings 1991, Heath 1974).

Although generally accepted, lack of direct evidence and inconsistencies with observations of continued cellulose microfibril production after disruption of cortical microtubules, have always hampered this model (Smith & Oppenheimer 2005). More recently, studies of mutants showing defects in microfibril and microtubule organization led Wasteneys to propose the 'microfibril length regulation hypothesis', in which cortical microtubules participate in regulating the length of cellulose microfibrils (Wasteneys 2004).

An interesting distinction between interphase microtubules of the plant and animal kingdoms is that plant microtubules are much more dynamic, as implied by a three- to four-times faster rate of fluorescence recovery after photobleaching (FRAP) (Hush et al 1994). Although the average rates of plus end polymerization and depolymerization are slower than animal cells, a noticeably reduced 'pause' time can perhaps explain the increased recovery rate. Furthermore, dynamic properties have been observed at both the plus and minus ends, a feature rarely seen in cells with microtubule organizing centres. The unattached microtubule minus ends exhibit slow depolymerization with pausing, whereas the plus ends undergo dynamic instability favoured towards growth. Due to this disparity in dynamic behaviour at each end, plant cortical microtubules are said to employ a mechanism known as 'hybrid treadmilling' (Ehrhardt & Shaw 2006, Lloyd & Chan 2006).

As the cells approach mitosis their cytoskeletal organization changes dramatically: cortically-based microtubules begin to depolymerize to leave only a circumferential band around the nucleus which demarcates the plane of cell division (Fig 4B). Called the preprophase band (PPB), it consists of an array of parallel cortical microtubules and actin filaments which breaks down just before division to leave an 'invisible' imprint. The importance of this structure is highlighted by mutational studies in which plants lacking PPBs show irregular cell expansion and cell division defects (McClinton & Sung 1997, Traas et al 1995).

Despite significant study into the timing of PPB appearance and its functional importance (Granger & Cyr 2001), the mechanism which drives its formation is still unclear. Fluorescence studies using a YFP-tagged plus-end binding protein to visualize and measure microtubule dynamics have helped to shed light on this process (Dhonukshe & Gadella 2003). In this model, PPB formation is thought to proceed in four stages: initiation, narrowing, maturation and eventual breakdown (FIG 5). During initiation, a broad PPB forms covering a large portion of the cell. The catastrophe frequency of these microtubules gradually starts to increase, providing a large pool of free tubulin dimers from which new microtubules form. This leads to narrowing of the PPB, and the continued cycle of increased catastrophe and subsequent MT growth rate promotes the formation of shorter microtubules in PPB maturation. Finally, it is proposed that during breakdown of the PPB the catastrophe rate reaches such a level (perhaps by total inactivation of MT-stabilizing proteins) that it cannot be overcome by increased MT growth rates, leading to its collapse. Nuclear envelope-derived microtubules, however, maintain higher growth rates and so survive, using the new tubulin pool from collapsed PPB MTs to construct the mitotic spindle (Dhonukshe & Gadella 2003). Interestingly, the fact that actin-depolymerizing drugs such as cytochalasin D affect the narrowing of the PPB (Granger & Cyr 2001), suggests an additional role for actin in PPB maturation.

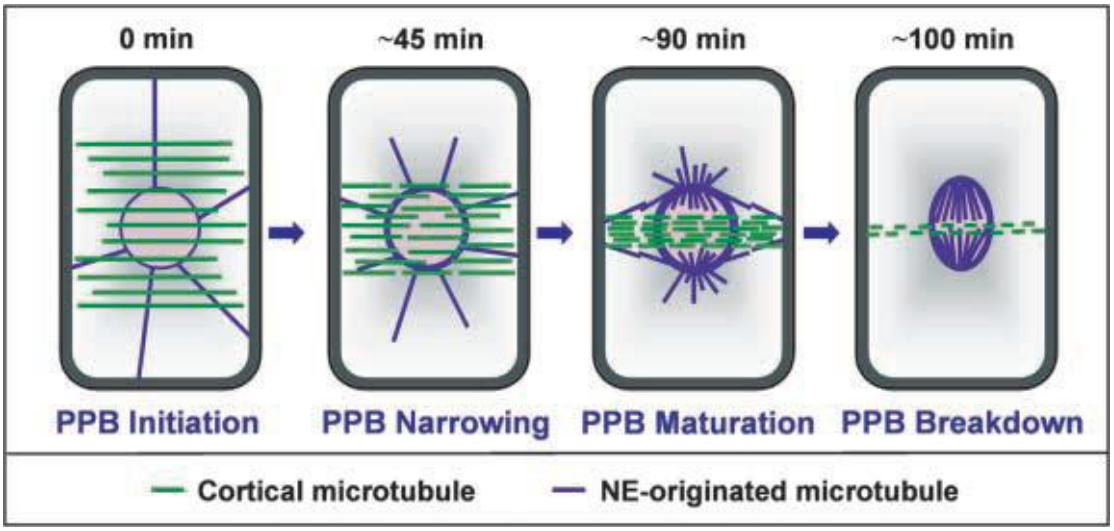

Figure 5: Schematic model of PPB formation by alteration of dynamic instability (Dhonukshe & Gadella 2003)

1.3.2. The Mitotic Spindle

In early prophase the PPB breaks down and is replaced by the mitotic spindle which serves to separate daughter chromosomes (Fig 4C). Apart from their structure at the poles, mitotic plant spindle closely resemble those in animal and fungal cells. They serve during division to attach and capture chromosomes at prophase, align them at metaphase and then separate them at anaphase.

Early study in animals cells led to the postulation of a 'search and capture' model for mitotic spindle formation (Kirschner & Mitchison 1986). As the microtubule minus ends are tethered to polarized centrosomes at either side of the nucleus, plus ends of growing microtubules emanate outwards and undergo rounds of growth and shrinkage. If these microtubules contact the kinetochore protein complexes at the centromeres of chromosomes, they are captured to form stable bundles. Eventually, with the help of a multitude of facilitating proteins, durable, bipolar spindles can be assembled (Zhang & Dawe 2011).

This model, however, does not account for the many types of animal cells which are capable of forming seemingly normal bipolar spindles without centrosomes, such as animal oocytes or somatic cells with laser ablated centrosomes (Zhang & Dawe 2011). Interestingly, these cells manage to nucleate spindle arrays at or near to condensed

chromosomes. This process was elucidated quite elegantly in an *in vitro* study of *Xenopus* eggs: the addition of DNA-coated beads to egg extracts lacking centrosomes led to the initiation of bipolar spindles with similar properties to their centrosome-mediated counterparts (Heald et al 1996). This alternative mechanism, dependent on the small GTPase Ran, is known as 'spindle self-organization' (FIG 6).

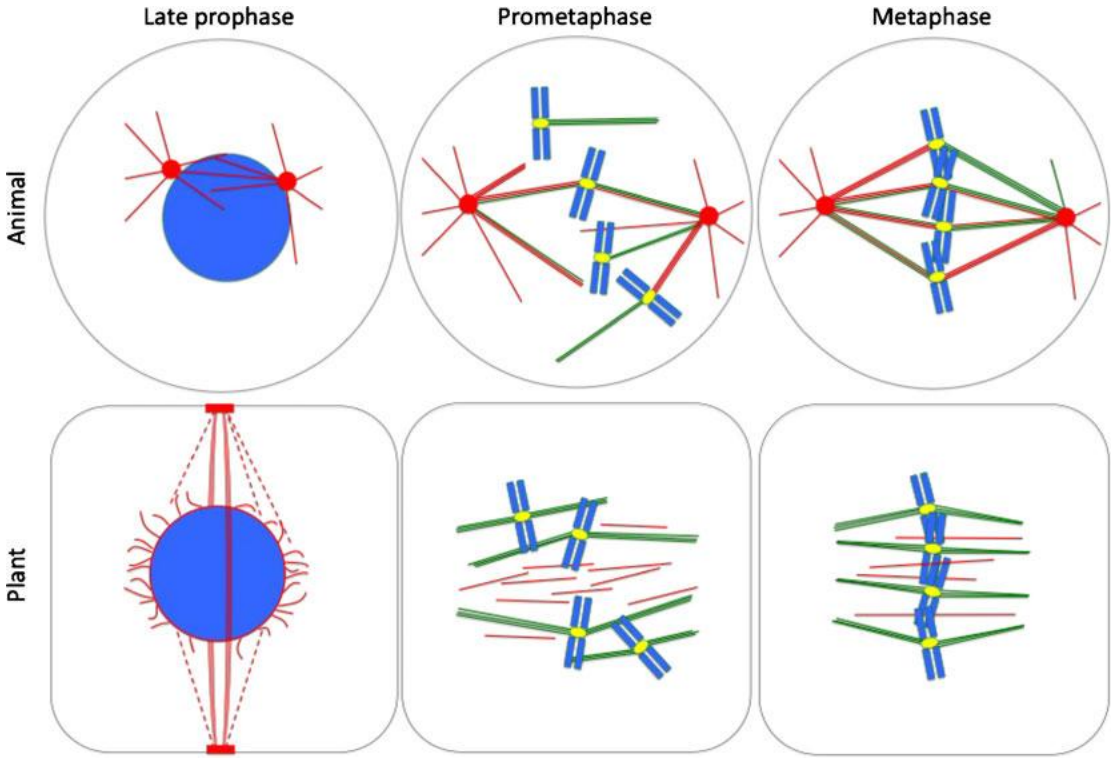

Figure 6: A comparison of spindle formation in animals and plants. The centrosomal or PPB-associated MTs are shown in red. Kinetochore-associated MTs are in green. In animal cells, MTs growing from the centrosomes and the kinetochores help to secure and align chromosomes correctly in the cell. In plants, the dotted red lines illustrate bridging MTs between the PPB and the nucleus, which are important along with spindle self-organisation (Zhang & Dawe 2011).

As plant cells lack organizing centrosomes, it has been argued that their spindles form with a similar self-organizing mechanism. Although definitive evidence is limited, the highly conserved nature of Ran in plants (Haizel et al 1997), combined with localisation and transgenic studies linking Ran-GAP to the spindle and PPB (Xu et al 2008, Yano et al 2006), strongly support a link between the Ran cycle and spindle assembly.

Despite this correlation, it is also important to note that although lacking centrosomes plants cells do have an early polarizing structure, the preprophase band. In addition to the cortical microtubules of the PPB during early mitosis, other microtubules randomly

dispersed around the nuclear periphery either encase the nuclear surface to form the prophase spindle, or radiate away to the cortex (Lloyd & Chan 2006). It has been shown that the PPB contributes to prophase spindle organization and bipolarity via the interaction of 'bridge' microtubules between the PPB and the nucleus (Ambrose & Cyr 2008). In this way the preprophase band acts like a centrosome pair: important for imposing polarity upon the mitotic spindle from the equator, rather than the poles, but dispensable for mitotic spindle assembly *per se* (Bannigan et al 2008).

1.3.3. Cytokinesis and the Phragmoplast

Cytokinesis in higher plants is a highly regulated process involving cytoskeletal-assisted targeting and fusion of membrane vesicles. As cytokinesis in plant cells effectively involves the formation of a new extracellular compartment within the cell, its complexity compared to animal cells is markedly increased. This process is thus co-ordinated by a plant-specific microtubule array, the phragmoplast (Fig 4D).

As the dividing cell reaches cytokinesis, microtubules from remnants of the mitotic spindle form a self-organizing double ring with the plus ends of each ring meeting and overlapping at the cell midzone (Euteneuer et al 1982). At late anaphase, the loosely dispersed spindle microtubules in the interzone laterally coalesce to form a cylindrical body. This then shortens in length and expands in width, with the addition of new microtubules at the growing edges as opposed to the spindle remnants involved in initial phragmoplast formation (Staehlin & Hepler 1996). As the cell plate expands, microtubules depolymerize at the centre and repolymerize at the edges of the expanding plate (Gu & Verma 1996, Gunning & Wick 1985). These microtubules direct cell wall-forming vesicles to the site of the centrifugally expanding cell plate, which eventually coalesce to form the separating cross-wall between two daughter cells (Wasteneys 2002).

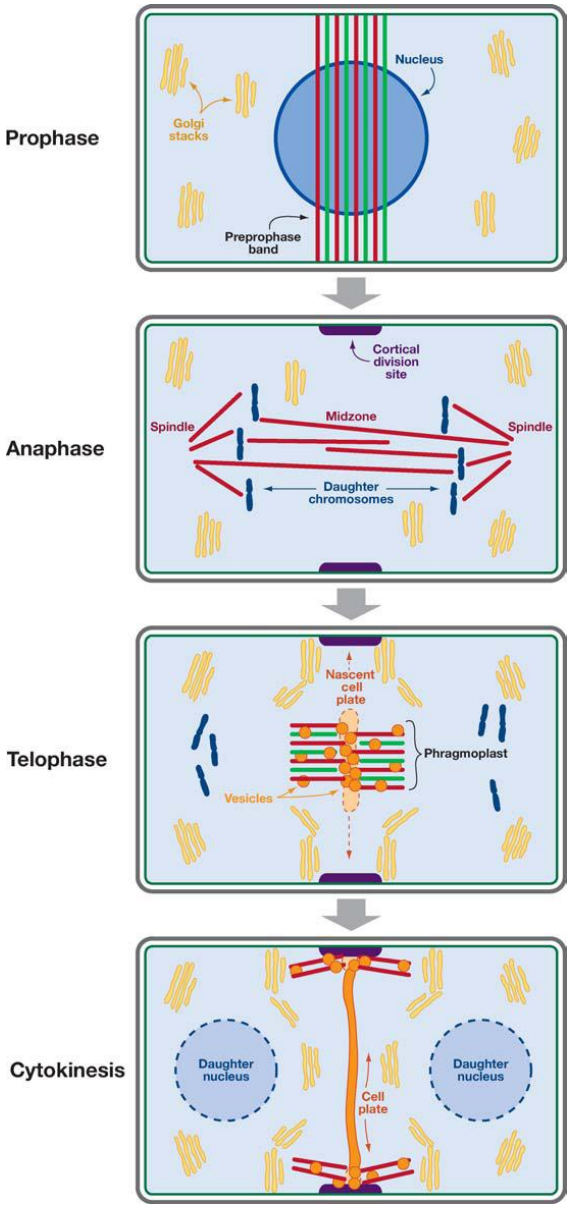

Figure 7: Cytokinesis in plant cells. Co-aligned MTs (red) and actin filaments (green) of the PPB determine the plane of cell division. During anaphase, overlapping spindle MTs initiate formation of the phragmoplast in the midzone. In telophase, an antiparallel bundle of MTs and actin filaments forms, allowing the accumulation of Golgi vesicles in the midzone. These fuse to form the cell plate, which expands outwards during cytokinesis accompanied by lateral translocation of MTs. Eventually the cell plate fuses with cortical attachment sites at the cell periphery (Jurgens 2005).

Initially, the fusion of cell plate forming vesicles is spatially constrained to form a small disk of intermediates which give rise to a transient membrane compartment, the cell plate, before finally forming the new plasma membrane between daughter cells. Arriving vesicles fuse to the edges of the expanding cell plate, simultaneously reorganizing by secreting cell wall components into the vesicular lumen and removing excess membrane material. Finally, the cell plate fuses to the edge of the parental plasma membrane at

cortical sites demarcated by the preprophase band, leading to formation of two distinct daughter cells (FIG 7)(Jurgens 2005).

Although aesthetic changes in the phragmoplast microtubule array had long been observed, details of the dynamic nature of these microtubules remained elusive. It was not until a pioneering study by Asada *et al* that any insight was gained into the mechanics of this intriguing structure. By using the newly developed technique of glycerination, cultured tobacco BY-2 cells were stably permeabilized and infused with DTAF (dichlorotriazonilamino fluorescein)-labelled tubulin at different points in cytokinesis. By comparing the incorporation of fluorescently-labelled tubulin into phragmoplast microtubules at different time points, they were able to determine their polymerization dynamics (Asada et al 1991).

Their results suggested that a treadmilling system was operating, in which the equatorial region of the phragmoplast combines microtubule polymerization at the plus end with translocation towards the minus end. The fact that translocation was induced effectively by GTP and less effectively by ATP, and inhibited by non-hydrolysable analogues of these nucleotides, points to the role of a force-generating mechanochemical enzyme in this process. Interestingly, a recent study using computer modelling to simulate microtubule dynamics during phragmoplast formation shows that most microtubules in the phragmoplast actually undergo dynamic instability (Smertenko et al 2011).

1.4. Microtubule Interacting Proteins

1.4.1. Microtubule Associated Proteins (MAPs)

The fact that microtubules are able to form distinct, stable arrays in response to developmental or environmental influences suggests the presence of proteins involved in regulating microtubule dynamics. Studies have shown that the reorganisation of microtubule arrays or the balance between catastrophic and rescue phases of dynamic instability are directly modulated by specialized Microtubule Associated Proteins (MAPs) (Lloyd & Chan 2004, Valiron et al 2001).

Early microtubule purifications isolated from cell extracts after rounds of assembly and disassembly led to the initial identification of MAPs as proteins which attach to microtubules *in vivo*. Most plant MAPs have functional homologues in all other eukaryotes, but not all animal and fungal MAPs are present in plants. A likely explanation for this may be that, although plant microtubules are structurally similar to their eukaryotic counterparts, plant microtubules differ significantly in their organization and dynamic properties.

A group of MAPs unique to and well-studied in animal cells are the so-called 'classical' or neuronal MAPs. Abundant in the microtubule-rich mammalian brain tissue, this group includes MAP2, MAP4 and Tau (Cleveland 1993). Located in all animal microtubule arrays, overexpression of these proteins induced MT bundling and resistance to MT-destabilizing drugs, highlighting their role as promoters of microtubule polymerization and stabilization (Ennulat et al 1989, Hoshi et al 1992). The microtubule-binding capacity of these proteins is conferred by a conserved C-terminal region of 18 amino acid repeats (Lewis et al 1988), and a proposed mechanism suggests that these MAPs bind longitudinally along the outer ridges of MTs, stabilizing the straight GDP-tubulin by longitudinal bridging of tubulin interfaces (Al-Bassam et al 2002).

Although homologues of these classical MAPs are not found in plants, the mechanism by which they bind and stabilize microtubules is common to other proteins found in plants. In fact, since the discovery of neuronal MAPs a diverse range of microtubule interacting proteins have been identified with conserved homologues in many organisms. Although many have yet to be fully classified, most can be distinguished by their preferential binding to different locations on the microtubule.

1.4.1.1. Plus end-tracking proteins (+TIPS)

CLIP-170

Microtubule plus end binding proteins (+TIPS) are a highly diverse group of proteins defined by their accumulation and tracking at microtubule plus ends (reviewed in Akhmanova & Steinmetz 2010). The first +TIP was identified as CLIP-170 (Cytoplasmic Linker Protein 170), when GFP-tagged CLIP-170 was seen to 'track' the growing plus

ends of microtubules using live cell video microscopy (Perez et al 1999). Since then, several CLIP family members have been found in a diverse range of phyla where they serve to regulate MT dynamics and link them to distinct cellular sites (Dujardin et al 1998, Pierre et al 1992). In this respect, they form part of a system which 'guides' microtubules to their target destinations by regional control of microtubule dynamics. The microtubule-binding region of CLIP proteins contains one or more CAP-Gly domains necessary for plus-end tracking.

A family of CLIP-associated proteins, or CLASPs, were identified using a yeast two-hybrid screen with the coiled coil region of the mammalian CLIP-115 as bait (Akhmanova et al 2001). Overexpression of CLASPs in fibroblast cells led to MT stabilization, and inhibition of CLASP function by antibody injections appeared to prevent the formation of stabilized, aligned microtubules (Akhmanova et al 2001). By binding to both MTs and CLIP proteins, they help to stabilize microtubules either directly or via interactions with bound CLIPs.

Although CLIP homologues have been identified in various animals and fungi, clear counterparts in plants have been difficult to determine. Interestingly, when a YFP-fused mammalian CLIP was expressed in tobacco BY-2 cells it was shown to bind to and track microtubule plus ends, hinting that conserved pathways for regulating CLIP binding to MTs exist in both plants and animals (Dhonukshe & Gadella 2003). Furthermore, a single, putative CLASP member related to the *Drosophila* MAST/ORBIT homologues has been identified in the plant genome, though its presence is surprising given the lack of CLIP family members (Bisgrove et al 2004, Gardiner & Marc 2003). Studies using reverse genetics and fluorescent fusion protein localization have shown that this *Arabidopsis* CLASP is a MAP involved in cell division and expansion (Ambrose et al 2011, Ambrose et al 2007).

EB1

Another well-studied family of +TIPs are the end-binding (EB) proteins, distinguished by a highlight conserved N-terminal calponin homology (CH) domain responsible for microtubule binding. Homologues have been identified in many organisms, with the *Arabidopsis* genome containing three proteins (Chan et al 2003). EB proteins were shown

to localize preferentially to the distal ends of spindle and cytoplasmic MTs (Galjart & Perez 2003). As EB proteins can autonomously track MT ends without the aid of other binding partners, they are seen as 'core' components of the +TIP network (Akhmanova & Steinmetz 2010).

EB1 functions primarily as an 'anti-pause' factor, regulating microtubule dynamics and promoting interactions with attachment sites around the cell. The EB1 protein also has a proposed role in the recruitment of other cytoplasmic proteins/MAPs to form complexes at the MT plus ends. The adenomatous polyposis coli (APC) tumour suppressor protein has been supposed as the binding target for human EB1, and early studies have identified the plant homolog TANGLED1 as a putative binding partner of plant EB1 (Smith et al 2001) .

In plant cells, several groups have investigated the subcellular localization patterns of GFP-fused *Arabidopsis* EB1 proteins, showing that the protein colocalizes with microtubules and exhibits plus-end tracking ability (Chan et al 2003, Dixit et al 2006, Mathur et al 2003). *Arabidopsis* EB1 protein also labels microtubule minus ends at sites from which microtubules can grow and shrink. These minus-end nucleation sites are mobile, supporting the idea of a flexible centrosome in plants (Chan et al 2003).

SPR1

A plant-specific +TIP was identified by a mutational screen which showed plants with right-handed helical growth in roots and etiolated hypocotyls (Furutani et al 2000). Called SPR1 (SPIRAL1), GFP-fusions showed that the protein localizes to MTs in all four plant arrays and is highly expressed in tissues undergoing rapid cell elongation. (Nakajima et al 2004, Sedbrook et al 2004). Interestingly, SPR1:GFP was seen to track the growing plus ends of microtubules in a similar way to CLIP-170, indicating its role as a +TIP (Sedbrook et al 2004). The *Arabidopsis* genome contains five other SPR1 homologues which only show sequence similarity in the N- and C-terminal regions but have high variability in the intervening sequences (Nakajima et al 2004). As this *SPR1* gene encodes a small, novel 12kDa polypeptide, it is plausible that this plant-specific protein family evolved to regulate the unique plant MT arrays (Bisgrove et al 2004)

1.4.1.2. Minus end-binding proteins

In addition to the proteins known to track the highly dynamic MT plus ends, there are also proteins involved in capping and stabilizing the less dynamic minus end. One such protein with known minus end-specific properties is the nucleating factor γ-tubulin. A member of the tubulin family (along with α- and β-subunits), γ-tubulin is highly conserved across all eukaryotes. It is found in complexes with an array of associated proteins, known as γ-tubulin complex proteins (GCPs), with which it forms either a small complex (γ-TuSC) of two γ-tubulin molecules, or a large ring complex (γ-TuRC) containing tubulin molecules associate with several GCPs (Raynaud-Messina & Merdes 2007) (FIG 8).

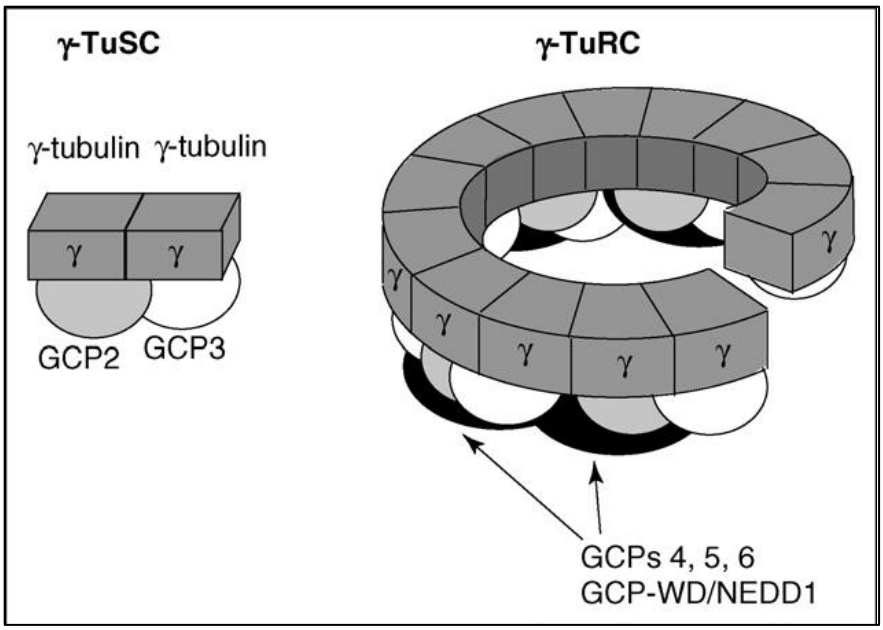

Figure 8: Schematic representation of the small complex (γ-TuSC), or the ring complex (γ-TuRC). The γ-TuSC consists of two γ-tubulin molecules associated with either GCP2 or 3. The ring or lock-shaped complex consists of several γ-tubulin molecules associated with GCPs 4, 5 and 6 (Raynaud-Messina & Merdes 2007).

Although, as described earlier, microtubules can quite easily nucleate *in vitro* providing the necessary conditions are met, γ-tubulin plays a key role in nucleation *in vivo*. Due to conflicting experimental evidence, different mechanisms for γ-tubulin-dependent microtubule nucleation have been proposed (Erickson 2000). The 'template model' suggests that γ-tubulin monomers associate laterally to form the ring complex upon which αβ-dimers form in a hollow tube. This model, however, does not explain MT nucleation from small complexes. The alternative 'protofilament model' posits that γ-tubulin

molecules longitudinally associate into short protofilaments, curved due to the conformational constraint of γ-tubulin monomers. αβ-subunits then associate with the terminal γ-tubulin molecules either laterally or longitudinally to form several protofilaments which close to form a tube. This model also serves to explain nucleation from γ-TuSCs and even monomeric γ-tubulin (Erickson 2000, Raynaud-Messina & Merdes 2007).

As well as serving vital roles in MT nucleation, studies have also linked γ-tubulin small complex proteins (γ-tubulin, GCP2 and 3) to mitosis and cell cycle progression. Cells lacking γ-TuSCs show aberrant spindle formation with monopolar arrays, and *Drosophila* embryos lacking γ-TuSCs are not viable (Raynaud-Messina & Merdes 2007, Yuba-Kubo et al 2005). The role of γ-TuRC proteins GCP4, 5 and 6, however, is considerably less clear. A recent study has shown that γ-TuRC GCPs may help to improve the fidelity of centrosome-dependent MT nucleation by γ-TuSCs (Verollet et al 2006). Other studies confirm that GCP4 and 5 are nonessential for normal MT nucleation, but *Drosophila* mutants are sterile (Vogt et al 2006). It is thought GCPs 4, 5 and 6 could function in higher eukaryotes to assemble the larger ring complexes required for the formation of specific MT arrays in differentiated cells (Oegema et al 1999). Interestingly, evidence pointing to γ-tubulin functioning as a pause and anti-catastrophe factor suggests a potential role in MT rescue events (Bouissou et al 2009).

As the role of γ-tubulin and its associated proteins in nucleation of MTs in animal and fungal cells is now well characterized, a similar function in plant cells has also been confirmed (Drykova et al 2003, Horio & Oakley 2003, Pastuglia et al 2006). Interestingly, though, the cellular localization of γ-tubulin in plant cells does not seem entirely congruous with a role in nucleation alone. In addition to its presence at established nucleation sites, such as on the nuclear surface, γ-tubulin was also highly enriched along MTs in all arrays and not restricted to MT minus ends (Liu et al 1994, Liu et al 1993, Panteris et al 2000). Mutational and RNAi knockdown studies on the two functionally redundant *Arabidopsis* γ-tubulin genes showed that γ-tubulin plays an essential role in the organization of all plant MT arrays through interphase and cell division (Binarova et al 2006, Pastuglia et al 2006). γ-tubulin depletion caused defects in spindle and phragmoplast formation as well as disruption to cortical MT organization.

1.4.1.3. Lattice-binding proteins

XMAP215

Although the dynamic behaviour of microtubules takes place at their tips, many proteins have been found which bind along the length of the microtubule and still influence MT dynamics. One particularly large and extensively studied family was first discovered in *Xenopus* as XMAP215. Initially identified from the purification of *Xenopus* extracts shown to stimulate the growth rate of microtubules *in vitro*, XMAP215 was characterized as a 215 kDa protein able to stimulate an eight-fold increase in MT growth rate (Gard & Kirschner 1987). Other studies with XMAP215 in *Xenopus* egg extracts alluded to its role as a stabilizing factor: immunodepletion of the protein dramatically increased catastrophe at the plus end, with a concurrent reduction in average microtubule length (Tournebize et al 2000). Interestingly, the addition of XMAP215 to depleted extracts restored the catastrophe frequency to that to control extracts, highlighting its influence on both catastrophe and growth in physiological conditions (Tournebize et al 2000).

The function of different domains in XMAP215 was elucidated by analysing the expression of GFP-tagged protein fragments; the N-terminal region was found in co-localize with MTs in egg extracts but not in cells, and the C-terminal region co-localized with MTs and centrosome in extracts and in cells. This suggested that the C-terminal region is responsible for microtubule binding (Popov et al 2000).

Genome sequencing has revealed homologues of this protein in a wide range of eukaryotic systems (Ohkura et al 2001). Proteins all share a conserved N-terminal repeating structure known as the TOG domain (Tumour Overexpressed Gene), named after the human XMAP215 homologue ch-TOG. These domains consist of approximately 200 amino acid residues and contain up to five HEAT motifs, responsible for protein-protein interactions. Except for fission yeast, it seems that all eukaryotic organisms contain only one member of this family.

The mechanism by which TOG domain proteins such as XMAP215 increase microtubule growth rate has been a contentious point. The traditional model suggested that XMAP215 acted as a tubulin ‘shuttle’ or ‘template’, bringing short oligomers of tubulin subunits to

the growing microtubule end (Gard & Kirschner 1987). This was supported by *in vitro* optical trapping experiments which showed that microtubules grew in distinct steps of 60nm, the approximate length of 7-8 tubulin dimers (Kerssemakers et al 2006).

This template model, however, is hard to reconcile with recent evidence showing that XMAP215 binds to tubulin molecules with a 1:1 stoichiometry. Furthermore, the flux of XMAP215 to the plus end is not fast enough to provide sufficient tubulin to account for the high MT growth rates. This, combined with the fact that XMAP215 actually depolymerises MTs in the absence of free tubulin, led to the development of a non-templating model which can account for these observations. It is argued that XMAP215 acts as a 'processive polymerase' which catalyses the addition of individual tubulin subunits as it moves with the growing MT (Brouhard et al 2008). In this way, XMAP215 would stabilize an intermediate step in the polymerization pathway, increasing the probability that the tubulin heterodimer is incorporated into the growing MT. Concurrently, as the free energy of this intermediate state would be less than both the unbound and bound states, this process would also operates in reverse, accelerating the exchange of tubulin dimers into and out of the lattice (Brouhard et al 2008). This model, therefore, provides a good explanation for both the polymerization and depolymerization properties of XMAP215.

The plant member of the MAP215 family was first identified in 2001 (Whittington et al 2001). Temperature-sensitive mutants in the *mor1* gene (microtubule organisation1) were seen to exhibit disorganised and shortened cortical microtubules at the restrictive temperature, a phenotype rescued by returning to the permissive temperature. This pointed to a similar role for MOR1 (or AtMAP215) in stabilizing and promoting the growth of cortical microtubules. A more severe *mor1* mutant was also identified, named *gemini pollen1*, which was lethal in homozygous plants and exhibited aberrant cytokinesis in haploid microspores (Twell et al 2002). Finally, a recent study with the temperature sensitive *mor1* mutant found that at the restrictive temperature all cell cycle arrays contained shorter microtubules compared to wild type (Kawamura et al 2006). Thus, the MOR1/GEM1 protein influences the dynamics of cortical, PPB, mitotic and phragmoplast microtubules. As its biochemical properties are similar to those of XMAP215 (Hamada et al 2004), it most likely acts with a similar 'processive' mechanism.

An interesting question raised by the study of TOR-domain protein function is, why do these proteins bind along the microtubule lattice if they only function at the tip? Although their function in MT polymerization and observations of plus tip tracking has led to their classification as +TIP proteins, evidence for XMAP215 binding to the microtubule lattice has been shown (Brouhard et al 2008). Once bound, they then laterally diffuse to the microtubule tip and thus increase the chance of protein-protein interactions. As mentioned earlier, the C-terminal regions of TOG proteins are thought to mediate microtubule lattice biding, containing positively charged serine, glycine and lysine residues capable of interacting with the negatively charged tubulin C-termini (Al-Bassam et al 2006). Additionally, XMAP215 binds to MTs with a very low affinity, allowing for high diffusion rates through repeated cycles of binding, release and re-binding (Widlund et al 2011). XMAP215 molecules would therefore localize to MT plus ends by recognising some additional features or via interaction with other +TIPS.

Katanin

Katanin, originally isolated from the eggs of the sea urchin *Strongylocentrotus purpuratus*, is a heterodimer consisting of a 60kDa microtubule-stimulated ATPase and a 80kDa (p80) subunit responsible for subcellular targeting and regulation of the microtubule-severing 60kda (p60) subunit (McNally & Vale 1993). In animal cells, katanin localizes to centrosomes where it cuts MTs from their anchored minus ends (McNally et al 1996)

Although first reported in animals, direct evidence for the severing action of katanin was uncovered in plants. The advantage of plant systems to their animal counterparts is that loss-of-function mutants are viable, and the action of katanin on interphase microtubules allows easy identification by light microscopy. In animal cells, however, the study of katanin is hindered by tightly bundled MT structures found in spindles, axons, dendrites and cilia (Roll-Mecak & McNally 2010).

The *Arabidopsis* genome encodes one p60 and four p80 subunit homologues, at least one of which associates with the catalytic subunit. Mutations to the katanin gene produce aberrant cortical microtubule orientation and cell expansion in root epidermal cells (Nakamura & Hashimoto 2009). Additionally, mutants display many cortical

microtubules which converge to common cortical sites, suggesting that katanin severs microtubules at their minus ends. In this way, katanin increases microtubule dynamics in the cytoplasm by facilitating microtubule treadmilling via the release of minus ends from their cortical attachment sites. In contrast, katanin overexpression causes cortical MT bundling followed by MT shortening (Stoppin-Mellet et al 2006). Therefore, katanin may also have a role in generating free cortical microtubules which are subsequently incorporated into bundles.

MAP65

The MAP65 proteins comprise the most abundant family of MAPs in plants. First discovered as three electrophoretically separable 65kDa proteins purified from tobacco BY-2 cells (Chang-Jie & Sonobe 1993), the MAP65 family has grown to encompass a range of proteins with different functions, with nine genes identified in *Arabidopsis* (Hussey et al 2002).

Initial biochemical studies of tobacco MAP65 demonstrated its ability to bind and bundle microtubules *in vitro* (Chang-Jie & Sonobe 1993). The development of antibodies against tobacco MAP65 led to the identification of three isotypes, MAP65-1a, -1b and -1c (Smertenko et al 2000). Interestingly, although the other two proteins were shown to bind universally to all MT arrays, NtMAP65-1a antibodies recognised only subsets of interphase microtubules and specifically highlighted the anaphase spindle and phragmoplast midzones (Smertenko et al 2000). Localization of the *Arabidopsis* MAP65-1 and MAP65-3 proteins also showed selective binding throughout the cell cycle and enrichment at the MT midzones, highlighting a general role of these MAPs in MT cross-bridge formation and stabilization (Muller et al 2004, Smertenko et al 2004).

The fact that both NtMAP65-1a and ATMAP65-1 are present at the cortical array and preprophase band, disappear during metaphase and subsequently reappear during anaphase and cytokinesis, suggests a process of stringent cell cycle control. It has been shown that although AtMAP65-1 is phosphorylated throughout the cell cycle, it is hyperphosphorylated by cyclin-dependent and mitogen-activated protein kinases (CDKs/MAPKs) during metaphase (Smertenko et al 2006). Furthermore, mutation of a putative CDK phosphorylation site restored its MT binding capacity, and led to

localization at the spindle midzone throughout spindle morphogenesis (Mao et al 2005). Combined with other mutagenesis studies, these data suggest that MAP65-1 is controlled throughout the cell cycle by its phosphorylation state, and that dephosphorylation is necessary for its appearance at anaphase and cytokinesis.

Although bacterially expressed recombinant AtMAP65-1 was shown to form 25nm cross-links between MTs *in vitro*, it did not show polymerization effects nor could it protect microtubules against cold-induced depolymerization (Smertenko et al 2004). It functions only when dimerised, with the C-terminal domains binding to adjacent MTs, and N-terminal regions contributing to dimer formation (Smertenko et al 2004). Similar biochemical studies on the tobacco subfamily NtMAP65-1b showed comparable bundling properties (Wicker-Planquart et al 2004). The bundling function of MAP65-1 has also been shown *in vivo* using GFP-protein fusions (Mao et al 2006), and recent studies have found that MAP65-1 and MAP65-2 play a critical role in the microtubule-dependent mechanism for stipulating axial cell growth in the expanding hypocotyl, independent of any mechanical role in microtubule array organization (Lucas et al 2011)

WAVE-DAMPENED

Another microtubule-bundling protein which binds along the MT lattice is WAVE-DAMPENED2 (WVD2). The *Arabidopsis* mutant was identified due to its distinct cell expansion defects including skewed root growth, thicker organs, short stature and dampened root waving on tilted agar surfaces (Yuen et al 2003). Analysis of these phenotypes revealed they were due to overexpression of the *WDV2* gene, which caused oblique orientation of cortical microtubules in elongating cells as opposed to transversely in the wild type (Yuen et al 2003).

The *WVD2* gene encodes a novel, plant-specific 23 kDa protein which contains a conserved domain shared with seven other *Arabidopsis* proteins (Yuen et al 2003). Furthermore, the C-terminus of these proteins shows limited sequence homology to that of the vertebrate MAP TPX2 (Targeting Protein for Xklp2), critical for mitotic spindle formation in *Xenopus* egg extracts (Wittmann et al 2000). WDV2 appears to localize to cortical microtubules, and analysis of the WDV2 protein *in vitro* demonstrated its ability to bind and bundle microtubules, consistent with observations in the *wdv2* mutants (Perrin

et al 2007). In this way, WDV2 appears to regulate cell expansion via its association with and organization of cortical microtubules.

MAP70

MAP70 is a recently discovered plant-specific MAP isolated biochemically in an attempt to identify MAPS not found by bioinformatics searches (Korolev et al 2005). The *Arabidopsis* gene AtMAP70-1 encodes a 70 kDa protein and forms part of a highly conserved five-member gene family. Studies using GFP-tagged protein *in vivo* showed continuous co-localization with all four microtubule arrays in both transiently and stably expressed plant suspension cultures, but did not label the phragmoplast midzone (Korolev et al 2005). GFP-fusions to variously truncated portions of the protein implicated a conserved central-coiled-coil domain along with part of a non-regular secondary structure region (NORS) in microtubule binding. Interestingly, MAP70-5 and its binding partner MAP70-1 have been identified as essential for secondary wall patterning in *Arabidopsis* wood cells (Pesquet et al 2010), highlighting the importance of the MAP70 family in vascularisation and cell wall deposition.

MAP18

MAP18 is another recently characterised pant-specific MAP purported to play a role in directional cell growth and cortical microtubule organization (Wang et al 2007). *In vitro* studies with the 18 kDa recombinant protein confirmed its MT-biding capability, and immunolocalization showed it focussed to dot-like regions along cortical microtubules. The fact that MAP18 inhibited MT polymerization in biochemical experiments, and overexpression in *Arabidopsis* caused cortical MT disruption and increased sensitivity to MT destabilizing drugs, all point to a role for MAP18 as a microtubule-destabilizing factor in *Arabidopsis* (Wang et al 2007).

1.4.2. Kinesins

1.4.2.1. Structure

Kinesins constitute a superfamily of microtubule motor proteins found ubiquitously in eukaryotic organisms. They are involved in a variety of cellular processes, such as organelle or vesicle transport, spindle formation, chromosome segregation and microtubule dynamics.

The first kinesin protein was identified based on its motility in the cytoplasm of giant axons from squid (Brady et al 1982, Vale et al 1985). Now known as kinesin-1, it consisted of two heavy chains with proposed motor activity linked to two light chains which mediated binding of the motor to its relevant cargo (FIG 9). For several years kinesin-1 was the only protein known to move along microtubules towards their plus ends, opposite to the previously discovered and better characterised dyneins. It was not until the gene sequence encoding a *Drosophila melanogaster* kinesin heavy chain (KHC) was made public that many other kinesin-related proteins were identified by sequence homology. Since then, a large number of kinesin proteins have been identified and divided into 14 separate groups, though many still remain unassigned (Endow et al 2010).

Although a startling amount of variation exists between proteins of different groups, all kinesins are characterized by a highly conserved motor domain. The force-producing KHCs contain the motor ‘head’ domain, which confers ATPase activity, a coiled-coil ‘stalk’ region and ‘tail’ which binds the kinesin light chains. The position of the head domain varies between groups: it is at the N-terminus of kinesin-1, the C-terminus of kinesin-14 and centrally located in kinesin-13 (Kim & Endow 2000).

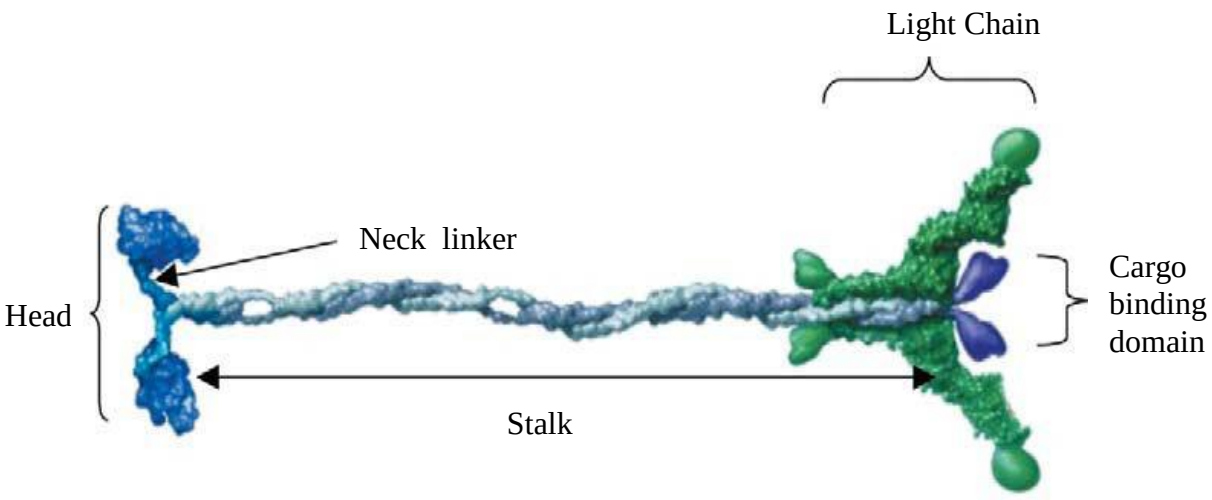

Figure 9: Structure of the homodimeric motor protein kinesin-1. The head domains bind ATP and microtubules, with an 8nm distance between them allowing processive movement along MTs in a step-by-step mechanism. The neck linker region confers directionality. The neck is connected to a 70nm coiled-coil stalk region which holds the two heads together. At the end of each stalk is situated the cargo binding domains (Yildiz & Selvin 2005).

The stalk region generally mediates protein dimerization, although there is variation in its exact role. In kinesin-1, for example, the stalk contains a flexible hinge region allowing the tail to fold back and inhibit motor domain binding to microtubules (Hackney & Stock 2000). It also has a role in coordinating the two head regions, allowing for processive movement of kinesin-1 along microtubules. The stalk region can mediate association of kinesins with other non-motor proteins: the budding yeast kinesin-14 Kar3, for example, can bind with itself or two other non-motor proteins, causing a conformational change which increases the motor speed (Barrett et al 2000, Manning et al 1999).

Between the head and stalk regions lies the flexible neck linker, a mechanical element which changes its conformation depending on the bound nucleotide state. By docking onto the motor core in the ATP-bound state and undocking after ATP hydrolysis, it is proposed that this neck region creates the power stroke necessary for motor motility (Rice et al 1999). This region has also been shown to confer directionality, as mutations in conserved neck residues which interact with the head region produce bidirectional motors (Endow & Higuchi 2000).

Although these structural features play an important role in regulating kinesin activity, the pivotal characteristic of kinesin proteins, their ability to hydrolyse ATP, is a function of the conserved catalytic core. The core domain consists of an eight-stranded β-sheet with three α-helices on each side. It contains very highly conserved switch I and II motifs whose conformations change during the ATP hydrolysis cycle, a mechanism very similar to their G-protein counterparts (Rice et al 1999, Yun et al 2001).

Kinesin-1 is a processive motor protein which can make over one hundred steps each time it binds to a microtubule. Each 8nm step, the distance between adjacent tubulin dimers along a microtubule protofilament, is tightly coupled to ATP hydrolysis: For every ATP molecule hydrolysed one step is taken which generates roughly 6-8 pN of force (Schnitzer & Block 1997). Processive motors such as kinesin-1 move along microtubules towards the microtubule plus ends using alternate heads with a 'hand-over-hand' mechanism (Kaseda et al 2003), whereas other motors, such as kinesin-14, detach from the microtubule immediately after hydrolysing a single ATP molecule (Endow & Higuchi 2000).

1.4.2.2. Cellular Function

Kinesin motor proteins play important roles in a diverse range of cellular processes. The classical kinesin-1 is essential for the transportation of vesicles and organelles to specific regions of the cytoplasm, known to bind cargoes associated with the mitochondria, endoplasmic reticulum, Golgi complex, endosomes and vesicles of the presynaptic axons in synaptic transmission, for example (Endow et al 2010). As well as vesicles/organelles, kinesin-1 also binds lysosomes, receptor and adaptor proteins, and signal-pathway-interacting proteins, highlighting its diverse range of cargos and role in spatially regulating signal transduction (Verhey & Rapoport 2001). The heterotrimeric kinesin-2 motor also has a transport function, involved in the intraflagellar transport required for the formation and maintenance of mammalian flagella and cilia (Rosenbaum & Witman 2002).

Kinesin family members function crucially in cell division, involved in forming the bipolar structure of the mitotic spindle, transport of chromosomes towards the equator of the spindle, chromosome segregation and poleward transport of chromosomes after

segregation (Yildiz & Selvin 2005). To carry out these functions, kinesin motors utilize several mechanisms (Sharp et al 2000). Microtubule sliding occurs when motors diffuse along a microtubule whilst remaining attached to another microtubule, a mechanism used by the *Drosophila* kinesin-14, Ncd, to bundle and slide microtubules in the formation of spindle poles (Skold et al 2005). Kinesins can also transport chromosomes along spindles directly, with kinesin-4 chromokinesin serving to segregate chromosomes towards opposite poles (Wang & Adler 1995). Finally, kinesin proteins allow chromosome transport by coupling kinetochore motility to spindle microtubule dynamics. It is thought that kinesin-7 could use its minus-end directed motility to transport kinetochores towards MT plus ends in metaphase, and subsequently anchor them to shortening MTs during anaphase (Lombillo et al 1995).

1.4.3. Catastrophic Kinesins

The kinesin super-family of proteins are molecular motors which utilize the energy derived from ATP hydrolysis to produce force. Traditionally, all of these mechanochemical enzymes were thought to translocate along the microtubule lattice in a uni-directional manner, "walking" along microtubules via a conformational change induced by ATP hydrolysis. However, the discovery that several kinesin family members exclusively depolymerize microtubules from both ends has challenged this idea.

Although there are three kinesin families known to exhibit depolymerizing activity (kinesin-8, kinesin-14 and kinesin-13), it is the kinesin-13s which are best characterized. Screens for motors involved in spindle function in *Xenopus* eggs led to the discovery of XKCM1 (*Xenopus* Kinesin Central Motor 1) (Walczak et al 1996), and early depletion/overexpression experiments highlighted the importance of these motors as catastrophe factors. This, coupled with a comprehensive collection of *in vitro* assays characterising the microtubule-depolymerizing function of XKCM1, provided compelling evidence for this new class of kinesin motor proteins (Desai et al 1999). The mammalian homolog of XKCM1, MCAK (Mitotic Centromere-Associated Kinesin), is one of the four kinesin-13 proteins found in mammals and is generally used as the prototypical subject for functional experiments.

Kinesin-13 proteins are homodimeric factors with a distinctive structure: their kinesin motor domain, containing the ATP- and microtubule-binding sites, is situated in the middle of the protein sequence. The kinesin-13 motor core shares a high sequence similarity to all kinesins, with many highly conserved regions such as the nucleotide-biding motif. Immediately N-terminal of the motor core lies a kinesin-13 class-specific region of 60 amino acids known as the neck region, and N-terminal to this is a 25-30 kDa domain involved in subcellular targeting and localization (Walczak et al 2002, Wordeman et al 1999). The C-terminus contains variable coiled-coil regions and is proposed to act with the N-terminus in dimerization (Maney et al 2001) (FIG 10).

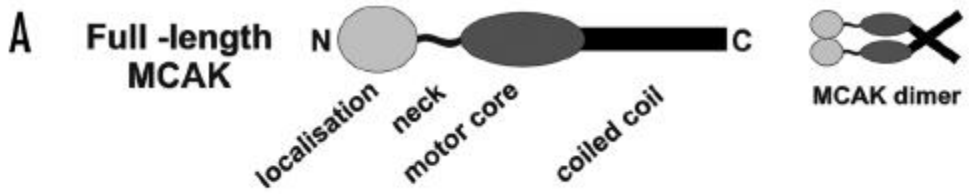

Figure 10: Schematic of the kinesin-13 protein structure. As shown, both the N- and C-terminal domains contribute to dimerization (Moores et al 2006)

1.4.3.1. Depolymerization mechanism

The depolymerizing activity of kinesin-13 essentially centres around the production of the bent, unstable conformation of tubulin at the microtubule ends (Desai et al 1999). In theory this could be achieved in two ways: either by selective stabilization of the bent tubulin conformation or by active catalysis of a straight-to-bend transition (Moores & Milligan 2006). The fact that kinesin-13 motors are able to depolymerize stabilized microtubule substrates provides compelling evidence that they actively deconstruct microtubules rather than waiting for exposed unstable tubulin dimers to act upon (Desai et al 1999).

Assays using the non-hydrolysable ATP analogue AMPPNP highlighted the key step in this depolymerization mechanism, as unpeeling of stabilized microtubules only occurred in the presence of this ATP (Desai et al 1999, Moores et al 2002). This provided the basis for a putative model of kinesin-13 motor action (FIG 11) (Moores et al 2002). In the first step, the kinesin-13 motor protein acts like a classical kinesin, binding a microtubule whilst exhibiting microtubule-induced ADP release. Next, binding of ATP causes a conformational change to the kinesin and its underlying tubulin dimer, causing the dimer

to bend outwards from the microtubule wall (FIG11-2). The hydrolysis and release of ATP facilitates detachment of the kinesin-13-tubulin complex from the protofilaments (FIG11-3), followed by release of the kinesin-13 molecule ready for another round of depolymerization (FIG11-4). Therefore, whereas conventional kinesins utilize the energy of ATP to generate a "power stroke", kinesin-13 uses it to bend microtubule protofilaments (Moores et al 2002).

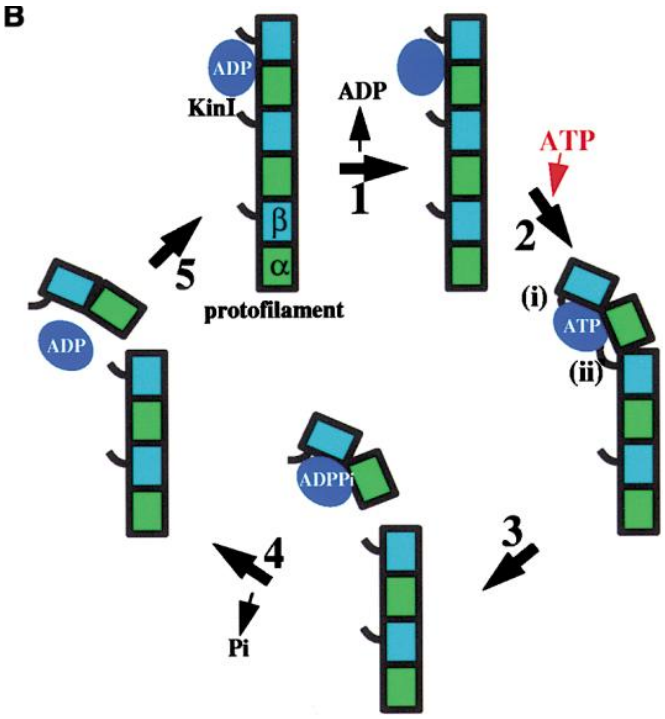

Figure 11: Model for the microtubule depolymerisation activity of kinesin-13 motors. Kinesin-13 binds to a microtubule, releasing ADP (1). When ATP binds a conformational change in the tubulin dimer is produced (2), and ATP hydrolysis leads to detachment of the tubulin-kinesin-13 complex from the microtubule protofilament (3). Subsequent separation of this complex released the kinesin-13 molecule ready for another round of depolymerization (Moores et al 2002).

Although the kinesin-13 motor core is built around the highly conserved eight-stranded β-sheet structure, the presence of several unique structures, particularly in loop two and α-helix four, may help to explain its function. Interestingly, positioning of a key energy-transducing element, the α4 helix, directly over the tubulin intra-dimer interface suggests its direct role in depolymerization. Despite this, mutational studies of kinesin-13-specfic residues in or around this helix only weaken the motor-MT interaction. However, mutations elsewhere in the motor core do not reduce MT binding but do disrupt the ATP-dependent bending of tubulin during the depolymerization cycle. Therefore, it is most

likely the cooperative effect of several kinesin-13-specific residues within the motor core which contribute to its depolymerization activity (Moores & Milligan 2006).

Although the MT depolymerization properties of kinesin-13 proteins are defined by the motor core, *in vitro* studies show that it functions poorly in comparison to full-length proteins (Hertzer et al 2006, Ovechkina et al 2002). The fact that monomeric neck+motor constructs show activity almost identical to that of full-length constructs highlights the role of this neck region in depolymerization (Hertzer et al 2006, Ovechkina et al 2002). However, the neck region alone does not exhibit depolymerization activity (Maney et al 1998), nor does it confer activity when expressed with a classical motile kinesin motor region (Maney et al 2001).

Structural analysis of neck+motor constructs have supported the hypothesis that the neck region provides additional MT attachment for the motor, via an abundance of positively charged residues, as it carries out its power stroke (Moores et al 2006, Ovechkina et al 2002). Removal of these positively charged residues either by deletion or alanine substitution drastically reduced the depolymerization activity of MCAK. Furthermore, replacement of this non-functional neck region with the K-loop of KIF1A, containing 6 positively charged residues, rescued the neckless mutants (Ovechkina et al 2002). Taken together, this shows that overall charge is an important functional property of the neck region, suggesting a role in assisting depolymerization by electrostatic tethering to microtubules. A more recent study suggests that the neck domain plays a role in blocking other proteins from binding to the same protofilament, thus increasing depolymerization efficiency (Mulder et al 2009).

Kinesin-13 proteins bind to the MT lattice and move rapidly along its surface to the plus or minus ends by diffusion (Helenius et al 2006). As described earlier for other lattice-binding MAPs, 1D diffusion is more efficient than 3D diffusion in allowing motors to quickly reach MT ends, but this diffusion is bi-directional and does not favour either pole.

1.4.3.2. Cellular Function and Localization

Functional analysis of these proteins is difficult as activity of MCAK seems to be closely linked to the ratio of tubulin dimers to polymer. In general terms, Kinesin-13 proteins depolymerize microtubules and regulate their dynamics, especially during cell division. MCAK localizes to kinetochores, spindle poles and microtubule plus ends where it has a role in chromosome dynamics, poleward microtubule flux and correct spindle positioning during mitosis (Wordeman 2010) (FIG 12 & 13).

During cell division the MT cytoskeleton undergoes several dramatic rearrangements. The initial stage involves the disintegration of interphase arrays and subsequent formation of mitotic spindle from polarized centrosomes. Although it is well established that kinesin-13 motors play a key role in spindle formation and dynamics, it has been hard to pick out conserved functions between systems.

One of the most well-established roles of kinesin-13 motors is in the initiation of spindle bi-polarity, as depletion of kinesin-13 in a range of organisms results in a high percentage of monopolar spindles or extremely dense bipolar spindles (Walczak et al 1996). Furthermore, the role of kinesin-13 motors in the ensuring the proper regulation of spindle dynamics is clear, as inhibition in almost all model system produces perturbation in microtubule polymer levels (Ems-McClung & Walczak 2010). Interestingly, though the subclasses of microtubule affected seem to be dependent on the cell type and kinesin-13 studied (Ems-McClung & Walczak 2010).

At the other end of mitotic spindles, kinesin-13 motors have also been localized at the kinetochore and have been ascribed several roles. Several studies support the role of MCAK in regulating kinetochore-microtubule attachments, though it is not known whether their role extends to the correction of prevention of aberrant connections.

Since their function as MT depolymerizers has been so well characterized, it has long been proposed that kinesin-13 motors play a role in the kinetochore-mediated MT depolymerization which leads to chromosome segregation in anaphase. Indeed, initial findings that inhibition of centromeric kinesin-13 led to anaphase defects supported this

idea (Maney et al 1998). However, the fact that the rates of chromosome segregations remained normal suggested that these defects were more likely due to attachment defects in late metaphase (Kline-Smith et al 2004). Despite this work in vertebrates, studies in insect systems showed clearly that insect kinesin-13s account for most of the chromosome movement in anaphase (Rogers et al 2004), highlighting the functional difference between species.

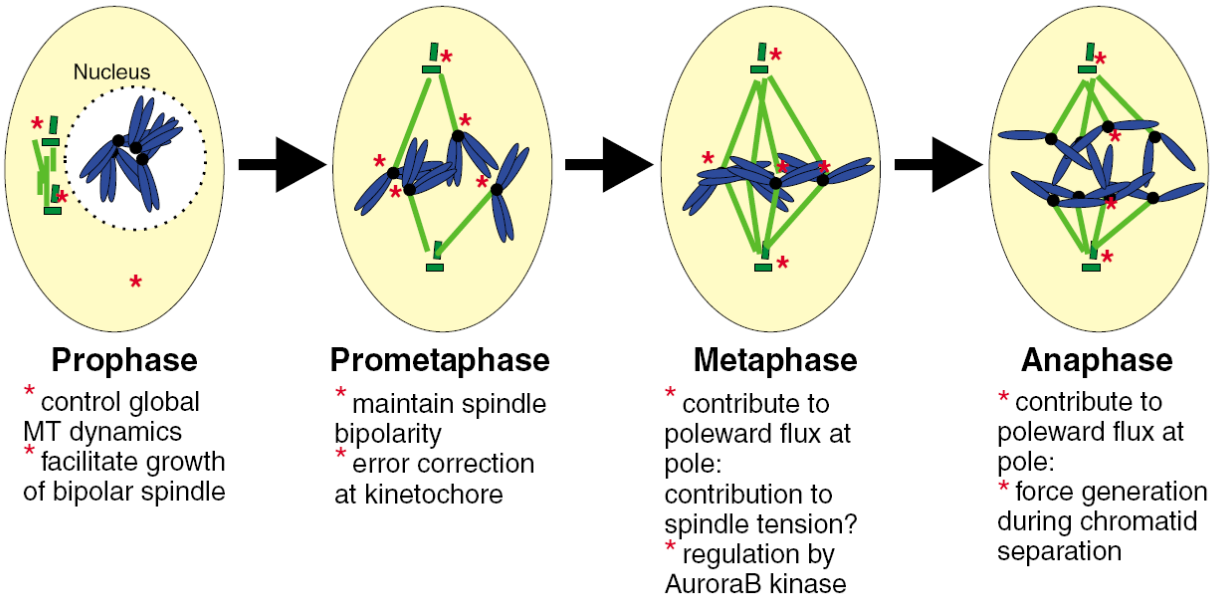

Figure 12: schematic of kinesin-13 protein function at different stages of mitosis. Blue: chromosomes, Black: kinetochores, Green: spindle MTs, Dark Green: centrioles, Red Asterisk: kinesin-13 (Moores & Milligan 2006)

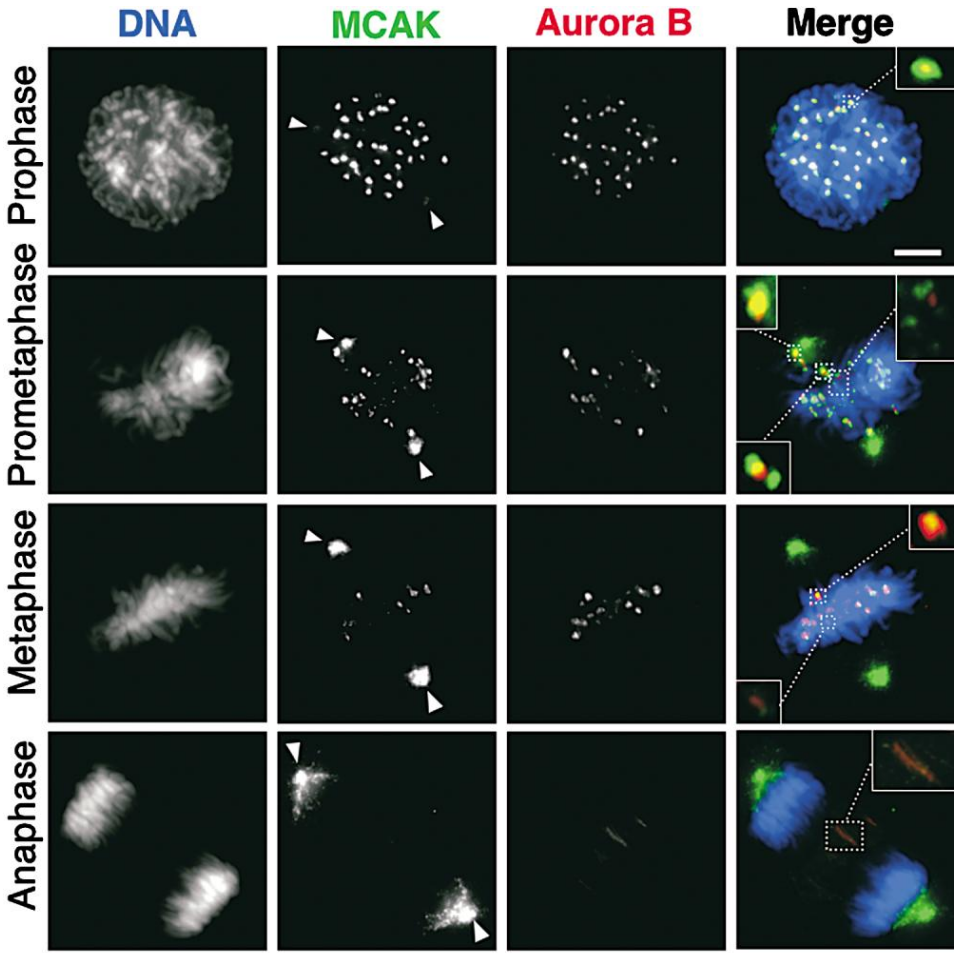

Figure 13: Localization of MCAK during mitosis. Aurora B is a regularity kinesin which colocalizes with MCAK (Adapted from Lan et al 2004).

1.5. Kinesin-13 in Plants

In the model plant system *Arabidopsis thaliana*, genes encoding at least 61 kinesin-like proteins have been identified (Reddy & Day 2001), the largest number of kinesins among all eukaryotic systems sequenced. Of this 61, only two *Arabidopsis* genes were found to group with the MCAK family of kinesin-13 proteins (FIG 14). AtKinesin-13A is the larger of the two proteins, consisting of 794 amino acids, whereas AtKinesin-13B is slightly smaller at 684 amino acids.

As these kinesins have only been recently identified, little is known about their structure and cellular function. A study by Lu *et al* in 2005 analysed the kinesin encoded by the At3g16630 gene, described as AtKinesin-13A. Identified as a protein encoded by 794 amino acids and a predicted molecular mass of 89 kDa, they showed that sequence similarity with MCAK and other kinesin-13 motors was limited only to the motor core

(Lu et al 2005). Lu *et al* used immunofluorescence and electron microscopy to localize AtKinesin-13A with the Golgi apparatus and demonstrated its role in plant trichome morphogenesis. In this way, they proposed that microtubules, kinesins and the Golgi apparatus work together to regulate plant cell morphogenesis in flowering plants.

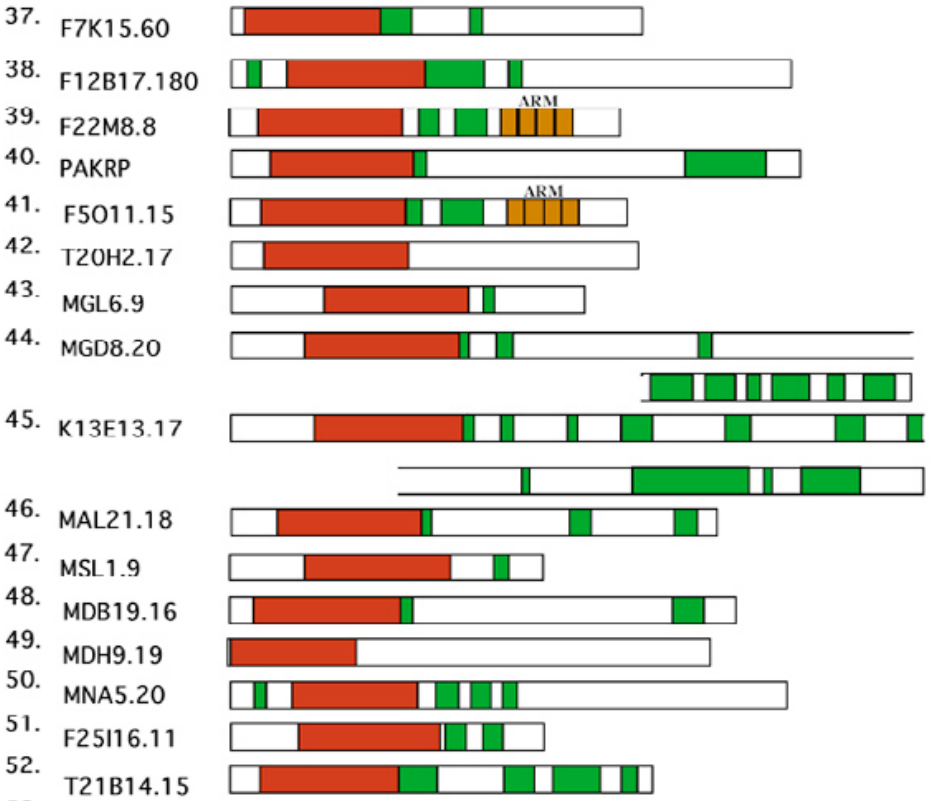

Figure 14: Section of a schematic diagram of all *Arabidopsis* kinesins. The motor domains are marked in red and the coiled coil domains in green. ARM are armadillo/β-catenin-like repeats. The two kinesin-13 proteins are numbers 43 (MGL6.9) and 47 (MSL1.9), both exhibiting internal motor domains. The larger MSL1.9 is termed AtKinesin-13A, and the smaller MGl6.9, AtKinesin-13B (Adapted from Reddy & Day 2001)

Importantly, though, the apparent lack of a "neck" region in the kinesin-13A protein was used to confirm their finding that it does not have the depolymerase activity normally associated with kinesin-13 motors. Detailed study into the neck region of MCAK mentioned above (Ovechkina et al 2002), however, showed that the charge of the neck region was more important than its length. Furthermore, the depolymerization activity seemed to be directly proportional to the number of positively charged residues in the neck region. Interestingly, sequence comparison between the two *Arabidopsis* kinesins and MCAK reveals that some positive residues in the neck region of AtKinesin-13A are conserved with MCAK. Furthermore, other positive residues can be identified in this

region, although not conserved in the MCAK sequence. Using the evidence mentioned above, it is likely that AtKinesin-13A could have some depolymerizing activity, albeit significantly less than the MCAK due to a much lower number of positively charged residues.

Another limitation of this study is the fact that the other kinesin-13 protein was completely ignored. As the antibody used to detect the AtKin13A protein in biochemical and immunofluorescence studies was raised against quite a large portion of the protein with significant similarity between both *Arabidopsis* proteins, the C-terminal 271 amino acids, it is highly likely that the antibody would be cross-reactive. Indeed, close examination of their immunoblot shows the presence of at least one smaller band which could be the smaller protein. It is difficult, therefore, to attribute the conclusions of this study to a particular kinesin-13 protein.

A more recent study conducted in our lab sought to analyse the individual properties of these two proteins. Antibodies were raised against specific regions of the two proteins from areas between the motor and C-terminal domains showing very little sequence similarity (Hawkins, personal communication). Analysis of protein localization using immunofluorescence showed that AtKinesin-13A (then called CMK-2) localized predominately to the preprophase band and mitotic spindle, consistent with that of its depolymerizing homologues in other organisms. AtKinesin-13B, however, was not found on mitotic spindle but was instead localized to discrete Golgi-like structures within the cytoplasm. Furthermore, cells and leaf tissue infiltrated with AtKinesin-13A showed shortened, fragmented microtubules, pointing to a function of this protein in microtubule depolymerization.

A fresh insight was shed onto these plant kinesins when a recent study suggested a role for Atkinesin-13A in regulating microtubule dynamics via is interaction with the ROP effector RIP3 (Mucha et al 2010). Importantly, they found that cells expressing RIP3 and AtKinesin-13A fusions would sometimes show fragmented microtubules.

1.6. Research Plan

This data, combined with other work from the Hussey lab (Hawkins, personal communication) suggests that at least one of the plant kinesin-13 proteins may actually function as a microtubule depolymerizer. In light of this recent work, this project aims to investigate in more detail the functions of AtKinesin-13A/B and their effect on microtubule dynamics.

The first aim is to analyse the function of both proteins *in vitro* using biochemical studies. Proteins will be expressed in both bacterial and insect cells before undergoing co-sedimentation and turbidimetric assays to assess their activity and microtubule-interacting properties.

The second aim of this project is to investigate the *in vivo* effects of these proteins on microtubule dynamics throughout the cell cycle. Tobacco BY-2 cell lines will be generated which express bothAtKinesin-13A and 13B, as well as a human HsKinesin-13 for comparison, under the expression of an estradiol-inducible promoter. This inducible system will allow transient expression of recombinant protein and allow me to analyse the effect of expression on cell growth, nuclear morphology and microtubule dynamics by immunofluorescence microscopy.

2. MATERIALS AND METHODS

2.1 MATERIALS

2.1.1 Plant Material

Arabidopsis thaliana of the Columbia (Col-O) ecotype were grown from LEHLE seeds.

2.1.2 *E. coli* strains

Table 1: bacterial strains used in protocols

Strain	Genotype	Application
DH5α		All gateway cloning
XL-1 Blue		Glycerol stocks
BL21 DE3 Rosetta 2^{TM}		Protein expression

2.1.3 *Agrobacterium* strains

Table 2: agrobacterium strains used in protocol

Strain	Resistance	Application
LBA4404	Rif & Strep	Transformation of BY-2 cells
GV3101	Rif & Gent	Transformation of BY-2 cells
C58C3	Nal & Strep	Floral dipping of *A. thaliana*

2.1.4 Vectors and Constructs

Table 3: vector details used for cloning

Vector name	Application	Size (bp)	Resistance Cassette	Source
pDONR207	Gateway Donor Vector	5585	Gentamicin (bacteria)	Invitrogen
pGAT4	Bacterial protein expression with N-terminal 6×His Tag.	5256	Ampicillin (bacteria)	
pMDC7	Gateway Destination vector for estrogen-inducible ectopic gene expression		Spectinomycin (bacteria) Hygromycin (plants)	
PIEx-7	Insect cell expression vector with N-terminal 6×His Tag.	3723	Ampicillin	Merck

2.2 METHODS

Molecular Biology

2.2.1 Transformations

2.2.1.1 Preparation of chemically competent cells

***E.coli* strains**

Glycerol stocks were streaked out onto LB agar plates (5g/l yeast extract, 10g/l tryptone, 5g/l NaCl, 20g/l Agar, pH 7.0) and grown overnight at 37^{o}C for14-16 hours. A single colony was used to inoculate 100ml SOB medium (2% tryptone (w/v), 0.5 % yeast extract

(w/v), 0.05% NaCl (w/v), 2.5mM KCl and 10mM $MgCl_2$, pH 7.0) in a 1L flask and incubated at room temperature (25^oC) until the OD_{600}= 0.4-0.6. The culture was then put on ice for 10 minutes and the cells pelleted by centrifugation at 2500 × g for 5 minutes at 4^oC. The supernatant was discarded and the pellet resuspended in 32ml of ice-cold TB buffer (10mM PIPES pH 6.7, 15mM $CaCl_2.2H_20$, 250mM KCl and 55mM $MnCl_2.4H_20$ to pH 6.7 using KOH), before another 10 minute incubation on ice. The cells were centrifuged again at 2500 × g for 5 minutes at 4^oC and the pellet resuspended in 8ml of ice-cold TB buffer. DMSO was added to a final concentration of 0.7% (v/v) before a final incubation on ice for 10 minutes. Cells were then separated into 400μm aliquots, frozen in liquid nitrogen and stored at -80^oC.

Agrobacterium strains

Agrobacterium tumefaciens strains were grown on YEB agar plates (5g/l beef extract, 1g/l yeast extract, 5g/l peptone, 5g/l sucrose, 0.5g/l $MgSO_4.7H_20$ and 20g/l agar at pH 7.2) supplemented with the relevant antibiotics (C58C3: 25mg/ml Nalidixic Acid, 100mg/ml streptomycin, GV3101: 25mg/ml Gentamicin, 25mg/ml rifampicin, LBA4404: 25mg/ml Rifampicin, 100mg/ml Streptomycin) for approximately 2 days at 30^oC. Individual colonies were then used to inoculate 5ml of YEB supplemented with appropriate antibiotics and incubated overnight at 30^oC. The overnight culture was then used to inoculate 500ml of YEB (with antibiotics) and grown at 30^oC for approximately 4-5 hours until the OD_{600}= 0.5-0.6. The culture was then chilled on ice and pelleted by centrifugation at 3000 × g for 5 minutes at 4^oC. The supernatant was discarded and the pellet gently resuspended in 50ml of ice-cold 0.15M NaCl, before being incubated for 15 minutes on ice. The cells were centrifuged again at 3000 × g for 5 minutes at 4^oC and the supernatant again discarded. The cells were resuspended in 5ml of ice-cold 20mM $CaCl_2$, separated into 100-200μl aliquots and quick-frozen in liquid nitrogen for storage at -80^oC.

2.2.1.2 Transformation of chemically competent cells using the Heat Shock method

E.coli strains

A 200µl aliquot of chemically competent *E.coli* cells was thawed on ice to which 1-20µl of plasmid DNA was added. The cells were incubated on ice for 30 minutes before being "heat-shocked" at 42^{o}C for 30 seconds and then placed back on ice for a further 2 minutes. 800µl of SOC medium (SOB medium, 20mM (0.36% (v/v) glucose) was added and the cells were left to recover at 37^{o}C for 1 hour with shaking. Cells were then spread onto suitably selective LB agar plates and incubated at 37^{o}C for 14-16 hours.

Agrobacterium strains

Approximately 1-2µg of plasmid DNA was added to thawed 200µl aliquots of chemically competent *Agrobacterium* cells on ice. Cells were immediately quick-frozen in liquid nitrogen and then incubated in a water bath at 37^{o}C for 5 minutes. 400µl of YEB medium was added to the cells, which were then left to recover at 30^{o}C for 2-4 hours. Cells were plated onto suitably selective YEB agar plates and grown for 48-72 hours at 30^{o}C.

2.2.2 Plasmid DNA purification

Plasmid DNA was purified using the Wizard Plus SV Miniprep DNA Purification System (Promega). DNA was eluted into 100µl of nuclease-free water and stored at -20^{o}C.

2.2.3 Restriction Digests

Digests were carried out in a total reaction mixture of 20µl containing 5µl of purified plasmid DNA, 10µl of 10x Reaction buffer, 3µl of sterile distilled water and 2µl of the relevant restriction enzyme. Reaction mixtures were incubated at their optimum temperature for 2 hours.

2.2.4 Agarose Gel Analysis

Agarose Gels were used to resolve PCR and restriction digest products. Gels were prepared by dissolving 1% (w/v) Agarose Low EEO (Melford) in 0.5× TAE buffer (0.04M Tris acetate, 1mM EDTA) by microwaving. Once the liquid had cooled, 5µl of Ethidium Bromide was added per 200ml of buffer and poured into trays with variously sized well combs. The gels, once set, were transferred to an electrophoresis tank and submerged in 1× TAE buffer. Samples were prepared by mixing with 5× DNA loading buffer (Bioline) and then loaded into wells alongside the Bioline Hyperladder I marker. 1% gels were run for 20-30 minutes at 100V and visualized by UV illumination using a BioRad Gel-Doc 1000 system.

2.2.5 Amplification of fragments using PCR

The Polymerase Chain Reaction was used to produce DNA fragments for cloning. For high fidelity reactions the Phusion (Finnzyme) DNA polymerase was used.

A typical Phusion PCR reaction mixture contained:

Component	**Volume (µl)**
sdH_20	34
5× GC Buffer	10
Forward Primer (10pmol/µl)	0.5
Reverse Primer (10pmol/µl)	0.5
10mM dNTPs	1
$MgCl_2$	1
DMSO	1.5
Template DNA	1
Phusion DNA polymerase	0.5

The thermocycler programme was typically composed of the following steps:

Stage 1	98^{o}C	30s	
Stage 2	98^{o}C	10s	
	68^{o}C	20s	30 cycles
	72^{o}C	30s	
Stage 3	72^{o}C	7min	

For reactions where a high fidelity was not important, for example when amplifying sequences for genotyping purposes, the non-proofreading BioTaq Red (Bioline) DNA polymerase was used. Again, a typical Taq mixture contained the following:

Component	**Volume (μl)**
sdH_20	34.5
10× NH_4 Reaction Buffer	10
Forward Primer (10pmol/μl)	0.5
Reverse Primer (10pmol/μl)	0.5
10mM dNTPs	1
$MgCl_2$	2.5
Template DNA	0.5
Phusion DNA polymerase	0.5

The PCR programme comprised of the same stages as above except the annealing temperature was set at 63^{o}C.

In both cases, the annealing temperature was always first set at 5^{o}C below that of the melting temperature of each timer, and then further optimized if initial reactions did not produce positive results.

2.2.6 The GATEWAY™ Cloning System

The GATEWAY system involves cloned DNA sequences being transferred between vectors using site-specific recombination, enabling the transfer of specific DNA sequences of interest into multiple vectors whilst maintaining the same reading frame and orientation. Rather than a series of restriction and ligation reaction reactions, this system involves two recombination steps: the BP reaction involving recombination between an attB-flanked PCR product and a Donor vector to form an entry clone, and the LR reaction which involves recombination between the entry clone and a destination vector to produce an expression clone.

2.2.6.1 BP Reaction

The BP reaction was used to insert Gateway PCR products into the donor vector pDONR207 involving the BP CLonase II Enzyme Mix (Invitrogen). Typical 10µl reactions were set up as follows:

Component	Volume (µl)
PCR product	0.5
pDONR207 vector	3
TE Buffer	4.5
BP Clonase II	2

After addition of BP Clonase the mixture was briefly vortexed and then incubated for 1 hour at 25^{o}C. 1µl of Proteinase K solution (Invitrogen) was added to terminate the reaction and the solution was incubated for a further 10 minutes at 37^{o}C.

Approximately 3µl of the BP reaction mixture was used to transform 150µl of competent DH5α cells (as described in 2.2.1) and the transformed cells were spread onto LB agar plates containing 25µg/ml Gentamicin. Plasmid DNA was purified from positive bacterial colonies and subsequently digested to confirm the presence of the correct insert (as in 2.2.3). Correct insertion into the desired region was also checked with sequencing using gene-specific primers (see appendix)

2.2.6.2 LR Reaction

This reaction involves recombining the fragment of interest out of the entry clone and into the appropriate destination vector. In this case the destination vector used was pMDC7, an estrogen-inducible vector derived from PER8. A typical 10µl reaction mixture was as follows

Component	Volume (µl)
Entry clone	0.3
pMDC7 vector	1
TE Buffer	6.7
LR Clonase II	2

After addition of LR Clonase II the mixture was gently vortexed and then incubated for 1 hour at 25^{o}C. The reaction was quenched with addition of 1µl Proteinase K solution and incubated for 10 minutes at 37^{o}C.

As with the BP reaction, the recombinant destination vector was transformed into DH5α cells and spread onto LB agar plates containing 100µg/ml Spectinomycin. The plasmid DNA was purified and the presence of correct insert checked as described above.

2.2.7 DNA Sequencing

Sequencing was carried out by the Durham University DNA Sequencing Service, using an Applied Biosystems 3730 DNA Analyzer.

Biochemistry

2.2.8 SDS-PAGE (Polyacrylamide Gel Electrophoresis) Analysis

Gel plates were thoroughly cleaned with detergent, distilled water and 70% ethanol and assembled. For analysis of the kinesin proteins, 7.5% resolving gel buffer was used (0.75M Tris-HCL, pH8.8, 10% (w/v) Ammonium persulphate, 10% (w/v) SDS). The polymerization catalyst TEMED was added to the resolving gel mixture, which was then

poured into the plates. A layer of ethanol was added on top of the gel to prevent drying and maintain a flat gel front. After polymerization, the ethanol was washed off and a well comb inserted. TEMED was added to 4% Stacking gel buffer (0.25M Tris-HCl, pH 6.8, 10% (w/v) Ammonium persulphate, 10% (w/v) SDS), which was subsequently poured into the gel assembly. After polymerization the gel combs were removed and excess stacking gel buffer washed off. The remaining gel components were disassembled and the gel was submerged vertically in a tank of gel running buffer (2.5mM Tris, 19mM Glycine, 0.01% SDS). Protein samples were mixed 1:1 with 2×SDS sample buffer (0.25M Tris-HCl pH 6.8, 4% (w/v) SDS, 20% (v/v) glycerol, 1% (v/v) mercaptoethanol) and loaded into wells alongside 3µl of Pageruler^{TM} Protein Ladder (Fermentas). A current of 25mA was applied to each gel and the proteins were left to run until the loading dye front reached the bottom of the gel. Gels were then stained for 30-60 minutes in gel staining solution (35% (v/v) EtOH, 7% (v/v) Acetic acid, 0.25% (v/v) Coomassie Briliant blue R-250) and then de-stained in de-stain solution (35% EtOH and 7% Acetic acid) before scanning.

2.2.9 Electroblotting and Western Blotting

Proteins were transferred from SDS-PAGE gels to nitrocellulose membranes. Gels were placed between two nitrocellulose membranes and surrounded by filter paper in a transfer assembly. This was then submerged vertically in a tank containing transfer buffer (48mM Tris, 38mM Glycine, 0.037% (w/v) SDS, 20% (v/v) methanol). The assembly was orientated so that the gel was nearest the –ve electrode and the membrane nearest the +ve electrode. A potential difference of 50V was applied across the gel/membrane for 1.5 hours or 20V if transferring overnight. After transfer the membrane was washed in distilled water and stained with 100× Amido black (0.5g Amidoblack in 50ml of 5% (v/v) Acetic acid).

After rinsing in distilled water the membrane was incubated for 20min in 2×TBST buffer (20mM Tris, 300mM NaCL, pH7.4) containing 5% (w/v) dried milk powder. After blocking the membrane was incubated with the primary antibody for 1 hour, typically diluted to 1:1000 in 2×TBST + milk buffer. The membrane was then washed for 1×1 min, 1×5min and 1×10min in 2×TBST before incubation with the secondary anti-mouse IgG

horseradish peroxidase-conjugated antibody (GE Healthcare) for 40 minutes. This antibody was typically diluted 1:3000 again in 2×TBST + milk. Incubation times and antibody concentrations differed depending on individual optimization.

The probed proteins were visualized in two ways. After incubation for approximately 5 minutes with 1ml of ECL reaction solution (Millipore), a piece of X-ray film was exposed and developed with timings dependent on signal strength. As an alternative to X-ray film, a Fujifilm Intelligent Dark Box II was used to take a picture directly of the membrane, eliminating the need for x-ray film and the associated chemicals.

2.2.10 Silver staining of proteins on nitrocellulose membranes

The membrane was thoroughly rinsed with distilled water to remove all excess ECL, amidoblack or antibody solutions. The membrane was then incubated for 2-5 minutes with shaking in the silver nitrate solution (2% (v/v) Na_3-citrate, 0.8% (v/v) $FeSO_4.7H_2O$, 0.2% (v/v) $AgNO_3$). After incubation the membrane was rinsed in distilled water and some photo-fixer usually added to increase the contrast. Finally, the membrane was rinsed again, scanned and air-dried.

2.2.11 Expression of His-tagged proteins

2.2.11.1 Bacterial Expression

Protein gene fragments were cloned into the pGAT4 expression vector (Novagen) and transformed into BL21 DE3 Rosetta 2^{TM} *E.coli* cells. Cells were grown in 50ml LB cultures (+ relevant antibiotics) at 37^{o}C overnight and used to inoculate 1L of pre-warmed LB medium with appropriate antibiotics. The 1L cultures were incubated at 37^{o}C until the OD_{600}= 0.4-0.8. When the OD reached desired value, IPTG was added to a final concentration of 1mM and the culture was incubated for 3-6 hours. After incubation the cultures were centrifuged at 6000rpm for 5 minutes to pellet the cells (Beckman JLA 10.500 fixed angle rotor).

2.2.11.2 Insect (Sf9) cell Expression

Protein gene fragments were first cloned into the pIEx-7 expression vector (Merck). This vector allows rapid, transient transfection in insect cells with a 6×Hist tag for purification. Expression is directed by the baculovirus hr5 enhancer and the IE1 (immediate early) promoter which recruit endogenous transcription machinery and thus circumvent the need for baculovirus production.

2.2.11.2.1 Storage and growth of Insect Cells

Sf9 insect cells were thawed from stocks stored at -70^{o}C. The thawing and passaging of cells was conducted as described in the Novagen 'Insect Cell Expression' manual. Cells were grown at 28^{o}C and passaged into fresh T-25 flasks at a ratio of 1:8 every 3-4 days under a laminar flow hood. Cells were grown in serum-free BacVector® Insect Cell Medium (Novagen) which was supplemented with 5% (v/v) fetal bovine serum for several passages after thawing.

2.2.11.2.2 Plasmid transfection

Insect cells were transfected with the GeneJuice (Novagen) liposome-based reagent. Table 5 below summarizes the components and their required volumes.

Table 4: Summary of the transfection ingredients

Transfection Ingredients	**6-well plate**	**10ml (125ml) flask**
Number of Cells	1×10^{4}	1×10^{7}
Culture volume/well	2.5ml	8ml
Amount of plasmid DNA	2µg	20µg
Volume of GeneJuice	10µl	100µl
Volume of serum-free medium added to DNA and GeneJuice for dilution	100µl	1ml
Volume of serum-fee edium added to transfection mixture after 15min incubation	0.8ml	N/A

For the small-scale optimization experiments, the 6-well plate format was used, whereas for larger suspension cultures the flask format was used. For 6-well plates, 1×10^6 (2.5ml) cells were transferred to each well one hour before transfection to equilibrate. For each well, both 2µg of DNA and10µl of GeneJuice were diluted with 100µl serum-free medium. The DNA was slowly added dropwise to the GeneJuice solution whilst shaking, and the mixture was left to incubate at room temperature for 15 minutes. After 15 minutes 0.8ml of serum-free medium was added to the transfection mixture, and this mixture was then added to each well after aspiration of medium from the cells. The lid was put on each plate and they were sealed with parafilm. For flask formats larger than 10ml, all other volumes and amounts were scaled up accordingly. Figure 15 below summarizes the insect cell transfection process.

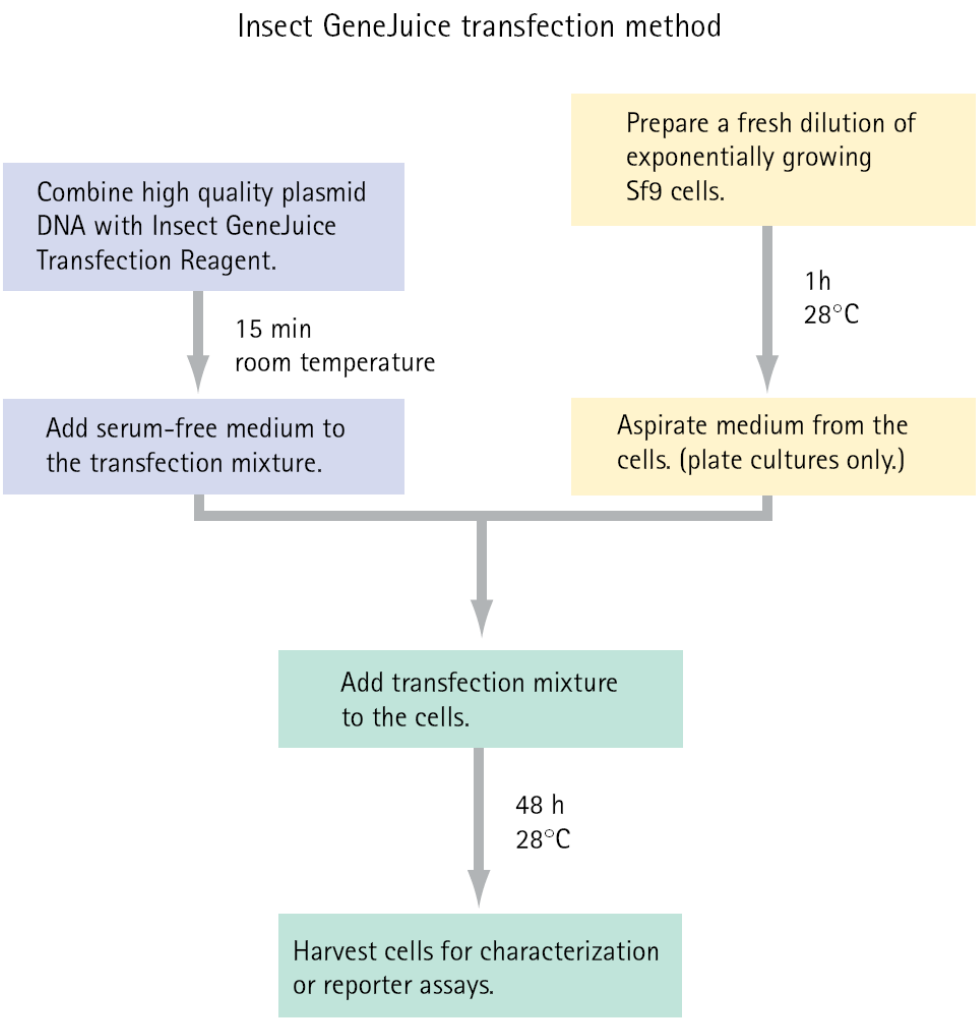

Figure 15: Schematic diagram of the stages involved in the GeneJuice transfection protocol

After transfection the cells were harvested to extract the recombinant protein. For the 6-well plate format, cells were scraped off the bottom of each well, transferred to a sterile Eppendorf tube and spun in a bench-top centrifuge at 3000rpm for 30s. The media was aspirated with a pipette and 100µl of 2×SDS sample buffer was added. Samples were boiled at 100^{o}C for 3 min, spun for 5min at top speed in a bench top centrifuge and loaded on 7% SDS-PAGE gels for analysis.

For large-scale suspension cultures, cells were harvested by centrifugation at 3000rpm on a Beckman JLA 10.500 fixed angle rotor to pellet the cells. Extraction was then carried out as described in the Nickel Column Purification section below.

2.2.12 Purification of His-tagged proteins

2.2.12.1 Removal of periplasmic fraction with osmotic shock (bacteria only)

After the initial centrifugation step, newly harvested bacterial cells were re-suspended in 5ml/g_{pellet} of sucrose buffer (50mM HEPES, 20% (w/v) sucrose, 1mM EDTA, pH 7.9) and then re-pelleted by centrifugation at 7000 × g for 30 minutes at 4^{o}C (Beckman JA-20 rotor). After centrifugation the supernatant was again discarded and the pellet re-suspended in 5ml/g_{pellet} of 5mM $MgSO_4$ ad incubated on ice for 10 minutes. Cells were then pelleted by a final centrifugation at 4500 × g for 20 minutes. The supernatant was discarded and the pellet was re-suspended in 1.5ml/g_{pellet} of extraction buffer (1M HEPES pH 7.0, 5M NaCl, 5mM mercaptoethanol) containing relevant protease inhibitors (PMSF, Leupeptin, pepstatin A, TAME) before continuing the nickel column purification protocol described below.

2.2.12.2 Nickel Column Purification

After initial centrifugation step, pelleted cells were resuspended in ice-cold protein extraction buffer (1M HEPES pH 7.0, 5M NaCl, 5mM mercaptoethanol) containing protease inhibitors (PMSF, Leupeptin, pepstatin A, TAME). The cells were then sonicated in order to disrupt the cell membranes and release expressed protein. Roughly 10 pulses were used, with the duration of each pulse lasting 1 second per ml of

resuspended cells. The pause between each pulse was the same as the duration of the pulse. The lysate was then centrifuged at 48,000 × g for 10 minutes (JA-20 fixed angle rotor).

The Ni-NTA (Qiagen) column was equilibrated with 2ml of resin slurry mixed with 3ml of extraction buffer without the protease inhibitors. The buffer was removed and the collected bacterial supernatant was passed through a 0.4μm filter membrane and loaded into the column. The supernatant and Ni-NTA were incubated on ice for 10 minutes with gentle shaking to allow binding of the His-tagged protein to the Ni-NTA beads. After incubation the supernatant was removed and the Ni-NTA beads were washed with imidazole buffer (1M HEPES pH 7.0, 5M NaCl) containing increasing concentrations of imidazole. Several washes with 20mM imidazole buffer were used until the resin returned to its original colour. Then, three washes with 40mM imidazole and two washes with 60mM imidazole were carried out. The expressed protein was finally eluted out three to four times with 1ml of elution buffer (50mM HEPES pH 7.0, 300mM NaCl, 250mM Imidazole). The yield and purity of the protein was assessed by SDS-PAGE analysis.

The concentration of purified proteins was measured using a Bradford protein assay. This spectroscopic assay uses the absorbance shift of the dye Coomassie Brilliant Blue G-250 in response to varying protein concentration. 5μl of the protein eluent was added to 1ml of Protein Assay Dye (Biorad), and the Ab_{595} was measured and compared to a protein standard curve.After measuring the concentration, eluted proteins were dialysed overnight in 100ml of dialysis buffer (80mM PIPES ph 6.8, 1mM $MgCl_2$, 1mM EGTA, 75mM KCl, 1mM DTT, 10μM ATP, 10% (w/v) sucrose)

***In vitro* protein experiments**

2.2.13 Microtubule Co-sedimentation assays

Tubulin used in these assays was isolated from porcine brain by two assembly/disassembly cycles followed by phosphocellulose chromatography, as described in (Shelanski et al 1973). The recombinant protein and tubulin were centrifuged at 200,000 × g for 10min at 4^{o}C to remove aggregates, and their concentrations measured

using a Bradford assay. For co-sedimentation, tubulin was added to a final concentration of 8μM and mixed with recombinant protein to a kinesin to tubulin ratio of 1:3. ATP and GTP were added and the reactions incubated at 37^{o}C for 30 minutes, and then centrifuged at 100,000 × g for 10 minutes (Beckman TLX Ultracentrifuge, rotor TLA120.1) In all negative controls, when microtubules were not added with the protein, reaction mixtures were made up to the final volume with MTSB buffer (50mM PIPES, 2mM EGTA, 2mM MgSO4, 100mM NaC, 5% (v/v) Glycerol). The supernatant was collected and the pellet was washed and re-suspended in SDS-PAGE sample buffer. Samples were analysed by SDS-PAGE and stained with Coomassie.

2.2.14 Microtubule polymerization assays

Porcine tubulin was used in all assays. Tubulin was stored at -80^{o}C, and before each assay it was rapidly thawed at 37^{o}C, incubated on ice for 10 minutes to depolymerize, and spun at for 200,000 × g 10 minutes at 4^{o}C to remove aggregates.

For bacterial proteins, tubulin was used at a final concentration of 8μM. The control run was set up with 80μl of tubulin and 20μl of dialysis buffer. ATP and GTP was added to a final concentration of 1mM. The dialysis buffer was replaced by kinesin protein for the other assays and the turbidity was monitored at 350nm and at 32^{o}C using a Helios beta spectrophotometer equipped with Unicam Peltier temperature control unit (Thermospectronic, UK).

Cell Biology

2.2.15 BY-2 Suspension Culture Transformation

Tobacco BY-2 (Bright Yellow) suspension cultures were used to test the effect of kinesin over-expression on microtubule dynamics and cell cycle progression. An estrogen receptor-based chemical-inducible system was used to regulate the expression of kinesin proteins in transformed BY-2 cells (Zuo et al 2000). This system uses a chimaeric transcription activator (XVE) created by the fusion of the DNA-binding domain of the

bacterial repressor LexA (X), the transactivating domain of VP16 (V) and the regulatory region of the human estrogen receptor (E).

The Gateway destination vector PMDC-7 (Curtis & Grossniklaus 2003) derived from the PER-8 estradiol-inducible vector, was used in these expression experiments. It confers resistance to spectinomycin in agrobacterium and hygromycin in plant cells. PMDC-7 vectors containing the relevant kinesin-13 gene constructs were transformed into the *agrobacterium* strains LBA4404 and GV3101 via the heat-shock method previously described. *Agrobacterium* colonies were used to inoculate 3ml cultures of YEB medium supplemented with the corresponding antibiotics and left to grow at 30^{o}C overnight. 0.1ml of *Agrobacterium* culture was mixed with 4ml of BY-2 cells in a 10cm petri dish and incubated for 2 days at 20^{o}C without shaking on a flat surface. The BY-2 cells were then spread onto plates containing BY-2 agar (4.31g/l Murashige & Skoog basal salt medium (sigma cat no M5519), 370mg/l KH_2PO_4, 2mg/ml 2.4-D and 30g/l sucrose, pH 5.8, 7g/l plant agar) and the relevant selection antibiotics (hygromycin, spectinomycin) as well as carbenicillin and vancomycin to kill the *agrobacterium*.

After 10-14 days calli should appear as small opaque dots. Calli were transferred to new selective medium before being used to set up transformed BY-2 liquid culture. 1cm calli were added to 20ml of BY-2 liquid media containing the relevant selection antibiotics in 100ml Erlenmeyer flasks.

2.2.16 Extraction of estradiol-induced protein

10ml of BY-2 cell culture was sieved through a 40-60µm mesh strainer and rinsed with BY-2 medium to remove residual β-estradiol. The sieved BY-2 cells were frozen with liquid nitrogen and crushed with a pre-chilled pestle and mortar. Two different techniques were then used to extract protein from the frozen cell powder.

2.2.16.1 TCA Extraction

Five volumes of 15% TCA was added to the cell powder and vigorously mixed until homogeneous. The mixture was then centrifuged at 4500rpm for 10 min and the supernatant discarded. The protein pellet was re-suspended and washed in acetone

solution (80% (v/v) acetone, 100mM Tris-HCl, pH8.5) before being centrifuged again at 4500 rpm for 5 min. This process was repeated twice and the resultant pellet was resuspended in 2×SDS loading buffer, boiled for 3 min at 100^{o}C, centrifuged and loaded on a gel. To determine whether recombinant kinesin protein was present, gels were transferred to nitrocellulose membranes and immunoblotted with anti-HA primary antibody (1:200 dilution).

2.2.16.2 Hot SDS Extraction

With this method, 0.5ml of boiling 2×SDS loading buffer was added to approximately 0.5ml of frozen BY-2 cell powder and mixed immediately. As above, samples were boiled for 3 min at 100^{o}C, centrifuged and loaded on gel. Western blotting was also carried out as above.

2.2.17 Fixation and Immunostaining of BY-2 suspension culture cells

BY-2 lines were induced with β-estradiol to a concentration of 1µM. 10ml of BY-2 cell cultures were sieved through a 40-60µm mesh strainer and 10ml of fixative solution was added (3.7% (w/v) paraformaldehyde, 50mM PIPES pH 6.8, 5mM EGTA, 2mM $MgSO_4$, 0.4% (v/v) Triton X-100). To make the fixative, the required amount of paraformaldehyde was placed in a 50ml centrifuge tube and half the required volume of water was added. After shaking the paraformaldehyde solution was incubated in a 65^{o}C water bath for 5 minutes after which 25µl/5ml of 0.1M NaOH was added. When the solution had cleared, the fixative was removed from the water bath and the rest of the fixative constituents were added.

Samples were mixed and incubated with the fixative for 30min at room temperature before being washed 3 times in PBS buffer (570mg/l Na_2HPO_4, 212mg/l KH_2PO_4, 8g/l NaCl, 1ml/l Tween 20, pH 7.0). Cells were then treated with an enzyme mixture for cell wall digestion (1% (w/v) Macerosyme, 0.2% (w/v) pectolyase, 0.4M mannitol, 5mM EGTA, 15mM MES pH 5.0) supplemented with protease inhibitors (100mM PMSF, 10mg/ml leupeptin, 1mg/ml pepstatin A) for 5 minutes before another 3 washes with PBS buffer.

200µl cell samples were placed on poly-L-lysine coated coverslips and incubated in a humid chamber for 10 min. Excess buffer was carefully removed with tissue paper and the cover slips were incubated for a further 5 min. Cover slips were then placed in 6-well plates containing PBS buffer to wash off unattached cells. Cover slips were then incubated in PBS buffer containing 2% (w/v) BSA for 20 min to block unspecific binding of antibodies. The cover slips were then incubated for one hour with primary antibody buffer containing PBS (+2% BSA) and the primary antibody of choice diluted to 1:500. Coverslips were washed 3 times with PBS and then incubated for 50 minutes with the secondary antibody solution. Finally, if nuclear staining was required cover slips were incubated with a PBS solution containing DAPI for 10 minutes, before mounting cover slips onto slides using VectaShield (Vector Laboratories). The edges were sealed with nail varnish. Slides were imaged by CLSM or on a fluorescence microscope for cell counting experiments.

2.2.18 Confocal Laser Scanning Microscopy (CLSM)

Immunostained slides were imaged using the Leica SP5 microscope. The antibodies used are listed below

Primary Antibodies	**Species Raised in**	**Secondary Antibodies**	**Species raised in**	**Conjugate**
Anti-HA	Mouse			TRITC
Anti-Tubulin	Rate	Anti-		FITC

2.2.19 Growth Curve experiments of induced BY-2 cells

To investigate the effect of AtKIN13A/B induction on the BY-2 cell cycle, growth curves were measured over a period of 10 days. Transformed BY-2 cell lines of AtK13A, AtK13B and HsK13 were seeded into 90ml BY-2 medium at 2g/90ml. Lines were induced with 1µM of β-estradiol and 0.3µM APM. 5ml samples were collected every three days, sieved through a mesh strainer, dried and weighed. When plotting on graph the error bars were calculated using the standard deviation of the means.

3. RESULTS

3.1. Biochemistry

3.1.1. Bacterial Expression

Expression and analysis of recombinant AtKin13A and 13B

Constructs for the full length *Arabidopsis* K13A and K13B genes were already available from the lab. These were then cloned into pGAT4 vectors and expressed as 6×His tagged fusion proteins in BL21 DE3 Rosetta 2 cells. After the removal of the periplasmic extract via osmotic shock, the recombinant proteins were purified as described in chapter 2. Samples were analysed by SDS-PAGE pre- and post-dialysis ('E' and 'D' respectively), with clear bands present for each protein at their predicted molecular weights (HsKin13: 81kDa, AtKin13A: 89kDa, AtKin13B: 77kDa). The presence of high molecular weight bands corresponding to roughly double the predicted size of Kin13A, points to the formation of dimer complexes (FIG 16A).

The microtubule-binding capability of the recombinant proteins was assessed with a co-sedimentation assay (FIG 16B). AtKIN13A and 13B were added to MAP-free porcine brain tubulin with a ratio of 1:3, along with ATP and GTP. After a 30 minute incubation period the supernatants and pellets were centrifuged, separated on SDS-PAGE gels and stained with Coomassie. The presence of bands at the predicted molecular weight of both proteins in the pellet, and not in the negative controls, shows that both proteins bind specifically to microtubules *in vitro*. For both proteins, faint high molecular weight bands in the pellet without microtubules suggest they are aggregates which precipitate non-specifically with microtubules in the pellet.

The presence of both kinesin proteins in the pellet was confirmed by western blotting. The supernatant and pellets containing tubulin and each kinesin were transferred to nitrocellulose membranes and probed with either anti-His (1:500 dilution) (FIG 16C) or specific anti-kinesin-13A/B (1:1000 dilution) (FIG 16D) primary antibodies. Although the proteins were expressed with a 6×His tag in order to aid extraction and detection, probing with the anti-His tag antibody was not particularly helpful as the presence of many bands in both pellets suggests a low specificity and some cross-reactivity with bacterial proteins still present after extraction. Probing with protein-specific primary

antibodies, however, confirmed the presence of bands at the predicted weights. Interestingly, the fact that no signal was detected in both supernatant samples highlights the specificity of these antibodies and shows that both kinesin proteins bind entirely to microtubules in the pellet.

The effect of both AtKin13A and AtKin13B on microtubule polymerization *in vitro* was tested using turbidimetric assays (FIG 16E). As microtubules scatter light much more effectively than free microtubule dimers, the turbidity of a solution is proportional to the amount of tubulin polymer and the length of microtubules (Hunter et al 2003). Both proteins were added to MAP-free porcine brain tubulin at a Kin13 to tubulin ratio of 1:3. The turbidity of the mixture was monitored at 350nm. As can be seen in FIG 16E, both kinesin proteins produced a dramatic increase in the turbidity of the microtubule mixture as compared to the control.

The fact that graphs for Kin13A and 13B are dissimilar could be significant. The turbidity in the Kin13A reaction mixture increased linearly, suggesting that what we are seeing is just an artefact of aggregation. To confirm this, a similar assay could be run with just the protein itself. The Kin13B graph, however, is more logarithmic which points to the presence of an enzymatic reaction and thus a functional protein.

Dimerization could in theory lead to bundling, but it is difficult to discern whether this is a physiological effect or not. Another issue is the fact that proteins expressed in prokaryotic systems may not undergo the post-translational modifications and folding necessary for correct functionality. The expressed kinesins may simply be inactive and the increased turbidity of the solution attributable to the formation of protein and tubulin aggregates. It was important, therefore, to express the protein in a eukaryotic system and repeat these *in vitro* assays.

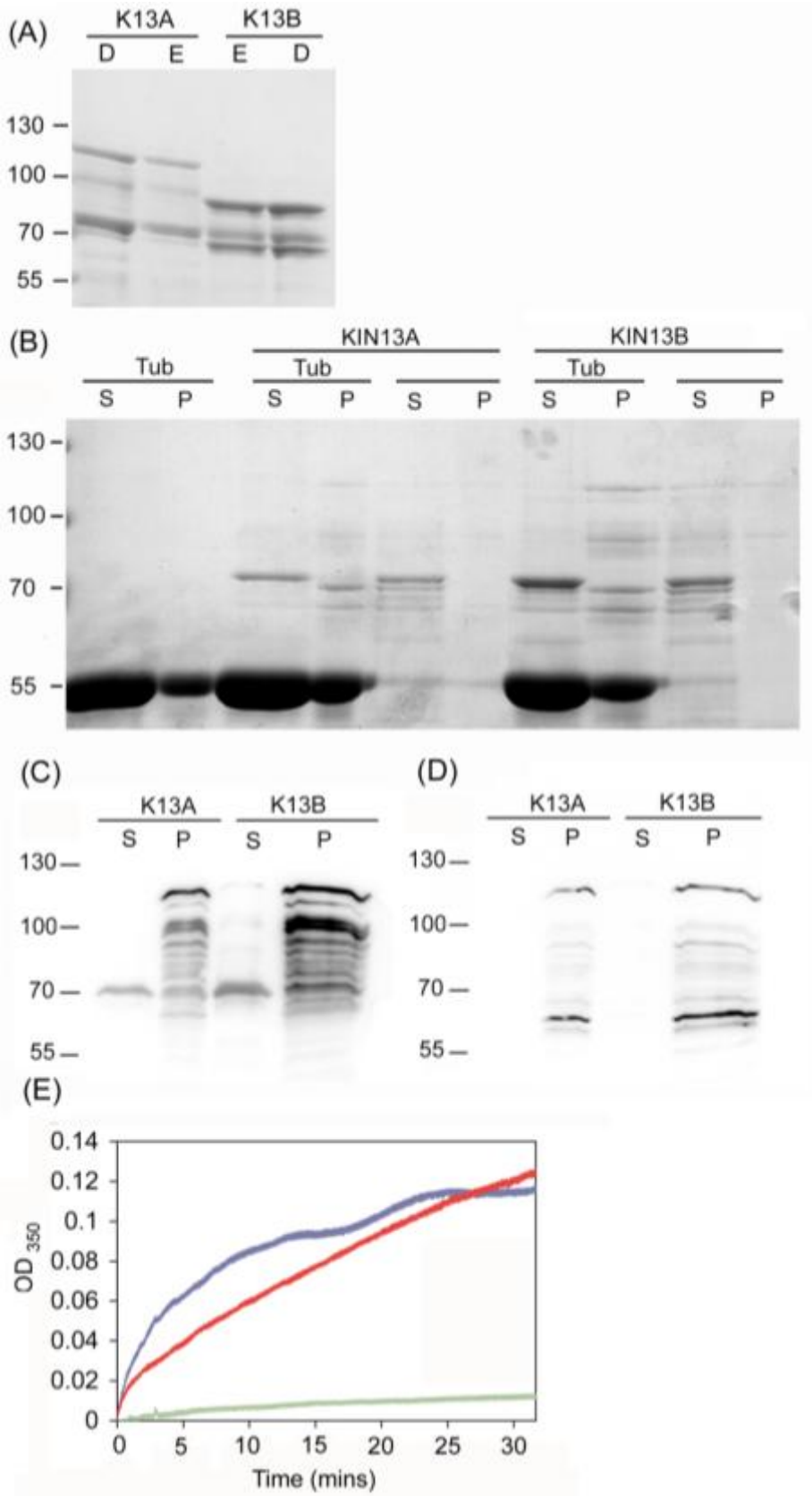

Figure 16: Biochemical analysis of recombinant AtKin13A/B proteins. Markers in kDa (A) Coomassie-stained SDS-PAGE gel of purified proteins pre(E)- and post(D)- dialysis. (B) Cosedimentation of AtK13A/B. supernatants (S) and pellets (P) were separated on SDS-PAGE gels and stained with Coomassie. (C) and (D) are immunoblots of the Cosedimentation assay probed with anti-His and anti-K13A/B antibodies respectively. (E) Effect of 3µM AtKin13A/B on the turbidity of a 10µM tubulin solution. The assay was performed at 32°C, and the turbidity was monitored at 350 nm. Atkin13A (red), AtKin13B (blue), control (green)

3.1.2. Insect Cell Expression

As the activity of the recombinant proteins may have been affected by the lack of eukaryotic post-translational machinery, similar biochemical studies were conducted on proteins expressed from insect Sf9 cells.

Expression and analysis of recombinant AtKin13A, 13B and HsK13

For expression in insect cells, AtK13A, AtK13B and HsK13 gene constructs were cloned into the pIEx-7 expression vector. This vector allows efficient expression of recombinant His-tagged proteins directly in insect cells, by-passing the time consuming process of baculovirus creation. Although a large number of insect Sf9 cell transfection reagents are commercially available, we used the GeneJuice (Novagen) liposome-based reagent (see chapter 2). Other reagents had been used, such as the Attractene (Qiagen) and Nanofection (PAA) transfection kits, but test experiments with both these methods failed. The inclusion of human Kinesin-13 would provide a useful control and functional comparison when conducting microtubule polymerization assays.

Before conducting large-scale expression experiments, a degree of optimization was required to check that this system worked and to determine the appropriate incubation time. An initial time-course transfection was conducted in 6-well plates with all three genes at three time points: 24, 48 and 72 hours (FIG 17A). After incubation cells were centrifuged, combined with SDS loading buffer and run on SDS-PAGE gels. Western blotting with anti-His primary antibodies confirmed the presence of recombinant protein and that a 72 hour induction time produced the highest yield. No bands were present in the AtKin13A lanes, suggesting that transfection of this protein was not successful.

Once optimized, a larger scale transfection experiment with AtKin13B was conducted. After the 72 hour incubation period, a similar Ni-NTA extraction protocol to bacterial expressed proteins was used, during which samples of the total cell extract (before nickel extraction), flow-through (unbound protein from the nickel column) and eluted protein were taken. Western blotting of these samples with anti-K13B antibodies (1:1000) showed the presence of a clear band of predicted molecular weight in the eluent, a band

not present in the flow-through (FIG 17B). This shows that all the recombinant protein bound to the nickel column, and that the extraction procedure managed to concentrate the recombinant protein from the total cell extract.

To assess the effect of the AtKin13B on microtubule dynamics, turbidimetric assays of different concentrations were carried out (FIG 17C). In both cases, there was a significant increase in turbidity compared to the control, with turbidity of the solution roughly doubling when twice the amount of protein was used. This suggests that AtKin13B has a concentration-dependent effect on the turbidity of tubulin solutions. The logarithmic shape of both curves is similar to that of bacterially-produced protein, and the curve with 3µM AtKin13B peaks at an absorbance of 0.1, identical to the bacterial protein (FIG 16E). This is interesting because the protein was expressed in a eukaryotic system, so is assumed to have folded correctly. It is likely that the logarithmic curve seen in the bacterial protein is reflective of correctly folded protein. This increase in turbidity could be due to an unexpected function of AtKin13B in stabilizing tubulin dimers. Incorrect folding of the full-length protein is unlikely to be as much of an issue here as a eukaryotic expression system was used, but the issue of protein dimerization is not entirely ruled out. More studies on this protein will have to be carried out to better ascertain the *in vitro* function.

The turbidimetric assay of HsKin13 (FIG 17D) was less encouraging as straight lines for each concentration used suggested the results may have been artefacts. The highest concentration of HsKin13 produced a low turbidity, as expected with the well-characterised depolymerization effect of human kinesin-13s. However, the turbidity of the tubulin solutions was higher with 0.2µM compared to 0.1µM, although in theory an inverse concentration-dependent relationship between HsKin13 and turbidity would mean these results should be the other way around. It is possible, therefore, that this result could be a mere artefact of protein aggregation or low protein concentration. Furthermore, the concentration of HsKin13 used was very low (0.1-0.4µM) which may have severely limited protein function.

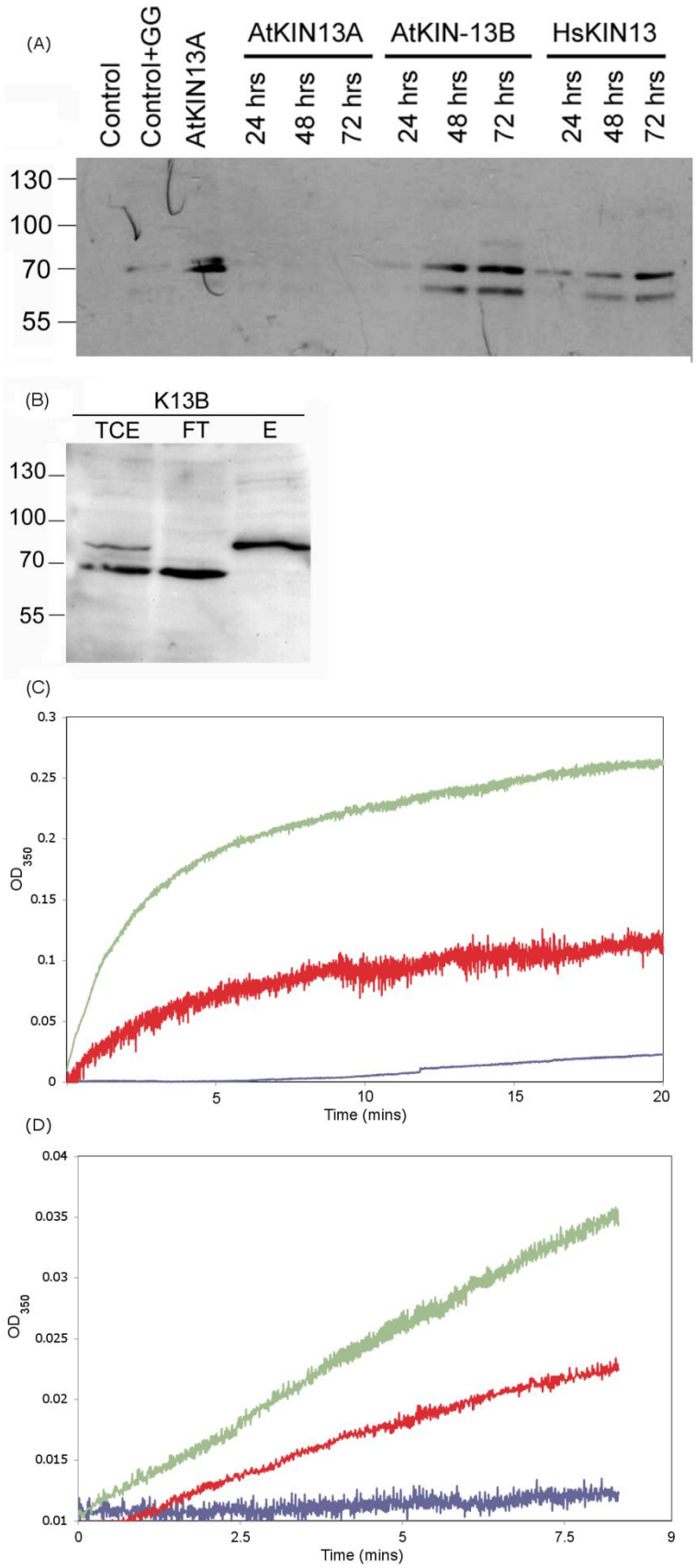

Figure 17: Biochemical Analysis of insect cell-expressed proteins. (A) Immunoblot of timecourse transfection experiment. (B) Immunoblot of AtK13B probed with anti-13B antibodies after large-scale transfection. (C) Effect of AtKin13B on the turbidity of a 10µM tubulin solution. The assay was performed at 32ºC, and the turbidity was monitored at 350 nm. Control 0µM (blue), 3µM (red), 6µM (green) (D) Turbidimetric assay of HsKin13. 0.2µM Hskin13 (green), 0.1µM (red) and 0µM (blue).

3.2. Cell Biology

3.2.1. Optimization of protein induction and extraction

Expression of recombinant proteins in BY-2 cells was carried out using a β-estradiol inducible expression system (see Methods). As β-estradiol induction had not been used in the lab before, some optimization was required. Firstly, two different methods of protein extraction were used to determine the amount of recombinant protein produced after induction (FIG 18A). Initial work using the TCA method produced variable results and often quite low yields. An attempt to precipitate the proteins in 100% acetone without the use of TCA was also unsuccessful. In contrast, the boiling SDS method, which involved adding crushed plant material directly to SDS loading buffer, produced much higher yields of total plant protein when run on an SDS-PAGE gel. Western blotting with anti-HA antibody confirmed that the hot SDS protein extraction was effective for both K13A and 13B, and the presence of single bands in each lanes showed that the HA antibody did not cross-react with native proteins (FIG 18B).

After establishing a reliable extraction protocol, a variety of western blotting conditions were tested to determine the most suitable blocking solutions and antibody concentrations for maximum protein detection. A single BY-2 HsKIN13 line was induced with 50μM β-estradiol and harvested after seven days. After protein extraction and transfer, the nitrocellulose membrane was cut into 12 strips, each with a different concentration of primary anti-HA antibody or blocking solution. Figure 18C shows that the western conditions which produce the best signal are: A blocking solution of 2×TBST with 5% milk, primary antibody dilution of 1:200 and primary antibody incubation time of 1 hour.

The next question we asked was how the level of recombinant protein produced was dependent on the concentration of β-estradiol used to induce the lines. Two BY-2 lines transformed with HsKin13 and AtKin13B were induced with a range of estradiol concentrations from 0.5μM to 10μM and harvested after 24 hours. As seen in Fig 19A, a range of low concentrations of estradiol did not produce much variation in the induction level of each recombinant protein, regardless of the construct used. The silver stained membrane shows that protein loading was equal (FIG 19B).

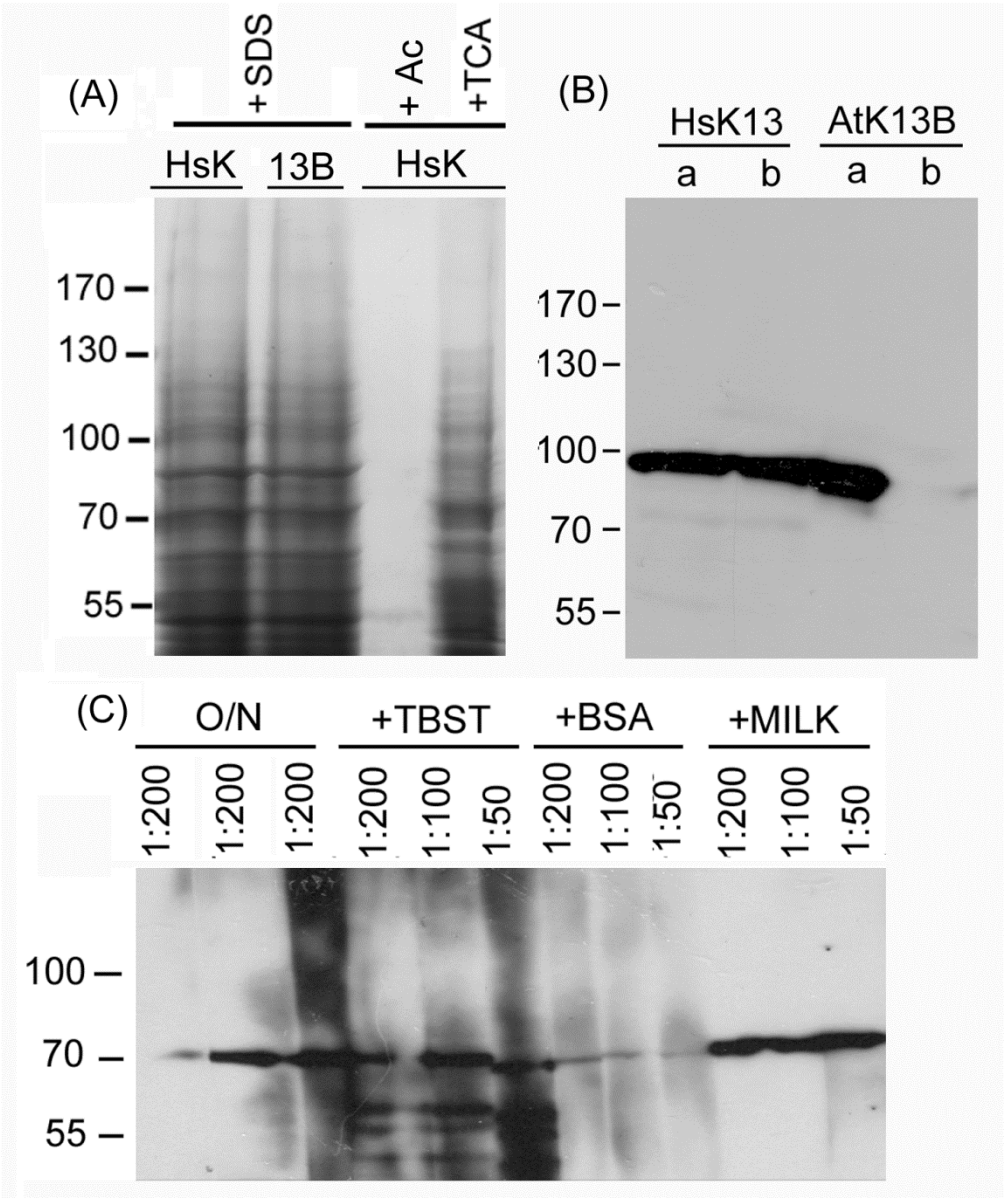

Figure 18: Optimization of estradiol-induced kinesin-13 proteins. (markers in kDa) (A) HsKin13 and AtKin13B proteins extracted with different methods, either hot SDS, 100% (v/v) acetone or the TCA method. Samples were run on SDS-PAGE gels and separated with Coomassie. (B) Immunoblot of protein from both lines extracted with the hot SDS method and probed with anti-HA antibody. (C) Optimization of immunoblotting conditions. Protein was extracted from a HsKin13 line after induction and transferred to nitrocellulose membrane. Each strip subjected to different dilution of primary anti-HA antibody and blocking solution.

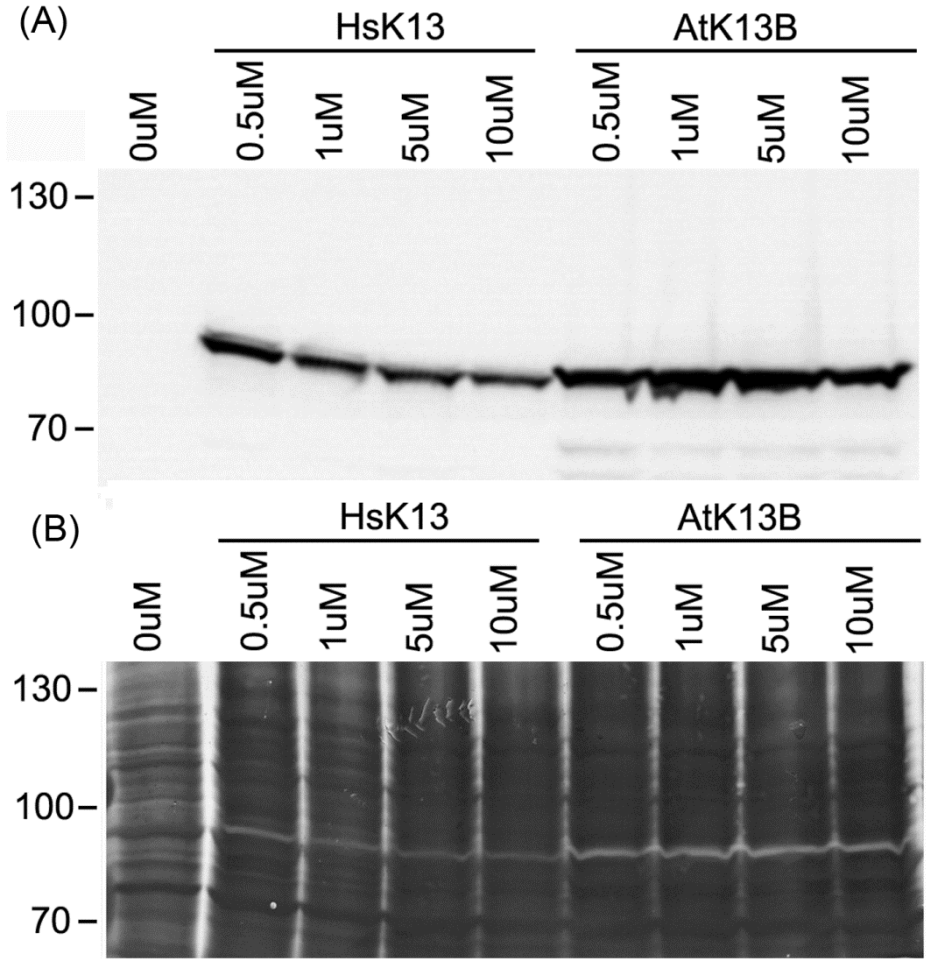

Figure 19: (A) Immunoblot of BY-2 lines transformed with HsK13 and AtKin13B induced with varying concentrations of β-estradiol. Membrane probed with anti-HA antibody. (B) Silver-stained nitrocellulose membrane used for the immunoblot in (A) (markers are kDa).

Although lower concentrations did not have a concentration-dependent effect on protein induction, it was still possible that more protein could be produced by increasing the estradiol concentration further. To test this, a BY-2 line transformed with AtKin13B was induced with a range of β-estradiol concentrations from 10μM to 100μM and samples were taken after one, two and 5 days to see how protein expression changed over time (FIG 20A).

After one day incubation, the amount of protein seemed to increase proportionately with an increase in estradiol concentration. This appears in contrast to the previous induction experiment with lower estradiol concentrations. Interestingly, though, from two days the level of induced protein did not change significantly with increasing estradiol concentrations but stayed at a high level. The band at 10μM is similar to that at 40μM, but after five days of induction the 40μM band is significantly thicker than DAY 2 or DAY 1. The presence of empty lanes at 10μM and 20μM concentrations at DAY 5 cannot be explained by incorrect loading, as the silver membrane in Fig 20B shows equal protein levels in each lane. Instead, it is possible that after 5 days of induction the BY-2 cells are able to overcome the elevated protein levels and start to degrade or break down recombinant protein. Therefore, it is only at estradiol concentrations above 20μM that recombinant protein levels are high enough to activate the degradation machinery.

As higher estradiol concentrations seemed to induce more protein, the phenotypic effects of these concentrations were analysed using fluorescence microscopy (FIG 21). DAPI staining allowed nuclear morphology to be judged. Samples induced with 20μM estradiol showed several cells containing giant nuclei, denoting a defect in karyokinesis at anaphase so chromosomes and nuclei could not properly separate. At 40μM estradiol there were several multi-nucleate cells and small blue dots in the cytoplasm thought to be mini- nuclei. In this case, defects in metaphase plate formation led to improper alignment of chromosomes so nuclei divided abnormally but no cytokinesis occurred. The phenotype at 100μM estradiol was the most dramatic, displaying both giant and lobed, multinucleate cells with highly condensed chromosomes.

Although the phenotypes were consistent with those observed with other microtubule-destabilising drugs, analysis of untransformed BY-2 cells suggested they may be artefacts of high estradiol concentrations. Control WT samples with no β-estradiol contained lots

of dividing cells with nuclei at all stages of mitosis (FIG 21). At 20μM estradiol many cells contained mini-nuclei, and at 40 and 100μM there were almost no cells undergoing cell division. Furthermore, the weight of cultures reduced massively at higher estradiol concentrations compared to uninduced controls, showing a marked cessation of cell growth (TABLE 1).

Table 1: Effect of high estradiol concentration on WT cell growth

B-estradiol concentration	g/10ml
0μM	6
10 μM	5.96
40 μM	0.14
100 μM	0.083

In summary, despite the fact that high concentrations of β-estradiol induce more recombinant protein in BY-2 cells, these concentrations also appear detrimental to normal cell growth. The concentration-dependent abnormalities in nuclear morphology of induced AtKin13B samples suggests a synergistic role between the induced protein and β-estradiol; perhaps estradiol has a microtubule-destabilising effect which causes cessation of growth in WT cells but more serious phenotypes when acting with overexpressed Kin13B. Although this may suggest a MT destabilizing role for *Arabidopsis* kinesin-13s, it is clear that non-toxic concentrations of estradiol must be used for future induction experiments.

Once extraction technique, western conditions and estradiol concentrations had been optimized, several lines for each kinesin-13 gene were screened to see how reproducible the induction system was and identify high expressing lines (FIG 20C). A β-estradiol concentration of 1μM was used, to avoid toxicity. Fig 20C shows that all constructs were expressed and stable proteins of the correct size were produced. However, the expression levels differed between each line. For HsKin13, line number 3 was the highest expresser, with a band significantly thicker than the other two, whereas for AtKin13B line 1 was the highest expressing line. In AtKin13A, only line 3 showed significant expression, with a very faint band in line 2 and nothing in line 1. How expression levels differ so much can be explained by two scenarios; either the samples contained a small number of

transformed cells with high expression levels, or they contained a larger number of transformed cells with low expression. This question cannot be answered without analysis of the lines by immunofluorescence.

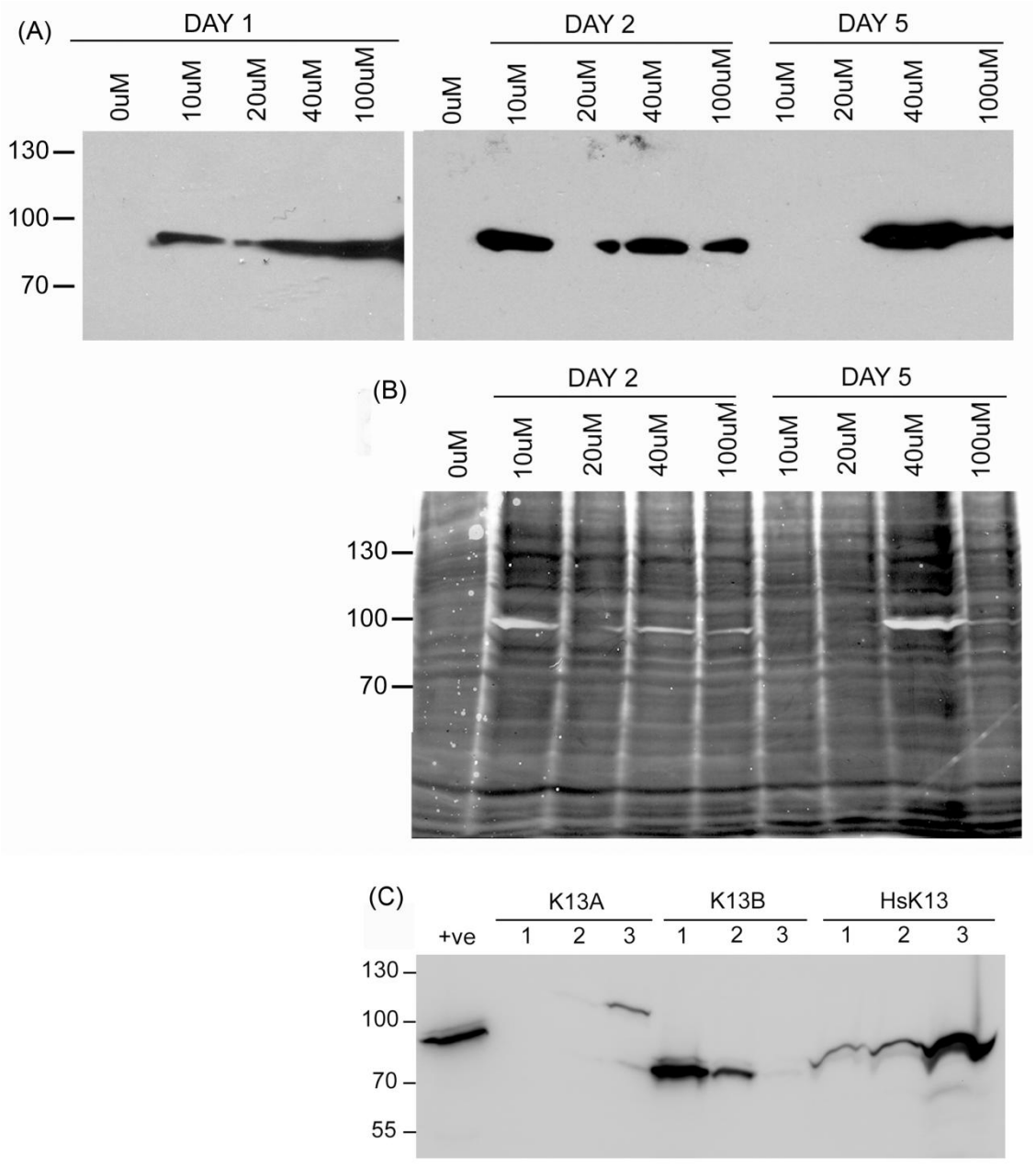

Figure 20: (A) immunoblot of a AtKin13B line induced at different concentrations. Protein was extracted at 3 different time points. (B) Silver-stained membrane of Day2 and Day5 samples (C) Immunoblot of three transformed BY-2 lines per gene construct, induced with 1µM estradiol. Markers are in kDa

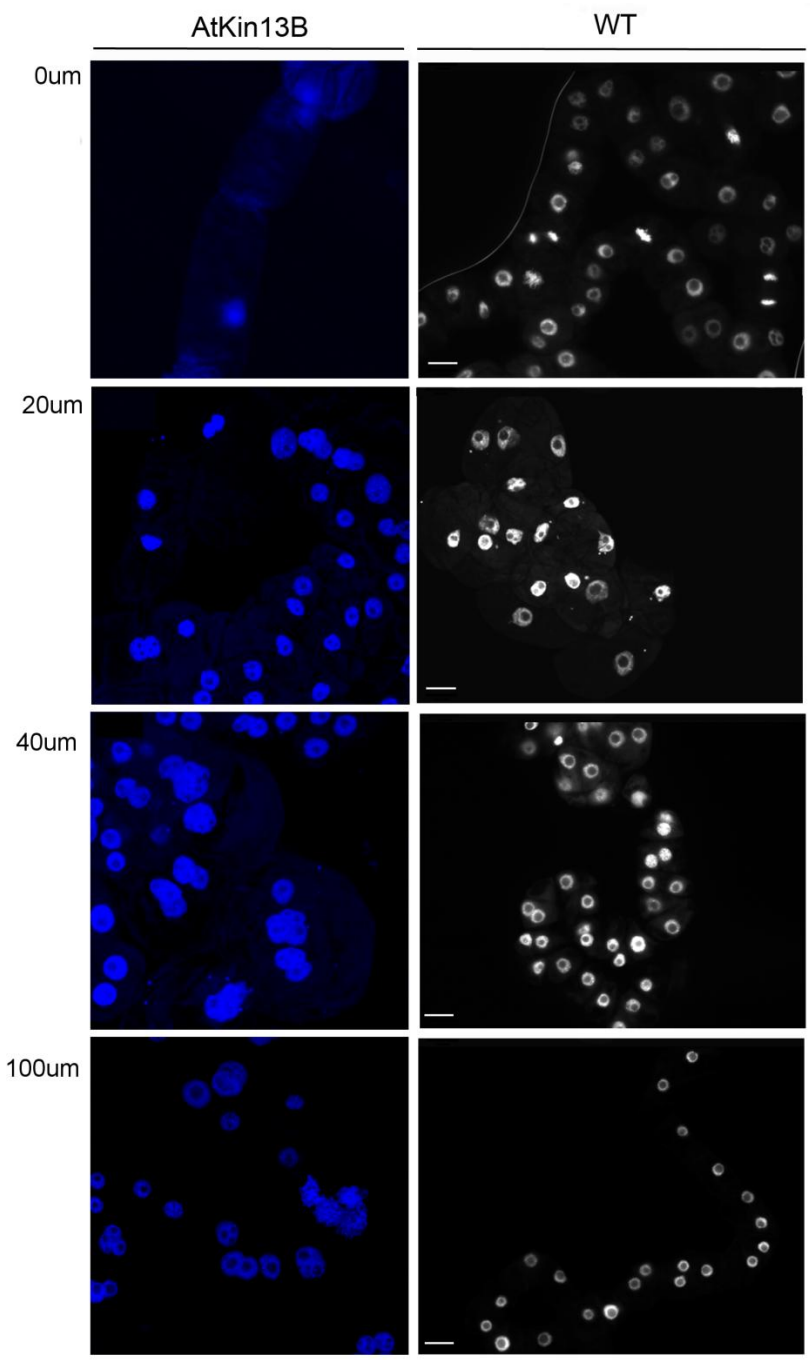

Figure 21: WT and AtKin13B BY-2 cells stained with DAPI (blue) at different concentrations of β-estradiol. The WT cells on the right were also stained with DAPI (white) and treated with differing estradiol concentrations. Scale bar = 25µm

3.2.2. Localization of kinesin-13 proteins through cell division

Immunofluorescence microscopy was used to confirm that active or correctly folded proteins were produced by the estradiol induction system, and to investigate their localization during cell division. Three lines for each construct were initially screened to check their expression levels, and the two highest expressers were induced for 72 hours with 1μM β-estradiol. Samples of each culture were immunostained with anti-tubulin and anti-HA antibodies, before being mounted on coverslips and viewed under the microscope (see Material & Methods 2.2.17).

The control WT images show stereotypical microtubule and nuclear formations at the four main stages of cell division (Fig 22A). At prophase, spindle MTs surround newly condensed chromosomes. During metaphase, spindle MTs emanating from both poles of the nucleus arrange chromosomes down the centre of the cell in a 'metaphase plate'. Chromosomes are pulled apart by opposing spindle fibres in anaphase, before decondensing during the formation of the phragmoplast.

At all stages of mitosis, HsKin13 seemed to colocalize with spindle microtubules. As spindle MTs surround dividing chromosomes it is hard to completely rule out chromosomal binding from prophase through to anaphase, but during telophase and phragmoplast formations it is clear that overexpressed HsKin13 localizes exclusively to microtubules (Fig 22B). Both AtKin13A and 13B show a different localization pattern (FIG 23A & B). From prophase to anaphase, staining is seen on the chromosomes but not with microtubules, with the areas of highest signal at the ends of chromosome arms. In both cases some weak staining is seen colocalizing with microtubules of the phragmoplast in telophase.

The strong staining at the ends of chromosomes arms can be explained by two possibilities. The primary antibodies could be restricted to the outer edges of chromosomes due to masking of epitopes during the fixation process or by geometric constraints preventing them penetrating further into the nucleus. Alternatively, the AtKin13 proteins may bind to chromosomes **indirectly** via other kinesins or chromosome-binding proteins enriched at the chromosome arms.

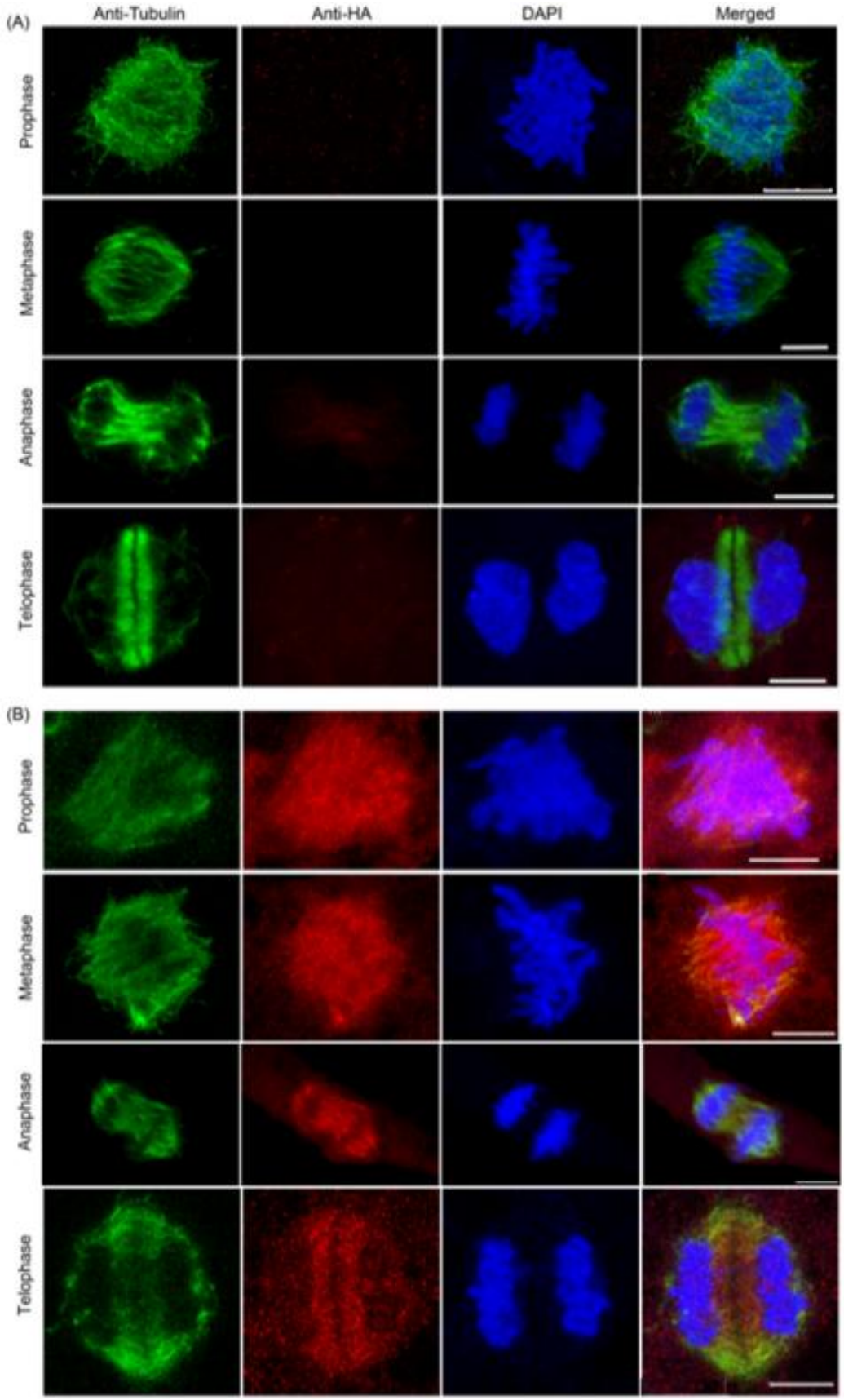

Figure 22: Immunostained BY-2 cells at different stages of cell division (scale bar: 10µm) (A) WT, untransformed BY-2 cells (B) HsK13 lines

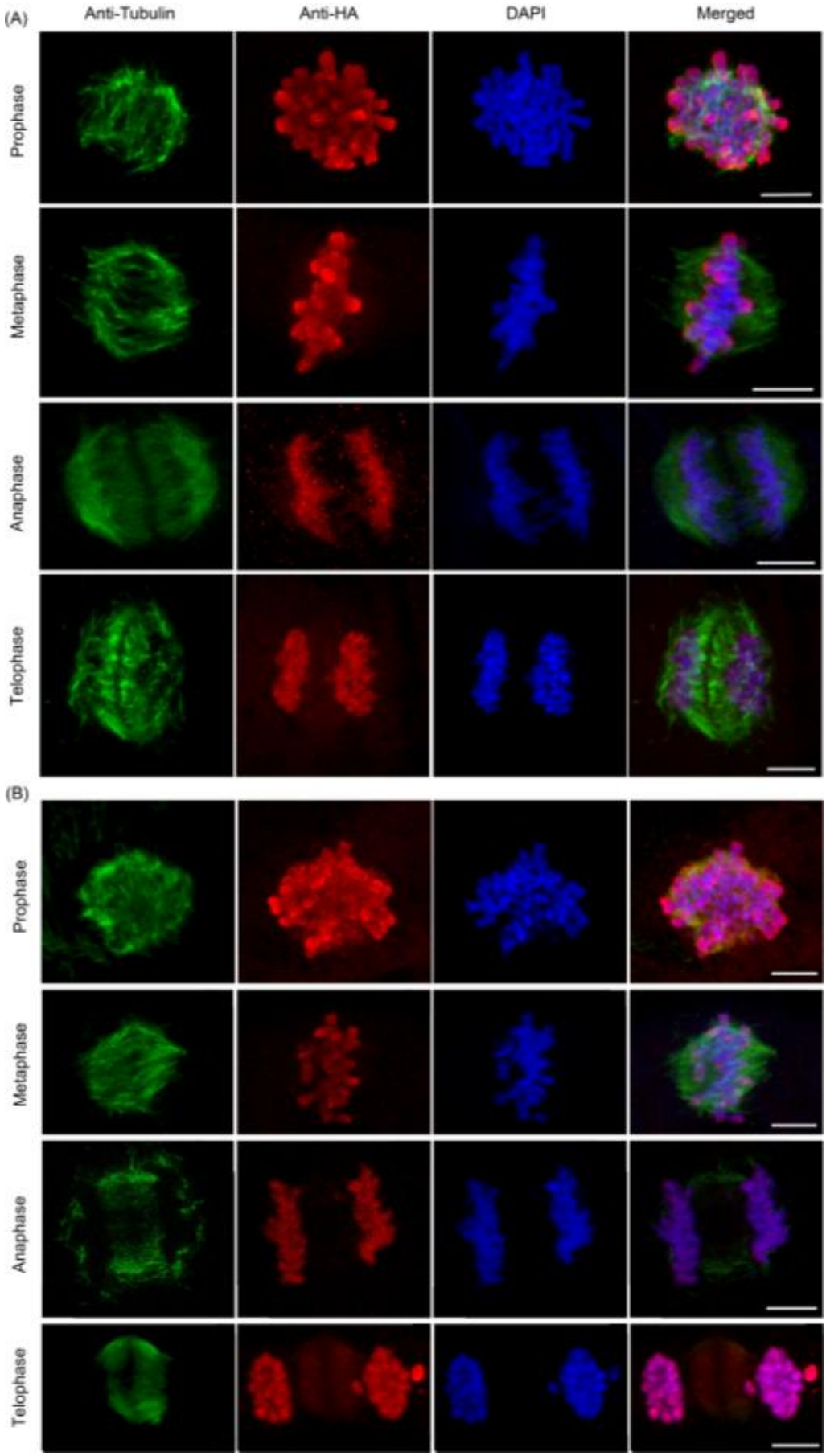

Figure 23: Immunostained BY-2 cells at different stages of cell division (scale bar: 10µm) (A) AtKin13A lines (B) AtKin13B lines

3.2.3. The Effect of Kinesin-13 induction on cell division and growth

To investigate the effect of these proteins on the cell cycle and progression through mitosis, cell counting studies were carried out. In these experiments, two lines for each construct were induced for 72 hours then fixed and stained with anti-tubulin antibody and DAPI. One thousand cells were counted for each line, with the number of cells at each stage of cell division recorded. Data for both lines were combined and averaged to increase reliability.

The graph in Figure 24 shows the proportion of cells at different mitotic stages. By comparing how the proportion of cells at each mitotic stage changes after protein overexpression, it is possible to determine when the protein has an effect. For HsKin13, there was no significant change in anaphase and telophase stages after induction, but the proportion of prophase cells reduced concurrent with an approximate 5% increase in metaphase cells. This suggests that overexpressed HsKin13 protein acts during the metaphase checkpoint to delay the transition to anaphase, perhaps by altering spindle dynamics. When the delay is overcome, however, the subsequent mitotic stages occur normally, suggesting that HsKin13 is inhibited or degraded during this time.

For AtKin13A, there is no statistically significant difference between uninduced and induced samples for any mitotic stages. As *Arabidopsis* kinesin-13s have severely reduced equivalents of the neck region known to confer the depolymerization activity of mammalian kinesin-13s, it is quite possible that AtKin13A has a more subtle effect on cell cycle progression which is not highlighted by this experiment.

With AtKin13B, there is a significant increase of over 10% for the proportion of metaphase cells after induction. As with HsKin13, this suggests that an *Arabidopsis* protein also acts during the metaphase checkpoint, with overexpression leading to a delay in the metaphase to anaphase transition. The proportion of anaphase cells and telophase cells both reduces after induction, which may be linked to delay at the metaphase checkpoint causing a more rapid separation of chromosomes and completion of mitosis. There is also a small increase in the percentage of prophase cells after induction, but may be due to natural variation.

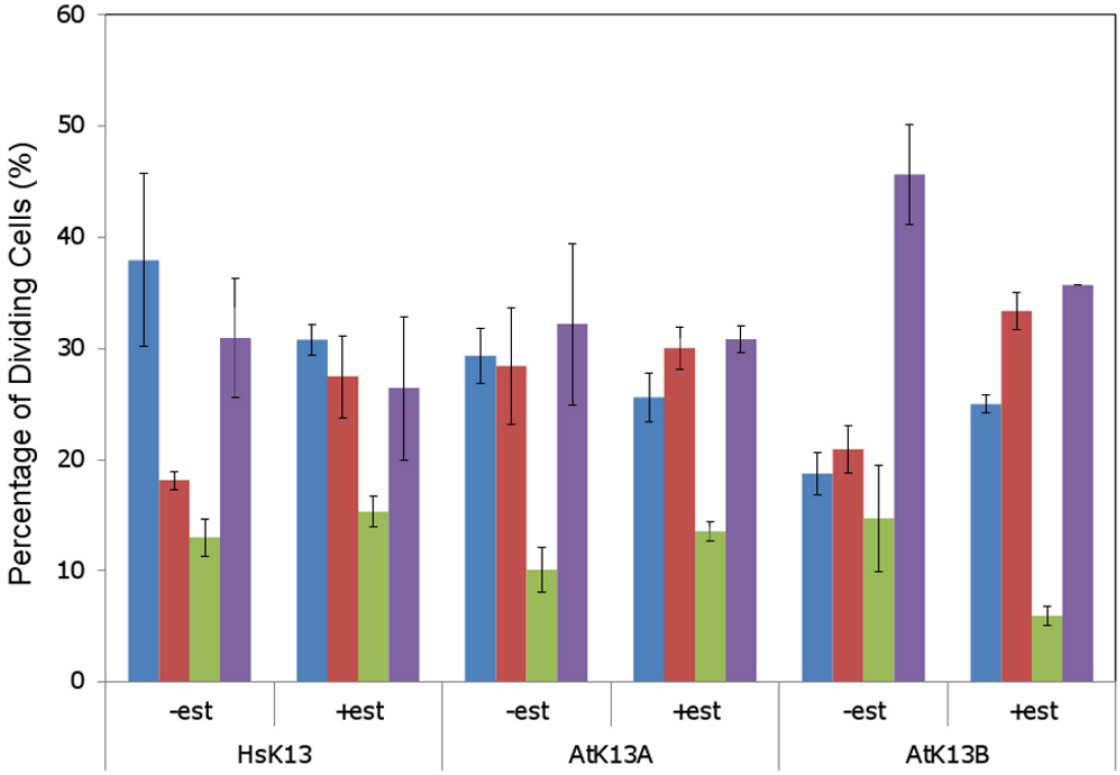

Figure 24: Graph showing the effect of kinesin-13 protein induction on different stages of cell division. 1000 cells at different stages of mitosis were counted in induced (+est) and uninduced (-est) samples to determine the percentage of dividing cells at each stage. Blue: prophase, Red: metaphase, Green: anaphase, Purple: telophase. Error bars represent the standard deviation of the mean.

The next question we asked was whether over-expression of the kinesin-13 proteins affected cell growth by altering microtubule dynamics. To do this we induced BY-2 lines of known cell weight and took samples every three days to measure the change in cell weight (and thus growth) over time. As well as induced/ uninduced lines, cultures were also treated with the microtubule-destabilising drug Amiprophos-Methyl (APM), known to affect culture growth by disrupting microtubule dynamics. If any of the kinesins had a destabilizing activity on microtubules, they would in theory accentuate the APM-mediated reduction in growth. If the proteins had a stabilizing function, however, they would be expected to counter-act the APM and result in normal cell growth, in a similar way to taxol.

For HsKin13 lines, there was no effect on cell growth either with APM on its own or APM with induced protein (FIG 25A). Cells appeared to grow normally to reach the stationary phase and the APM did not seem to affect growth at all. With AtKin13A both induced and uninduced samples treated with APM showed reduced growth compared to the controls (FIG 25B). Interestingly, cells treated with both APM and induced with estradiol grew slightly slower than APM on its own, hinting that AtKin13A may have a destabilizing effect on microtubules. However, this argument is hampered by the lack of a statistically significant difference between the two curves, due to overlapping error bars. Furthermore, the two uninduced cultures grew slower than expected from controls, barely reaching the stationary phase by day 9.

AtKin13B (FIG 25C) cultures treated with APM and induced with estradiol grew at a much slower rate than the untreated samples. Importantly, the uninduced APM-treated culture grew normally and reached the stationary phase, but the induced sample did not. This suggests that overexpression of AtKin13B significantly disrupts cells growth, presumably by altering microtubule dynamics and progression though the cell cycle.

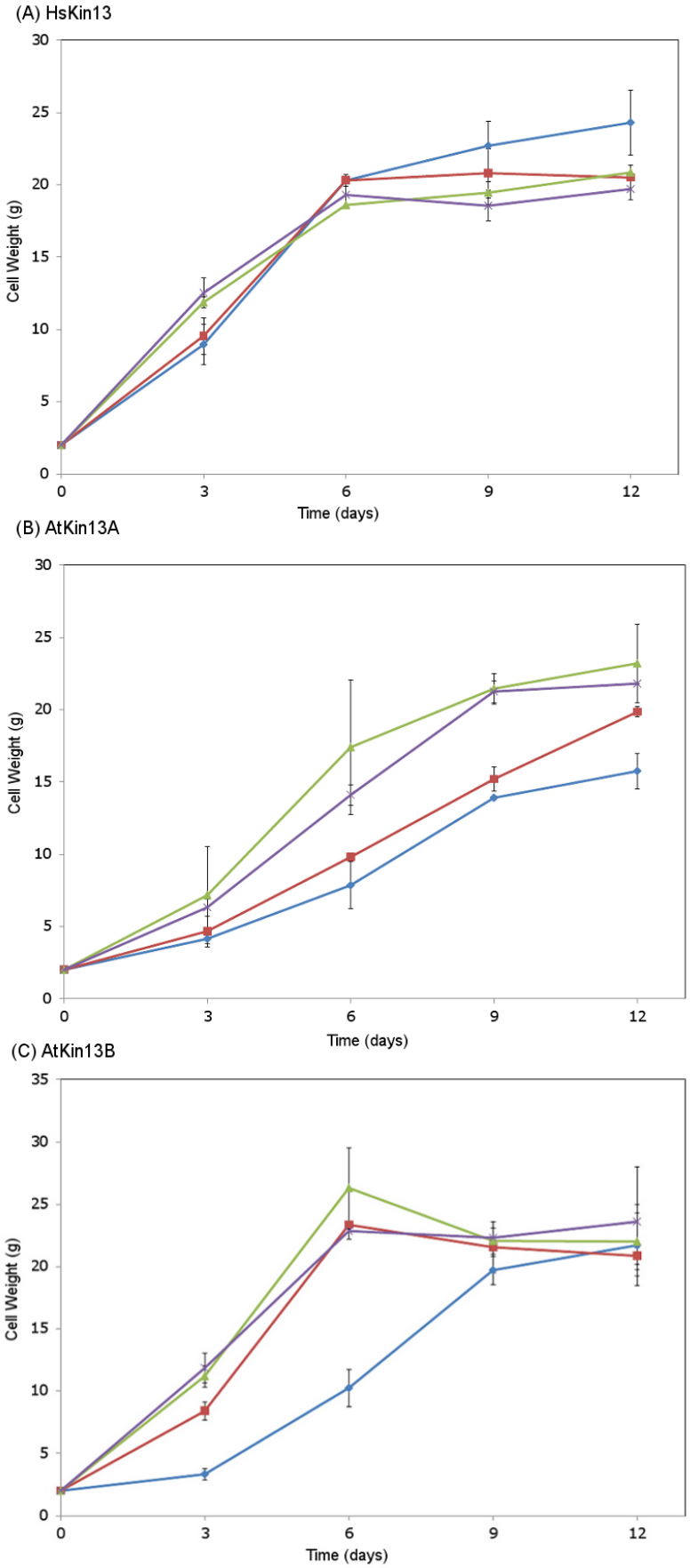

Figure 25: Graphs showing the effect of protein induction and APM treatment on cell proliferation. Green: +est, Purple: -est, Red: +APM – est, Blue: + APM +est.

4. DISCUSSION

The aim of this project was to investigate the function of the *Arabidopsis* Kinesin-13 proteins. To achieve this, *in vitro* studies using bacterial and insect cell-expressed proteins were conducted to assess their activity and effect on microtubule dynamics. The *in vitro* properties of these proteins were analysed in tobacco BY-2 cells using an oestrogen-inducible expression system and immunofluorescence microscopy, with human Kinesin-13 used as a comparison. The results of these experiments are discussed below.

4.1. Expression and analysis of recombinant AtKin13A and 13B

4.1.1. Bacterial Expression

The results described earlier show that full-length kinesin-13s can be produced in both bacterial and insect cell expression systems. The bacterially expressed proteins showed specific tubulin binding in co-sedimentation assays.

The turbidimetric experiments to assess the effect on tubulin dynamics produced some interesting results. The increase in turbidity seen with both proteins can be explained in two ways: either the protein increases the total amount of polymer by promoting MT polymerization, or it could induce bundling of already assembled microtubules. However, this data is in conflict with the well-characterized effects of other kinesin-13 proteins on microtubules, which induce a reduction in the total amount of MT polymer or in the rate of MT polymerization. In fact, similar studies with the mammalian kinesin-13 homologue MCAK show a rapid reduction in turbidity (Hunter et al 2003, Moores et al 2002). It is possible, therefore, that plant kinesin-13 proteins possess functional characteristics which are unique for this type of kinesin.

As mentioned, one explanation for these results is that plant kinesins could increase the amount of MT polymer by increasing the number of microtubule ends from which new microtubules can seed. By destabilizing and shortening microtubules, more MT fragments would be available for nucleation, leading to an overall increase in turbidity. Although MCAK has been characterized as a particularly powerful depolymerase (Hunter et al

2003), it is important to bear in mind that the structural dissimilarities between human and plant kinesin-13 (Lu et al 2005) may affect their respective functions, so this remains a plausible explanation.

Dimerization could in theory lead to bundling, and has been identified as a necessary property of the plant microtubule-bundling protein MAP-65 (Smertenko et al 2004). If each kinesin protein bound to another protein as well as a tubulin molecule, which in turn bound to other tubulin molecules, then large kinesin/tubulin aggregates could rapidly build up in the solution. The formation of these aggregates would produce a gradual increase in turbidity, and it is unclear whether a logarithmic or linear curve would be produced. The fact that there was no change in the amount of tubulin in the pellet of co-sedimentation assays points to aggregation or bundling, rather than a depolymerising effect. If the purified protein could depolymerise microtubules, the density of tubulin in the pellet would reduce as seen with vertebrate kinesin-13s (Desai et al 1999, Hunter et al 2003).

As mentioned, the logarithmic curve produced with AtKin13B seems suggestive of an enzymatic reaction, whereas the linear AtKin13A curve is more indicative of inactive protein, though it could be a logarithmic reaction with a much slower rate. To confirm this, the AtKin13A assay could be repeated with the protein alone, so if aggregation was in operation the curve would be an identical shape. To check that these results were not due to incorrect protein folding, turbidimetric assays were repeated with an insect cell eukaryotic expression system.

4.1.2. Insect Cell Expression

This experiment shows that the GeneJuice (Novagen) transfection system can be used to successfully produce recombinant kinesin proteins. Furthermore, the results for AtKin13B were almost identical to those from the bacterial expression system, producing a logarithmic curve. The magnitude of the curve increased depending on the kinesin concentration, as the turbidity of the solution doubled when twice as much protein was added. The fact that both bacterial and insect cell expression assays are the same suggests that either this represents the real *in vitro* activity of AtKin13B, or in both cases the protein was improperly folded and produced an artefact caused by aggregation. As

mentioned earlier, an increase in turbidity is hard to reconcile with the expected function of kinesin-13s as depolymerisers. However, any functional comparisons can only be made with their well-characterized vertebrate counterparts, which have several structural dissimilarities, most notably lacking the neck region implicated in the depolymerizing activity. Perhaps these *in vitro* experiments highlight an unexpected property of plant kinesin-13s as microtubule stabilizers.

To improve this data, the more robust baculovirus transfection technique can be used to express these proteins in insect cells, allowing larger-scale experiments on the recombinant proteins. The GeneJuice transfection did work, but results in low yields of recombinant protein. It is clear that more work is needed in this area to investigate the biochemical properties of these proteins before solid conclusions can be made.

4.2. High concentrations of estradiol affect BY-cell proliferation

The results in Fig 21 show that β-estradiol is toxic to tobacco BY-2 cells at concentrations higher than 10μM, causing a cessation of cell growth and nuclear morphology defects. Although higher estradiol levels induce more protein, this benefit is far outweighed by the detrimental effect on the cells. Increasing concentrations of β-estradiol produced different morphology defects: 20μM estradiol seemed to disrupt karyokinesis by producing cells with giant nuclei, whereas 40μM estradiol led to the formation of multinucleate cells with defects in early metaphase. 100μM concentrations of estradiol produced severe defects, with several giant, lobed and multinucleate cells with highly condensed chromosomes. The toxic effect of β-estradiol was confirmed by analysing WT BY-2 samples, which also contained mini-nuclei and a huge reduction in the number of mitotic cells. Furthermore, Table 1 highlighted the marked cessation of cell growth compared to WT, untreated cells.

Although β-estradiol is mammalian hormone, studies have shown that one of its metabolites 2-methoxyestradil (2ME2) suppresses microtubule dynamics and arrests mitosis without directly destabilizing microtubules. As well as affecting microtubule dynamics, 2ME2 also induced spindle asymmetry and prevented cell growth (Kamath et al 2006). However, when used in *Arabidopsis* plants for inducible protein expression, β-estradiol was not shown to be toxic to the host (Zuo et al 2000). It may be that tissue

cultures are more vulnerable to estradiol than whole plants, but it is still surprising that a mammalian hormone can also have a toxic effect on plant cells. After further optimization of β-estradiol, the concentration of 1 μM was established as a safe and effective level to use.

Despite the fact that high estradiol concentrations massively reduced cell proliferation in all samples, it is interesting to note that the transformed cell line showed more severe phenotypes than the WT cells. This suggests that overexpression of AtKin13B may act synergistically with the estradiol to produce nuclear morphology defects; the destabilizing function of AtKin13B combining with the suppression of microtubule dynamics by estradiol, for example. AtKin13B may, therefore, have some subtle role in regulating microtubule dynamics which only becomes apparent when expressed in cells also treated with microtubule-destabilising drugs.

4.3. *Arabidopsis* kinesin-13A and 13B localize to chromosomes during cell division

The confocal images in figures 22 and 23 show that there is disparity between the mitotic localization of mammalian and plant kinesin-13. HsKin13 was shown to localize exclusively at spindle microtubules, whereas AtKin13A and 13B were present on chromosomes, with some staining at the spindle microtubules of anaphase and telophase. Previous studies in animal cells have localized MCAK to the spindle poles, kinetochores and microtubule plus ends (Moores & Milligan 2006, Wordeman 2010), but it is interesting that in this case localization seems to be exclusively to the spindle.

As HsKin13 is being expressed in a foreign system, it could be that crucial binding partners or regulatory proteins lacking in plant cells disrupt the usual HsKin13 localization. It is well established, for example, that mammalian MCAK is regulated directly by the mitotic protein Aurora B kinase, which inhibits its microtubule depolymerizing activity via phosphorylation (Andrews et al 2004, Wordeman et al 1999). Aurora B has also been shown to recruit MCAK to the inner centromere during prometaphase (Wordeman et al 1999). Although Aurora-like kinases have been identified in *Arabidopsis* (Demidov et al 2005) and shown to be required for chromosome segregation in tobacco BY-2 cells (Kurihara et al 2006), they are clearly separate from

animal and fungal Auroras. Furthermore, the localization of HsKin13 to the spindle in BY-2 cells may occur because the mammalian-specific proteins required for targeting to the centromeres, as well as the centrosomes themselves, are not present. Aurora B kinase is just one example of the species-specific kinases and chromosome-interacting proteins involved in kinesin-13 function, so it is not surprising that a different localization pattern has emerged.

As mentioned, AtKin13A and B both localized to the chromosomes at prophase and metaphase, as well as at the anaphase spindle and phragmoplast microtubules. Both plant kinesins showed strong staining at the ends of the chromosome arms which could have been because antibodies were restricted due to epitope masking and geometric constraints.

However, another explanation is that the kinesins bind to or interact with other chromosome-interacting proteins enriched at the chromosome arms. The chromokinesins, another class of kinesin proteins with their motor domains situated at the N-terminus, have been shown to localize to chromosome arms during mitosis (Mazumdar & Misteli 2005). The human kinesin-10 protein KID (Kinesin-like DNA-binding protein), a plus-end directed motor that binds both MT and chromosomes (Tokai et al 1996, Yajima et al 2003), has been reported to play a role in chromosome movement and the orientation of chromosome arms in metaphase (Levesque & Compton 2001). Four flowering plant kinesin-10 genes have been identified in plants, but their function is currently unknown (Reddy & Day 2011). Interestingly, though, a comprehensive analysis of plant kinesins found that the only domain common to both plants and animals is the DNA-binding motif present in kinesin-10 (Richardson et al 2006). It is possible, therefore, that plant kinesin-13 and kinesin-10 proteins may function together to regulate the microtubule-dependent process of chromosome orientation.

4.4. AtKinesin-13B overexpression delays progression through mitosis

The cell cycle chart in Figure 24 shows that overexpression of AtKin13B leads to an increase in the proportion of metaphase cells. This suggests that overexpressed Kin13B delays dividing cells at the metaphase checkpoint, thus delaying subsequent progression

through to anaphase. The checkpoint is in place to ensure that cell division does not continue until proper connections between the spindle and kinetochores are established. At this stage, sensing of the bipolar tension acting on chromosomes of the metaphase plate initiates entry into anaphase by releasing inhibition of the anaphase-promoting complex (APC) (Musacchio & Salmon 2007). Interestingly, in animal cells Aurora B kinase functions as a mitotic error-checker (Kallio et al 2002), detecting and destabilizing incorrect attachments via its regulation of MCAK. In this way, overexpression of AtKin13B may disrupt spindle microtubule dynamics during metaphase and affect their co-ordinated, bipolar attachment to chromosomes.

As Figure 24 shows, overexpression of HsKin13 also increases the proportion of metaphase cells, although to a lesser extent than AtKin13B. As MCAK is known to be involved in activating the spindle checkpoint, it is not surprising that overexpression disrupts this process. Furthermore, HsKin13 may have a lesser effect than Kin13B because BY-2 cells lack the necessary mammal-specific kinases required for full activation.

The fact that only one stage of mitosis is significantly affected by Kin13B overexpression implies that its activity is cell cycle-regulated. The regulation of MCAK by Aurora B kinase is already well characterised, and it is likely that plant-specific kinases operate during mitosis to control when the kinesin-13 proteins are active. AtKin13A induction appeared to have no significant effect on cell cycle progression. More study is needed into the function of these proteins through the cell cycle, the relationship between these proteins and their associated kinases, and the phosphorylation mechanism in operation.

4.5. AtKinesin-13B overexpression reduces cell proliferation

As earlier work suggested the combination of AtKin13B overexpression and high β-estradiol concentration appeared to reveal a subtle microtubule-disrupting effect, protein induction was combined with the anti-microtubule drug Amiprophos-Methyl (APM). APM has been well-characterized as an anti-microtubule drug which directly inhibits microtubule dynamics in plant cells via destabilization (Falconer & Seagull 1987, Morejohn & Fosket 1984). If the kinesins had a destabilizing effect, therefore,

overexpression would amplify the reduction cell proliferation caused by APM treatment alone. If they acted as stabilizers in a similar way to the drug taxol, the detrimental effects of APM should in theory be reversed.

As shown in Figure 25C, overexpression of AtKin13B in APM-treated BY-2 cells led to a significant reduction in cell proliferation and growth. This reduction in growth could be explained by the cell cycle results above. In untreated cells AtKin13B overexpression leads to a delay in the metaphase checkpoint which is eventually overcome, but with the addition of APM the effect of AtKin13B overexpression on weakened microtubules is enhanced and cell division is detrimentally affected. This effect, however, was not apparent in both HsKin13 and AtKin13A lines. Human kinesin-13 may not have the same function it shows in its native environment due to the lack of regulatory proteins mentioned above. For AtKin13A, the cultures were still growing and did not reach the stationary phase, so it is hard to predict what overexpression would have caused in older cells.

4.6. Conclusion

These experiments show that AtKin13B appears to function during metaphase in aiding activation of the metaphase spindle checkpoint and subsequent progression through the cell cycle. Biochemical studies into its relationship with microtubules, combined with *in vivo* induction data, suggest that AtKin13B may have a subtle destabilizing effect on microtubules, contrary to is previous characterization as a Golgi-associated protein (Lu et al 2005). It is clear that this protein is tightly regulated during cell division, and so it would not be surprising that, like its mammalian counterpart MCAK, it is phosphorylated and de-phosphorylated by specific mitotic kinases. Further work is needed into the function of this protein and the nature of any regulatory interactions.

Biochemical studies with AtKin13A showed that it binds specifically to microtubules, however its effect on microtubule dynamics was difficult to determine. The *in vitro* assays suggested that bacterially-expressed protein forms aggregates in solution, and overexpression in BY-2 cells had no significant effect on the cell cycle. Interestingly, AtKin13A localized to chromosomes in a similar pattern to AtKin13B, so both proteins

may have a similar role in cell cycle regulation. Previous experiments conducted in the lab have shown that this protein may have a microtubule-destabilizing effect (Tim Hawkins, personal communication). It is clear that further work with the estradiol-inducible BY-2 system is needed to investigate the potential properties of this protein.

Human Kinesin-13, a well-characterised microtubule depolymerizer, was used in this study as a functional comparison for the *Arabidopsis* kinesin-13s. When expressed in tobacco BY-2 cells, it localized exclusively to spindle microtubules throughout the cell cycle, inconsistent with studies of MCAK in animal cells (Moores & Milligan 2006, Wordeman 2010). Plant cells, however, lack centrosomes and other animal-specific regulatory proteins, so this result is not surprising. In BY-2 cells, HsKin13 overexpression delayed BY-2 cells at metaphase, suggesting a similar function to MCAK in regulation of the spindle checkpoint. These results show that the activity of kinesin-13 proteins is species-specific and the effect of animal kinesins in plant systems is markedly reduced.

5. APPENDICES

Primer sequences

	Forward	**Reverse**
AtKin13A Gateway	GGGGACAAGTTTGTACAAA AAAGCAGGCTTCACCATGGG CGGCCAAATGCAGCAAAAC	TTAAGCATAATCTGGAACATCAT ATGGATACCGAGGAACTCTCTTA CGGCTCA
AtKin13B Gateway	GGGGACAAGTTTGTACAAA AAAGCAGGCTTCACCATGAG CGGAAGACAGAGATCTGTTG	TTAAGCATAATCTGGAACATCAT ATGGGTACCCAGTGGTAGAGAC TAATACA
HsKin Gateway	GGGGACAAGTTTGTACAAA AAAGCAGGCTTCACCATGGC CATGGACTCGTCGCTTCA	TTAAGCATAATCTGGAACATCAT ATGGATACTGGGGCCGTTTCTTG CTGCTTAT
HA Gateway	N/A	GGGGACCACTTTGTACAAGAAA GCTGGGTCTTAAGCATAATCTGG AACATCATATGG

6. REFERENCES

Akhmanova A, Hoogenraad CC, Drabek K, Stepanova T, Dortland B, et al. 2001. CLASPs are CLIP-115 and-170 associating proteins involved in the regional regulation of microtubule dynamics in motile fibroblasts. *Cell* 104: 923-35

Akhmanova A, Steinmetz MO. 2010. Microtubule plus TIPs at a glance. *Journal of Cell Science* 123: 3415-19

Al-Bassam J, Ozer RS, Safer D, Halpain S, Milligan RA. 2002. MAP2 and tau bind longitudinally along the outer ridges of microtubule protofilaments. *Journal of Cell Biology* 157: 1187-96

Al-Bassam J, van Breugel M, Harrison SC, Hyman A. 2006. Stu2p binds tubulin and undergoes an open-to-closed conformational change. *Journal of Cell Biology* 172: 1009-22

Alberts, A J, J L, M R, K R, P W. 2002. Molecular Biology of The Cell, 4th Edition. New York: Garland Science

Ambrose C, Allard JF, Cytrynbaum EN, Wasteneys GO. 2011. A CLASP-modulated cell edge barrier mechanism drives cell-wide cortical microtubule organization in Arabidopsis. *Nature Communications* 2: 12

Ambrose JC, Cyr R. 2008. Mitotic Spindle Organization by the Preprophase Band. *Molecular Plant* 1: 950-60

Ambrose JC, Shoji T, Kotzer AM, Pighin JA, Wasteneys GO. 2007. The Arabidopsis CLASP gene encodes a microtubule-associated protein involved in cell expansion and division. *Plant Cell* 19: 2763-75

Andrews PD, Ovechkina Y, Morrice N, Wagenbach M, Duncan K, et al. 2004. Aurora B regulates MCAK at the mitotic centromere. *Developmental Cell* 6: 253-68

Asada T, Sonobe S, Shibaoka H. 1991. MICROTUBULE TRANSLOCATION IN THE CYTOKINETIC APPARATUS OF CULTURED TOBACCO CELLS. *Nature* 350: 238-41

Bannigan A, Lizotte-Waniewski M, Riley M, Baskin TI. 2008. Emerging molecular mechanisms that power and regulate the anastral mitotic spindle of flowering plants. *Cell Motility and the Cytoskeleton* 65: 1-11

Barrett JG, Manning BD, Snyder M. 2000. The Kar3p kinesin-related protein forms a novel heterodimeric structure with its associated protein Cik1p. *Molecular Biology of the Cell* 11: 2373-85

Binarova P, Cenklova V, Prochazkova J, Doskocilova A, Volc J, et al. 2006. gamma-Tubulin is essential for acentrosomal microtubule nucleation and coordination of late mitotic events in Arabidopsis. *Plant Cell* 18: 1199-212

Bisgrove SR, Hable WE, Kropf DL. 2004. +TIPs and microtubule regulation. The beginning of the plus end in plants. *Plant Physiology* 136: 3855-63

Bouissou A, Verollet C, Sousa A, Sampaio P, Wright M, et al. 2009. gamma-Tubulin ring complexes regulate microtubule plus end dynamics. *Journal of Cell Biology* 187: 327-34

Brady ST, Lasek RJ, Allen RD. 1982. FAST AXONAL-TRANSPORT IN EXTRUDED AXOPLASM FROM SQUID GIANT-AXON. *Science* 218: 1129-31

Brouhard GJ, Stear JH, Noetzel TL, Al-Bassam J, Kinoshita K, et al. 2008. XMAP215 is a processive microtubule polymerase. *Cell* 132: 79-88

Buey RM, Diaz JF, Andreu JM. 2006. The nucleotide switch of tubulin and microtubule assembly: A polymerization-driven structural change. *Biochemistry* 45: 5933-38

Burns RG. 1991. ALPHA-TUBULIN, BETA-TUBULIN, AND GAMMA-TUBULINS - SEQUENCE COMPARISONS AND STRUCTURAL CONSTRAINTS. *Cell Motility and the Cytoskeleton* 20: 181-89

Caplow M, Ruhlen RL, Shanks J. 1994. THE FREE-ENERGY FOR HYDROLYSIS OF A MICROTUBULE-BOUND NUCLEOTIDE TRIPHOSPHATE IS NEAR ZERO - ALL OF THE FREE-ENERGY FOR HYDROLYSIS IS STORED IN THE MICROTUBULE LATTICE. *Journal of Cell Biology* 127: 779-88

Caplow M, Shanks J. 1996. Evidence that a single monolayer tubulin-GTP cap is both necessary and sufficient to stabilize microtubules. *Molecular Biology of the Cell* 7: 663-75

Caudron N, Valiron O, Usson Y, Valiron P, Job D. 2000. A reassessment of the factors affecting microtubule assembly and disassembly in vitro. *Journal of Molecular Biology* 297: 211-20

Chan J, Calder GM, Doonan JH, Lloyd CW. 2003. EB1 reveals mobile microtubule nucleation sites in Arabidopsis. *Nature Cell Biology* 5: 967-71

Chang-Jie J, Sonobe S. 1993. Identification and preliminary characterization of a 65 kDa higher-plant microtubule-associated protein. *Journal of Cell Science* 105: 891-901

Chretien D, Fuller SD, Karsenti E. 1995. STRUCTURE OF GROWING MICROTUBULE ENDS - 2-DIMENSIONAL SHEETS CLOSE INTO TUBES AT VARIABLE RATES. *Journal of Cell Biology* 129: 1311-28

Cleveland DW. 1993. Tubulin and associated proteins. *Guide Book Series; Guidebook to the cytoskeletal and motor proteins*: 101-05

Conde C, Caceres A. 2009. Microtubule assembly, organization and dynamics in axons and dendrites. *Nature Reviews Neuroscience* 10: 319-32

Curtis MD, Grossniklaus U. 2003. A gateway cloning vector set for high-throughput functional analysis of genes in planta. *Plant Physiology* 133: 462-69

Demidov D, Van Damme D, Geelen D, Blattner FR, Houben A. 2005. Identification and dynamics of two classes of Aurora-like kinases in arabidopsis and other plants. *Plant Cell* 17: 836-48

Desai A, Mitchison TJ. 1997. Microtubule polymerization dynamics. *Annual Review of Cell and Developmental Biology* 13: 83-117

Desai A, Verma S, Mitchison TJ, Walczak CE. 1999. Kin I kinesins are microtubule-destabilizing enzymes. *Cell* 96: 69-78

Dhonukshe P, Gadella TWJ. 2003. Alteration of microtubule dynamic instability during preprophase band formation revealed by yellow fluorescent protein-CLIP170 microtubule plus-end labeling. *Plant Cell* 15: 597-611

Dimitrov A, Quesnoit M, Moutel S, Cantaloube I, Pous C, Perez F. 2008. Detection of GTP-Tubulin Conformation in Vivo Reveals a Role for GTP Remnants in Microtubule Rescues. *Science* 322: 1353-56

Dixit R, Chang E, Cyr R. 2006. Establishment of polarity during organization of the acentrosomal plant cortical microtubule array. *Molecular Biology of the Cell* 17: 1298-305

Drechsel DN, Kirschner MW. 1994. THE MINIMUM GTP CAP REQUIRED TO STABILIZE MICROTUBULES. *Current Biology* 4: 1053-61

Drykova D, Cenklova V, Sulimenko V, Volc J, Draber P, Binarova P. 2003. Plant gamma-tubulin interacts with alpha beta-tubulin dimers and forms membrane-associated complexes. *Plant Cell* 15: 465-80

Dujardin D, Wacker UI, Moreau A, Schroer TA, Rickard JE, De Mey JR. 1998. Evidence for a role of CLIP-170 in the establishment of metaphase chromosome alignment. *Journal of Cell Biology* 141: 849-62

Dutcher SK. 2001. The tubulin fraternity: alpha to eta. *Current Opinion in Cell Biology* 13: 49-54

Ehrhardt DW, Shaw SL. 2006. Microtubule dynamics and organization in the plant cortical array. *Annual Review of Plant Biology* 57: 859-75

Ems-McClung SC, Walczak CE. 2010. Kinesin-13s in mitosis: Key players in the spatial and temporal organization of spindle microtubules. *Seminars in Cell & Developmental Biology* 21: 276-82

Endow SA, Higuchi H. 2000. A mutant of the motor protein kinesin that moves in both directions on microtubules. *Nature* 406: 913-16

Endow SA, Kull FJ, Liu H. 2010. Kinesins at a glance. *Journal of Cell Science* 123: 3420-24

Ennulat DJ, Liem RKH, Hashim GA, Shelanski ML. 1989. 2 SEPARATE 18-AMINO ACID DOMAINS OF TAU PROMOTE THE POLYMERIZATION OF TUBULIN. *Journal of Biological Chemistry* 264: 5327-30

Erickson HP. 2000. gamma-tubulin nucleation: template or protofilament? *Nature Cell Biology* 2: E93-E96

Euteneuer U, Jackson WT, McIntosh JR. 1982. POLARITY OF SPINDLE MICROTUBULES IN HAEMANTHUS ENDOSPERM. *Journal of Cell Biology* 94: 644-53

Falconer MM, Seagull RW. 1987. AMIPROPHOS-METHYL (APM) - A RAPID, REVERSIBLE, ANTI-MICROTUBLE AGENT FOR PLANT-CELL CULTURES. *Protoplasma* 136: 118-24

Furutani I, Watanabe Y, Prieto R, Masukawa M, Suzuki K, et al. 2000. The SPIRAL genes are required for directional central of cell elongation in Arabidopsis thaliana. *Development* 127: 4443-53

Fygenson DK, Flyvbjerg H, Sneppen K, Libchaber A, Leibler S. 1995. SPONTANEOUS NUCLEATION OF MICROTUBULES. *Physical Review E* 51: 5058-63

Galjart N, Perez F. 2003. A plus-end raft to control microtubule dynamics and function. *Current Opinion in Cell Biology* 15: 48-53

Gard DL, Kirschner MW. 1987. A MICROTUBULE-ASSOCIATED PROTEIN FROM XENOPUS EGGS THAT SPECIFICALLY PROMOTES ASSEMBLY AT THE PLUS-END. *Journal of Cell Biology* 105: 2203-15

Gardiner J, Marc J. 2003. Putative microtubule-associated proteins from the Arabidopsis genome. *Protoplasma* 222: 61-74

Giddings. 1991. Microtubule-mediated control of microfibril deposition; a re-examination of the hypothesis *The Cytoskeletal Basis of Plant Growth and Form*: 85-100

Gigant B, Wang CG, Ravelli RBG, Roussi F, Steinmetz MO, et al. 2005. Structural basis for the regulation of tubulin by vinblastine. *Nature* 435: 519-22

Grafmueller A, Voth GA. 2011. Intrinsic Bending of Microtubule Protofilaments. *Structure* 19: 409-17

Granger CL, Cyr RJ. 2001. Use of abnormal preprophase bands to decipher division plane determination. *Journal of Cell Science* 114: 599-607

Grego S, Cantillana V, Salmon ED. 2001. Microtubule treadmilling in vitro investigated by fluorescence speckle and confocal microscopy. *Biophysical Journal* 81: 66-78

Gu XJ, Verma DPS. 1996. Phragmoplastin, a dynamin-like protein associated with cell plate formation in plants. *Embo Journal* 15: 695-704

Gunning BE, Wick SM. 1985. Preprophase bands, phragmoplasts, and spatial control of cytokinesis. *Journal of cell science. Supplement* 2: 157-79

Hackney DD, Stock MF. 2000. Kinesin's IAK tail domain inhibits initial microtubule-stimulated ADP release. *Nature Cell Biology* 2: 257-60

Haizel T, Merkle T, Pay A, Fejes E, Nagy F. 1997. Characterization of proteins that interact with the GTP-bound form of the regulatory GTPase ran in Arabidopsis. *Plant Journal* 11: 93-103

Hamada T, Igarashi H, Itoh TJ, Shimmen T, Sonobe S. 2004. Characterization of a 200 kDa microtubule-associated protein of tobacco BY-2 cells, a member of the XMAP215/MOR1 family. *Plant and Cell Physiology* 45: 1233-42

Hashimoto T. 2003. Dynamics and regulation of plant interphase microtubules: a comparative view. *Current Opinion in Plant Biology* 6: 568-76

Heald R, Tournebize R, Blank T, Sandaltzopoulos R, Becker P, et al. 1996. Self-organization of microtubules into bipolar spindles around artificial chromosomes in Xenopus egg extracts. *Nature* 382: 420-25

Heath IB. 1974. UNIFIED HYPOTHESIS FOR ROLE OF MEMBRANE-BOUND ENZYME COMPLEXES AND MICROTUBULES IN PLANT-CELL WALL SYNTHESIS. *Journal of Theoretical Biology* 48: 445-49

Helenius J, Brouhard G, Kalaidzidis Y, Diez S, Howard J. 2006. The depolymerizing kinesin MCAK uses lattice diffusion to rapidly target microtubule ends. *Nature* 441: 115-19

Hertzer KM, Ems-McClung SC, Kline-Smith SL, Lipkin TG, Gilbert SP, Walczak CE. 2006. Full-length dimeric MCAK is a more efficient microtubule depolymerase than minimal domain monomeric MCAK. *Molecular Biology of the Cell* 17: 700-10

Horio T, Oakley BR. 2003. Expression of arabidopsis gamma-tubulin in fission yeast reveals conserved and novel functions of gamma-tubulin. *Plant Physiology* 133: 1926-34

Hoshi M, Ohta K, Gotoh Y, Mori A, Murofushi H, et al. 1992. MITOGEN-ACTIVATED-PROTEIN-KINASE-CATALYZED PHOSPHORYLATION OF MICROTUBULE-ASSOCIATED PROTEINS, MICROTUBULE-ASSOCIATED PROTEIN-2 AND MICROTUBULE-ASSOCIATED PROTEIN-4, INDUCES AN ALTERATION IN THEIR FUNCTION. *European Journal of Biochemistry* 203: 43-52

Hunter AW, Caplow M, Coy DL, Hancock WO, Diez S, et al. 2003. The kinesin-related protein MCAK is a microtubule depolymerase that forms an ATP-hydrolyzing complex at microtubule ends. *Molecular Cell* 11: 445-57

Hush JM, Wadsworth P, Callaham DA, Hepler PK. 1994. QUANTIFICATION OF MICROTUBULE DYNAMICS IN LIVING PLANT-CELLS USING FLUORESCENCE REDISTRIBUTION AFTER PHOTOBLEACHING. *Journal of Cell Science* 107: 775-84

Hussey PJ, Hawkins TJ, Igarashi H, Kaloriti D, Smertenko A. 2002. The plant cytoskeleton: recent advances in the study of the plant microtubule-associated proteins MAP-65, MAP-190 and the Xenopus MAP215-like protein, MOR1. *Plant Molecular Biology* 50: 915-24

Jurgens G. 2005. Cytokinesis in higher plants. *Annual Review of Plant Biology* 56: 281-99

Kallio MJ, McCleland ML, Stukenberg PT, Gorbsky GJ. 2002. Inhibition of aurora B kinase blocks chromosome segregation, overrides the spindle checkpoint, and perturbs microtubule dynamics in mitosis. *Current Biology* 12: 900-05

Kamath K, Okouneva T, Larson G, Panda D, Wilson L, Jordan MA. 2006. 2-methoxyestradiol suppresses microtubule dynamics and arrests mitosis without depolymerizing microtubules. *Molecular Cancer Therapeutics* 5: 2225-33

Kaseda K, Higuchi H, Hirose K. 2003. Alternate fast and slow stepping of a heterodimeric kinesin molecule. *Nature Cell Biology* 5: 1079-82

Kawamura E, Himmelspach R, Rashbrooke MC, Whittington AT, Gale KR, et al. 2006. MICROTUBULE ORGANIZATION 1 regulates structure and function of microtubule arrays during mitosis and cytokinesis in the Arabidopsis root. *Plant Physiology* 140: 102-14

Kerssemakers JWJ, Munteanu EL, Laan L, Noetzel TL, Janson ME, Dogterom M. 2006. Assembly dynamics of microtubules at molecular resolution. *Nature* 442: 709-12

Kim AJ, Endow SA. 2000. A kinesin family tree. *Journal of Cell Science* 113: 3681-+

Kirchner K, Mandelkow EM. 1985. TUBULIN DOMAINS RESPONSIBLE FOR ASSEMBLY OF DIMERS AND PROTOFILAMENTS. *Embo Journal* 4: 2397-402

Kirschner M, Mitchison T. 1986. BEYOND SELF-ASSEMBLY - FROM MICROTUBULES TO MORPHOGENESIS. *Cell* 45: 329-42

Kline-Smith SL, Khodjakov A, Hergert P, Walczak CE. 2004. Depletion of centromeric MCAK leads to chromosome congression and segregation defects due to improper kinetochore attachments. *Molecular Biology of the Cell* 15: 1146-59

Komarova YA, Akhmanova AS, Kojima S, Galjart N, Borisy GG. 2002. Cytoplasmic linker proteins promote microtubule rescue in vivo. *Journal of Cell Biology* 159: 589-99

Korolev AV, Chan J, Naldrett MJ, Doonan JH, Lloyd CW. 2005. Identification of a novel family of 70 kDa microtubule-associated proteins in Arabidopsis cells. *Plant Journal* 42: 547-55

Kueh HY, Mitchison TJ. 2009. Structural Plasticity in Actin and Tubulin Polymer Dynamics. *Science* 325: 960-63

Kurihara D, Matsunaga S, Kawabe A, Fujimoto S, Noda M, et al. 2006. Aurora kinase is required for chromosome segregation in tobacco BY-2 cells. *Plant Journal* 48: 572-80

Lan WJ, Zhang X, Kline-Smith SL, Rosasco SE, Barrett-Wilt GA, et al. 2004. Aurora B phosphorylates centromeric MCAK and regulates its localization and microtubule depolymerization activity. *Current Biology* 14: 273-86

Levesque AA, Compton DA. 2001. The chromokinesin Kid is necessary for chromosome arm orientation and oscillation, but not congression, on mitotic spindles. *Journal of Cell Biology* 154: 1135-46

Lewis SA, Wang DS, Cowan NJ. 1988. MICROTUBULE-ASSOCIATED PROTEIN MAP2 SHARES A MICROTUBULE BINDING MOTIF WITH TAU-PROTEIN. *Science* 242: 936-39

Liu B, Joshi HC, Wilson TJ, Silflow CD, Palevitz BA, Snustad DP. 1994. GAMMA-TUBULIN IN ARABIDOPSIS - GENE SEQUENCE, IMMUNOBLOT, AND IMMUNOFLUORESCENCE STUDIES. *Plant Cell* 6: 303-14

Liu B, Marc J, Joshi HC, Palevitz BA. 1993. A GAMMA-TUBULIN-RELATED PROTEIN ASSOCIATED WITH THE MICROTUBULE ARRAYS OF HIGHER-PLANTS IN A CELL CYCLE-DEPENDENT MANNER. *Journal of Cell Science* 104: 1217-28

Lloyd C, Chan J. 2004. Microtubules and the shape of plants to come. *Nature Reviews Molecular Cell Biology* 5: 13-22

Lloyd C, Chan J. 2006. Not so divided: the common basis of plant and animal cell division. *Nature Reviews Molecular Cell Biology* 7: 147-52

Lombillo VA, Nislow C, Yen TJ, Gelfand VI, McIntosh JR. 1995. ANTIBODIES TO THE KINESIN MOTOR DOMAIN AND CENP-E INHIBIT MICROTUBULE

DEPOLYMERIZATION-DEPENDENT MOTION OF CHROMOSOMES IN-VITRO. *Journal of Cell Biology* 128: 107-15

Lowe J, Li H, Downing KH, Nogales E. 2001. Refined structure of alpha beta-tubulin at 3.5 A resolution. *Journal of Molecular Biology* 313: 1045-57

Lu L, Lee YRJ, Pan RQ, Maloof JN, Liu B. 2005. An internal motor kinesin is associated with the golgi apparatus and plays a role in trichome morphogenesis in Arabidopsis. *Molecular Biology of the Cell* 16: 811-23

Lucas JR, Courtney S, Hassfurder M, Dhingra S, Bryant A, Shaw SL. 2011. Microtubule-Associated Proteins MAP65-1 and MAP65-2 Positively Regulate Axial Cell Growth in Etiolated Arabidopsis Hypocotyls. *Plant Cell* 23: 1889-903

Mandelkow EM, Mandelkow E. 1985. UNSTAINED MICROTUBULES STUDIES BY CRYO-ELECTRON MICROSCOPY - SUBSTRUCTURE, SUPERTWIST AND DISASSEMBLY. *Journal of Molecular Biology* 181: 123-35

Mandelkow EM, Mandelkow E, Milligan RA. 1991. MICROTUBULE DYNAMICS AND MICROTUBULE CAPS - A TIME-RESOLVED CRYOELECTRON MICROSCOPY STUDY. *Journal of Cell Biology* 114: 977-91

Maney T, Hunter AW, Wagenbach M, Wordeman L. 1998. Mitotic centromere-associated kinesin is important for anaphase chromosome segregation. *Journal of Cell Biology* 142: 787-801

Maney T, Wagenbach M, Wordeman L. 2001. Molecular dissection of the microtubule depolymerizing activity of mitotic centromere-associated kinesin. *Journal of Biological Chemistry* 276: 34753-58

Manning BD, Barrett JG, Wallace JA, Granok H, Snyder M. 1999. Differential regulation of the Kar3p kinesin-related protein by two associated proteins, Cik1p and Vik1p. *Journal of Cell Biology* 144: 1219-33

Mao GJ, Buschmann H, Doonan JH, Lloyd CW. 2006. The role of MAP65-1 in microtubule bundling during Zinnia tracheary element formation. *Journal of Cell Science* 119: 753-58

Mao GJ, Chan J, Calder G, Doonan JH, Lloyd CW. 2005. Modulated targeting of GFP-AtMAP65-1 to central spindle microtubules during division. *Plant Journal* 43: 469-78

Margolis RL, Wilson L. 1978. OPPOSITE END ASSEMBLY AND DISASSEMBLY OF MICROTUBULES AT STEADY-STATE INVITRO. *Cell* 13: 1-8

Margolis RL, Wilson L. 1981. MICROTUBULE TREADMILLS - POSSIBLE MOLECULAR MACHINERY. *Nature* 293: 705-11

Mathur J, Mathur N, Kernebeck B, Srinivas BP, Hulskamp M. 2003. A novel localization pattern for an EB1-like protein links microtubule dynamics to endomembrane organization. *Current Biology* 13: 1991-97

Mazumdar M, Misteli T. 2005. Chromokinesins: multitalented players in mitosis. *Trends in Cell Biology* 15: 349-55

McClinton RS, Sung ZR. 1997. Organization of cortical microtubules at the plasma membrane in Arabidopsis. *Planta* 201: 252-60

McNally FJ, Okawa K, Iwamatsu A, Vale RD. 1996. Katanin, the microtubule-severing ATPase, is concentrated at centrosomes. *Journal of Cell Science* 109: 561-67

McNally FJ, Vale RD. 1993. IDENTIFICATION OF KATANIN, AN ATPASE THAT SEVERS AND DISASSEMBLES STABLE MICROTUBULES. *Cell* 75: 419-29

Melki R, Carlier MF, Pantaloni D, Timasheff SN. 1989. COLD DEPOLYMERIZATION OF MICROTUBULES TO DOUBLE RINGS - GEOMETRIC STABILIZATION OF ASSEMBLIES. *Biochemistry* 28: 9143-52

Mitchison T, Kirschner M. 1984a. DYNAMIC INSTABILITY OF MICROTUBULE GROWTH. *Nature* 312: 237-42

Mitchison T, Kirschner M. 1984b. MICROTUBULE ASSEMBLY NUCLEATED BY ISOLATED CENTROSOMES. *Nature* 312: 232-37

Moores CA, Cooper J, Wagenbach M, Ovechkina Y, Wordeman L, Milligan RA. 2006. The role of the kinesin-13 neck in microtubule depolymerization. *Cell Cycle* 5: 1812-15

Moores CA, Milligan RA. 2006. Lucky 13 - microtubule depolymerisation by kinesin-13 motors. *Journal of Cell Science* 119: 3905-13

Moores CA, Yu M, Guo J, Beraud C, Sakowicz R, Milligan RA. 2002. A mechanism for microtubule depolymerization by KinI kinesins. *Molecular Cell* 9: 903-09

Morejohn LC, Fosket DE. 1984. INHIBITION OF PLANT MICROTUBULE POLYMERIZATION INVITRO BY THE PHOSPHORIC AMIDE HERBICIDE AMIPROPHOS-METHYL. *Science* 224: 874-76

Mucha E, Hoefle C, Huckelhoven R, Berken A. 2010. RIP3 and AtKinesin-13A - a novel interaction linking Rho proteins of plants to microtubules. *Eur J Cell Biol* 89: 906-16

Mulder AM, Glavis-Bloom A, Moores CA, Wagenbach M, Carragher B, et al. 2009. A new model for binding of kinesin 13 to curved microtubule protofilaments. *Journal of Cell Biology* 185: 51-57

Muller S, Smertenko A, Wagner V, Heinrich M, Hussey PJ, Hauser MT. 2004. The plant microtubule-associated protein AtMAP65-3/PLE is essential for cytokinetic phragmoplast function. *Current Biology* 14: 412-17

Musacchio A, Salmon ED. 2007. The spindle-assembly checkpoint in space and time. *Nature Reviews Molecular Cell Biology* 8: 379-93

Nakajima K, Furutani I, Tachimoto H, Matsubara H, Hashimoto T. 2004. SPIRAL1 encodes a plant-specific microtubule-localized protein required for directional control of rapidly expanding Arabidopsis cells. *Plant Cell* 16: 1178-90

Nakamura M, Hashimoto T. 2009. A mutation in the Arabidopsis gamma-tubulin-containing complex causes helical growth and abnormal microtubule branching. *Journal of Cell Science* 122: 2208-17

Nogales E, Wang HW. 2006. Structural mechanisms underlying nucleotide-dependent self-assembly of tubulin and its relatives. *Current Opinion in Structural Biology* 16: 221-29

Oegema K, Wiese C, Martin OC, Milligan RA, Iwamatsu A, et al. 1999. Characterization of two related Drosophila gamma-tubulin complexes that differ in their ability to nucleate microtubdes. *Journal of Cell Biology* 144: 721-33

Ohkura H, Garcia MA, Toda T. 2001. Dis1/TOG universal microtubule adaptors - one MAP for all? *Journal of Cell Science* 114: 3805-12

Oliva MA, Trambaiolo D, Loewe J. 2007. Structural insights into the conformational variability of FtsZ. *Journal of Molecular Biology* 373: 1229-42

Ovechkina Y, Wagenbach M, Wordeman L. 2002. K-loop insertion restores microtubule depolymerizing activity of a "neckless" MCAK mutant. *Journal of Cell Biology* 159: 557-62

Panda D, Miller HP, Wilson L. 2002. Determination of the size and chemical nature of the stabilizing "cap" at microtubule ends using modulators of polymerization dynamics. *Biochemistry* 41: 1609-17

Panteris E, Apostolakos P, Graf R, Galatis B. 2000. Gamma-tubulin colocalizes with microtubule arrays and tubulin paracrystals in dividing vegetative cells of higher plants. *Protoplasma* 210: 179-87

Pastuglia M, Azimzadeh J, Goussot M, Camilleri C, Belcram K, et al. 2006. gamma-tubulin is essential for microtubule organization and development in Arabidopsis. *Plant Cell* 18: 1412-25

Perez F, Diamantopoulos GS, Stalder R, Kreis TE. 1999. CLIP-170 highlights growing microtubule ends in vivo. *Cell* 96: 517-27

Perrin RM, Wang Y, Yuen CYL, Will J, Masson PH. 2007. WVD2 is a novel microtubule-associated protein in Arabidopsis thaliana. *Plant Journal* 49: 961-71

Pesquet E, Korolev AV, Calder G, Lloyd CW. 2010. The Microtubule-Associated Protein AtMAP70-5 Regulates Secondary Wall Patterning in Arabidopsis Wood Cells. *Current Biology* 20: 744-49

Pierre P, Scheel J, Rickard JE, Kreis TE. 1992. CLIP-170 LINKS ENDOCYTIC VESICLES TO MICROTUBULES. *Cell* 70: 887-900

Piette BMAG, Liu J, Peeters K, Smertenko A, Hawkins T, et al. 2009. A Thermodynamic Model of Microtubule Assembly and Disassembly. *Plos One* 4

Popov AV, Pozniakovsky A, Arnal I, Antony C, Ashford AJ, et al. 2000. XMAP215 regulates microtubule dynamics through two distinct domains. *Molecular Biology of the Cell* 11: 197A-97A

Raff EC, Fackenthal JD, Hutchens JA, Hoyle HD, Turner FR. 1997. Microtubule architecture specified by a beta-tubulin isoform. *Science* 275: 70-73

Ravelli RBG, Gigant B, Curmi PA, Jourdain I, Lachkar S, et al. 2004. Insight into tubulin regulation from a complex with colchicine and a stathmin-like domain. *Nature* 428: 198-202

Raynaud-Messina B, Merdes A. 2007. gamma-tubulin complexes and microtubule organization. *Current Opinion in Cell Biology* 19: 24-30

Reddy ASN, Day IS. 2001. Kinesins in the Arabidopsis genome: A comparative analysis among eukaryotes. *BMC Genomics* 2: 1-13

Reddy ASN, Day IS. 2011. Microtubule Motor Proteins in the Eukaryotic Green Lineage Functions and Regulation. *Plant Cytoskeleton* 2: 119-41

Rice LM, Montabana EA, Agard DA. 2008. The lattice as allosteric effector: Structural studies of alpha beta- and gamma-tubulin clarify the role of GTP in microtubule assembly. *Proceedings of the National Academy of Sciences of the United States of America* 105: 5378-83

Rice S, Lin AW, Safer D, Hart CL, Naber N, et al. 1999. A structural change in the kinesin motor protein that drives motility. *Nature* 402: 778-84

Richardson DN, Simmons MP, Reddy ASN. 2006. Comprehensive comparative analysis of kinesins in photosynthetic eukaryotes. *Bmc Genomics* 7

Rogers GC, Rogers SL, Schwimmer TA, Ems-McClung SC, Walczak CE, et al. 2004. Two mitotic kinesins cooperate to drive sister chromatid separation during anaphase. *Nature* 427: 364-70

Roll-Mecak A, McNally FJ. 2010. Microtubule-severing enzymes. *Current Opinion in Cell Biology* 22: 96-103

Rosenbaum JL, Witman GB. 2002. Intraflagellar transport. *Nature Reviews Molecular Cell Biology* 3: 813-25

Schek HT, III, Gardner MK, Cheng J, Odde DJ, Hunt AJ. 2007. Microtubule assembly dynamics at the nanoscale. *Current Biology* 17: 1445-55

Schnitzer MJ, Block SM. 1997. Kinesin hydrolyses one ATP per 8-nm step. *Nature* 388: 386-90

Sedbrook JC, Ehrhardt DW, Fisher SE, Scheible WR, Somerville CR. 2004. The Arabidopsis SKU6/SPIRAL1 gene encodes a plus end-localized microtubule-interacting protein involved in directional cell expansion. *Plant Cell* 16: 1506-20

Sharp DJ, Rogers GC, Scholey JM. 2000. Microtubule motors in mitosis. *Nature* 407: 41-47

Shelanski M, Gaskin F, Cantor CR. 1973. MICROTUBULE ASSEMBLY IN ABSENCE OF ADDED NUCLEOTIDES. *Proceedings of the National Academy of Sciences of the United States of America* 70: 765-68

Shelden E, Wadsworth P. 1993. OBSERVATION AND QUANTIFICATION OF INDIVIDUAL MICROTUBULE BEHAVIOR INVIVO - MICROTUBULE DYNAMICS ARE CELL-TYPE SPECIFIC. *Journal of Cell Biology* 120: 935-45

Skold HN, Komma DJ, Endow SA. 2005. Assembly pathway of the anastral Drosophila oocyte meiosis I spindle. *Journal of Cell Science* 118: 1745-55

Smertenko A, Saleh N, Igarashi H, Mori H, Hauser-Hahn I, et al. 2000. A new class of microtubule-associated proteins in plants. *Nature Cell Biology* 2: 750-53

Smertenko AP, Chang H-Y, Sonobe S, Fenyk SI, Weingartner M, et al. 2006. Control of the AtMAP65-1 interaction with microtubules through the cell cycle. *Journal of Cell Science* 119: 3227-37

Smertenko AP, Chang HY, Wagner V, Kaloriti D, Fenyk S, et al. 2004. The Arabidopsis microtubule-associated protein AtMAP65-1: Molecular analysis of its microtubule bundling activity. *Plant Cell* 16: 2035-47

Smertenko AP, Piette B, Hussey PJ. 2011. The origin of phragmoplast asymmetry. *Current biology : CB* 21: 1924-30

Smith LG, Gerttula SM, Han SC, Levy J. 2001. TANGLED1: A microtubule binding protein required for the spatial control of cytokinesis in maize. *Journal of Cell Biology* 152: 231-36

Smith LG, Oppenheimer DG. 2005. Spatial control of cell expansion by the plant cytoskeleton. *Annual Review of Cell and Developmental Biology* 21: 271-95

Staehlin LA, Hepler PK. 1996. Cytokinesis in higher plants. *Cell* 84: 821-24

Stoppin-Mellet V, Gaillard J, Vantard M. 2006. Katanin's severing activity favors bundling of cortical microtubules in plants. *Plant Journal* 46: 1009-17

Tokai N, FujimotoNishiyama A, Toyoshima Y, Yonemura S, Tsukita S, et al. 1996. Kid, a novel kinesin-like DNA binding protein, is localized to chromosomes and the mitotic spindle. *Embo Journal* 15: 457-67

Tournebize R, Popov A, Kinoshita K, Ashford AJ, Rybina S, et al. 2000. Control of microtubule dynamics by the antagonistic activities of XMAP215 and XKCM1 in Xenopus egg extracts. *Nature Cell Biology* 2: 13-19

Traas J, Bellini C, Nacry P, Kronenberger J, Bouchez D, Caboche M. 1995. NORMAL DIFFERENTIATION PATTERNS IN PLANTS LACKING MICROTUBULAR PREPROPHASE BANDS. *Nature* 375: 676-77

Twell D, Park SK, Hawkins TJ, Schubert D, Schmidt R, et al. 2002. MOR1/GEM1 has an essential role in the plant-specific cytokinetic phragmoplast. *Nature Cell Biology* 4: 711-14

Vale RD, Reese TS, Sheetz MP. 1985. IDENTIFICATION OF A NOVEL FORCE-GENERATING PROTEIN, KINESIN, INVOLVED IN MICROTUBULE-BASED MOTILITY. *Cell* 42: 39-50

Valiron O. 2011. New insights into microtubule elongation mechanisms. *Communicative & integrative biology* 4: 10-3

Valiron O, Caudron N, Job D. 2001. Microtubule dynamics. *Cellular and Molecular Life Sciences* 58: 2069-84

Verhey KJ, Rapoport TA. 2001. Kinesin carries the signal. *Trends in Biochemical Sciences* 26: 545-50

Verollet C, Colombie N, Daubon T, Bourbon HM, Wright M, Raynaud-Messina B. 2006. Drosophila melanogaster gamma-TuRC is dispensable for targeting gamma-tubulin to the centrosome and microtubule nucleation. *Journal of Cell Biology* 172: 517-28

Vogt N, Koch I, Schwarz H, Schnorrer F, Nuesslein-Volhard C. 2006. The gamma TuRC components Grip75 and Grip128 have an essential microtubule-anchoring function in the Drosophila germline. *Development* 133: 3963-72

Voter WA, Erickson HP. 1984. THE KINETICS OF MICROTUBULE ASSEMBLY - EVIDENCE FOR A 2-STAGE NUCLEATION MECHANISM. *Journal of Biological Chemistry* 259: 430-38

Walczak CE, Gan EC, Desai A, Mitchison TJ, Kline-Smith SL. 2002. The microtubule-destabilizing kinesin XKCM1 is required for chromosome positioning during spindle assembly. *Current Biology* 12: 1885-89

Walczak CE, Mitchison TJ, Desai A. 1996. XKCM1: A Xenopus kinesin-related protein that regulates microtubule dynamics during mitotic spindle assembly. *Cell* 84: 37-47

Walker RA, Obrien ET, Pryer NK, Soboeiro MF, Voter WA, et al. 1988. DYNAMIC INSTABILITY OF INDIVIDUAL MICROTUBULES ANALYZED BY VIDEO LIGHT-MICROSCOPY - RATE CONSTANTS AND TRANSITION FREQUENCIES. *Journal of Cell Biology* 107: 1437-48

Wang HW, Nogales E. 2005. Nucleotide-dependent bending flexibility of tubulin regulates microtubule assembly. *Nature* 435: 911-15

Wang SZ, Adler R. 1995. CHROMOKINESIN - A DNA-BINDING, KINESIN-LIKE NUCLEAR-PROTEIN. *Journal of Cell Biology* 128: 761-68

Wang X, Zhu L, Liu B, Wang C, Jin L, et al. 2007. Arabidopsis MICROTUBULE-ASSOCIATED PROTEIN18 functions in directional cell growth by destabilizing cortical microtubules. *Plant Cell* 19: 877-89

Wasteneys GO. 2002. Microtubule organization in the green kingdom: chaos or self-order? *Journal of Cell Science* 115: 1345-54

Wasteneys GO. 2004. Progress in understanding the role of microtubules in plant cells. *Current Opinion in Plant Biology* 7: 651-60

Wegner A, Engel J. 1975. KINETICS OF COOPERATIVE ASSOCIATION OF ACTIN TO ACTIN-FILAMENTS. *Biophysical Chemistry* 3: 215-25

Whittington AT, Vugrek O, Wei KJ, Hasenbein NG, Sugimoto K, et al. 2001. MOR1 is essential for organizing cortical microtubules in plants. *Nature* 411: 610-13

Wicker-Planquart C, Stoppin-Mellet V, Blanchoin L, Vantard M. 2004. Interactions of tobacco microtubule-associated protein MAP65-1b with microtubules. *Plant Journal* 39: 126-34

Widlund PO, Stear JH, Pozniakovsky A, Zanic M, Reber S, et al. 2011. XMAP215 polymerase activity is built by combining multiple tubulin-binding TOG domains and a basic lattice-binding region. *Proceedings of the National Academy of Sciences of the United States of America* 108: 2741-46

Wittmann T, Wilm M, Karsenti E, Vernos I. 2000. TPX2, a novel Xenopus MAP involved in spindle pole organization. *Journal of Cell Biology* 149: 1405-18

Wordeman L. 2010. How kinesin motor proteins drive mitotic spindle function: Lessons from molecular assays. *Seminars in Cell & Developmental Biology* 21: 260-68

Wordeman L, Wagenbach M, Maney T. 1999. Mutations in the ATP-binding domain affect the subcellular distribution of mitotic centromere-associated kinesin (MCAK). *Cell Biology International* 23: 275-86

Xu XM, Zhao Q, Rodrigo-Peiris T, Brkljacic J, He CS, et al. 2008. RanGAP1 is a continuous marker of the Arabidopsis cell division plane. *Proceedings of the National Academy of Sciences of the United States of America* 105: 18637-42

Yajima J, Edamatsu M, Watai-Nishii J, Tokai-Nishizumi N, Yamamoto T, Toyoshima YY. 2003. The human chromokinesin Kid is a plus end-directed microtubule-based motor. *Embo Journal* 22: 1067-74

Yano A, Kodama Y, Koike A, Shinya T, Kim H-J, et al. 2006. Interaction between methyl CpG-binding protein and Ran GTPase during cell division in tobacco cultured cells. *Annals of Botany* 98: 1179-87

Yildiz A, Selvin PR. 2005. Kinesin: walking, crawling or sliding along? *Trends in Cell Biology* 15: 112-20

Yuba-Kubo A, Kubo A, Hata M, Tsukita S. 2005. Gene knockout analysis of two gamma-tubulin isoforms in mice. *Developmental Biology* 282: 361-73

Yuen CYL, Pearlman RS, Silo-Suh L, Hilson P, Carroll KL, Masson PH. 2003. WVD2 and WDL1 modulate helical organ growth and anisotropic cell expansion in Arabidopsis. *Plant Physiology* 131: 493-506

Yun MY, Zhang XH, Park CG, Park HW, Endow SA. 2001. A structural pathway for activation of the kinesin motor ATPase. *Embo Journal* 20: 2611-18

Zhang H, Dawe RK. 2011. Mechanisms of plant spindle formation. *Chromosome Research* 19: 335-44

Zuo JR, Niu QW, Chua NH. 2000. An estrogen receptor-based transactivator XVE mediates highly inducible gene expression in transgenic plants. *Plant Journal* 24: 265-73